Dissecting Motor Adaptation in Visually Guided Reaching Movements

Thesis Advisor
Professor Maurice A. Smith

Author
Howard Gwohow Wu

Dissecting Motor Adaptation in Visually Guided Reaching Movements

Abstract

Movement is essential to human life because it provides us with the freedom of mobility and the power to affect our surroundings. Moreover, movements are vital to communication: from hand and finger movements when writing, mouth and throat movements when speaking, to painting, dancing, and other forms of artistic self expression. As people grow and experience new environments, adaptively maintaining the accuracy of movements is a critical function of the motor system. In this dissertation, I explore the key mechanisms that underlie the adaptability of simple visually guided reaching movements. I specifically focus on two key facets of this adaptability: how motor learning rate can be predicted by motor variability and how motor learning affects the mechanisms which underlie movement planning.

Inspired by reinforcement learning, I hypothesized that greater amounts of motor variability aligned with a task will produce more effective exploration, leading to faster learning rates. I discovered that this relationship predicts person-to-person and task-to-task differences in learning rate for both reward-based and error-based learning tasks. Moreover, I found that the motor system actively and enduringly reshapes motor output variability, aligning it with a task to improve learning. These results indicate that the structure of motor variability is an actively-regulated, critical feature of the motor system which plays a fundamental role in determining motor learning ability.

Combining prominent theories in motor control, I created a model which describes the planning of visually guided reaching movements. This model computes a weighted average of two independent feature-based motor plans: one based on the goal location of a movement, and the other based on an intended movement vector. Employing this model to characterize the generalization of adaptation to movements and movement sequences, I find that both features, movement vector and goal location, contribute significantly to movement planning, and that each feature is remapped by motor adaptation. My results show that multiple features contribute to the planning of both point-to-point and sequential reaching movements. Moreover, a computational model which is based on the remapping of multiple features accurately predicts how visuomotor adaptation affects the planning of movement sequences.

Table of Contents

Acknowledgements

First, I would like to thank my advisor, Professor Maurice Smith, for his mentorship, training, and intellectual challenges which have defined the last six years I have spent as a graduate student. The quantitative and analytic rigor which he brings to every situation has been one of his greatest gifts, and I can only hope that some of it has rubbed off onto me. Moreover, his personal generosity, inclusiveness, and giving nature have set an example for me and every person who has worked within the lab. I would also like to thank the other members of my dissertation committee, Professor Bence Ölveczky and Professor Robert Howe, for their guidance and support, and in particular, Bence for his contributions and collaboration on the variability project detailed in Chapter 2.

Next, I thank my fellow graduate students (Gary Sing, Luis Nicolas Gonzalez-Castro, Jordan Brayanov, Alkis Hadjiosif, Yohsuke Miyamoto, and Andrew Brennan) and post-docs (Bijan Najafi, Wilsaan Joiner, Thrishantha Nanayakkara, and Biljana Petreska) in the Harvard Neuromotor Control Lab for the countless hours of relaxation time, collaborative work, and intense discussions and debates we have shared both inside and outside of lab. In particular, I would like to thank Yohsuke Miyamoto for designing, running, and analyzing the data relating to the reward-based learning experiments described in Chapter 2, and for always being up for throwing around a football.

I would like to thank my friends, particularly two of my old roommates, Steven Hou and Alex Chan, for their support and camaraderie during these past years. I thank Shimin Kai for her general awesomeness in putting up with me during much of my graduate studies. Lastly, I thank my family: my great grandmother, my grandparents, my aunts and uncles, my cousins, my parents and my sister for giving me the opportunity to develop into the person that I am today.

Chapter 1 – Introduction

The nervous system is one of the most essential but least understood systems in the human body, with functions ranging from the control of basic processes, such as the regulation of breathing[36,47,65], to the planning and execution of complex strategies, such as those involved in air-to-air dogfights. The nervous system is also required for the processing of sensory inputs, the production of creative thought, and, in particular, the formation of memory during learning[65]. Consequently, neurological disorders and stroke can impact nearly every aspect of a person's life, with some of the most debilitating disorders being related to motor control, such as cerebral palsy, Parkinson's disease, and Huntington's disease, which affect either the planning or execution of movements.

These motor disorders are particularly debilitating because movement underlies nearly all interactions with the world. Movement provides us with the freedom of mobility and the power to affect our surroundings by manipulating the objects around us. Moreover, perhaps the most basic and fundamental application of movement is communication: from the written word, to oral communications, to artistic self expressions. These varied functions underscore the importance of movement and highlight the need to develop an understanding of the basic processes which underlie healthy motor function. Knowledge of how a healthy motor control system functions will not only serve to advance the understanding of the pathology associated with each disorder, but also lead to more effective forms of treatment in the future.

One of the earliest motor skills that infants develop is the ability to perform visually guided reaching movements[48,51,140]. By four months of age, infants are able to accurately reach

towards either stationary[48,140] or moving[51] visual targets. From the time of initial development, the adaptability of reaching movements is essential for maintaining accurate performance in the face of changing biomechanical properties (such as growing arms or fatiguing muscles) or when learning new dynamics (such as moving underwater or learning how to operate a new tool).

This dissertation focuses on two key features that underlie the adaptability of visually guided reaching movements: how motor learning rate can be predicted by motor variability and how motor learning affects the mechanisms which underlie movement planning. In the remainder of this chapter, I briefly discuss some basic concepts relating to motor control and motor learning which will be referred to in the following chapters.

1.1 – Algorithms for motor learning

To differentiate between different algorithms that underlie motor learning, we focus on the type of information that the algorithm uses as a learning signal. Although information can be conveyed through multiple sensory modalities (visual, proprioceptive, auditory), we focus on its informational content to identify two algorithms for motor learning: error-based learning[82,113,125] and reinforcement learning[62,120]. In error-based learning, the motor system relies on a signed error signal, the difference between a desired and actual outcome. Whereas in reinforcement learning, the motor system utilizes a reward signal based on the success of a particular movement, without information on what is required to attain more reward[62,120].

1.1.1 – Error-based learning

Although it is likely that multiple learning algorithms contribute to motor learning[31,55,56,142], adaptation of visually guided reaching movements has generally been studied

as a form of error-based learning[31,142]. Specifically, when errors occur during reaching movements, the motor system updates its estimates of internal and external factors to incorporate the new information. In an attempt to minimize errors, the following movement will be based on this updated information. Critically, these error signals provide information about how to improve performance, creating a means to estimate the gradient of an error signal related to a previous action. For example, if a reaching movement overshoots a target, error-based learning will attempt to reduce the extent of the subsequent movement. Thus when error information is available, error-based learning provides a robust avenue for achieving accurate movements in novel environments.

1.1.2 – Reinforcement learning

Reinforcement learning theory[62,120] is an area of machine learning in computer science which breaks learning down into the interaction of two processes: exploration and exploitation. Exploration consists of trying different, novel actions to search for increased rewards, while exploitation is the leveraging of current knowledge to achieve maximal known rewards. Critically, variability is an essential element in reinforcement learning because it drives action exploration. Through exploration, actions which yield greater amounts of reward are discovered, and motor commands which generate these actions are reinforced such that the same or similar actions are more likely to be repeated. Thus without variability, learning cannot occur because new actions which yield progressively higher rewards will never be discovered. Reinforcement learning is particularly effective when the reduction of error is a complicated process, or when error signals are unavailable entirely. But since reward signals contain less information than error signals, reinforcement learning is less clearly directed and tends to progress more slowly than error-based learning.

1.2 – Motor adaptation tasks

1.2.1 – Force-field adaptation

Force-field adaptation is a popular paradigm used by motor control experimentalists to create novel dynamic environments for subjects to learn[11,104,109,111,113,125]. In this task, subjects grasp a robotic manipulandum and make visually guided reaching movements while forces are generated by the robotic manipulandum onto the subject's hand, causing the movement to deviate from what was planned. Often, subjects experience motion state dependent force-fields based on the instantaneous velocity and position of the hand during movement because previous work has shown that novel dynamics are learned as functions of motion state rather than time[22,23,39,109]. One of the more common types of force-fields is a velocity-dependent curl force-field in which forces perturbing the hand are proportional in magnitude but perpendicular in direction to the hand's velocity.

In general, error-based learning algorithms have been applied to model the progression of force-field adaptation[111,113,125], such that when perturbing forces are experienced, the error signal is the difference between the predicted and observed movement. Notably, both visual and proprioceptive error signals have been found to drive force-field adaptation[83,102]. Using these multiple sources of error information to adapt subsequent movements, the motor system attempts to counteract the perturbing force by generating an equal but opposite counteracting force[111,113].

1.2.3 – Visuomotor rotation adaptation

Another common paradigm used to study motor adaptation is the visuomotor rotation task[41,55,63,72,74,82,103,137]. In this task, vision of the hand is obstructed while a cursor representing

hand position is shown on a screen. Subjects are told to move this cursor to visual targets which appear on the screen. A visual perturbation is imposed by rotating the cursor around the movement start location so that it no longer accurately reflects hand position. In order to successfully maneuver the cursor to the target in a straight line, subjects need to adapt by moving their hand at a deviated angle relative to the visual target. Interestingly, since the imposed perturbation is purely visual in nature, the visual error signal conflicts with the unaltered proprioceptive information. Despite this conflict, subjects robustly recalibrate their movements to adapt to these visual perturbations, perhaps indicating that visual information overrides proprioceptive information.

A recent studied demonstrated that visuomotor rotations are adapted through implicit error-based learning, such that this adaptation is independent of explicit strategies[82]. Mazzoni and Krakauer provided subjects with an explicit strategy for perfect task performance. However, they found that although subjects displayed minimal errors initially, directional errors increased as more movements were made under the visuomotor rotation. These results imply that the error driving motor adaptation is not based purely on sensory feedback, but rather that the error is an implicit discrepancy, specifically the motor system's estimate of the intended movement compared to the visual feedback of the movement. They concluded that the motor system adapts movement plans to reduce this sensory prediction error, despite the explicit strategy which was provided that produced perfect task performance.

1.3 – The planning and adaptation of visually guided reaching movements

1.3.1 – Internal models for movement planning and the adaptive control of movement

A central theory in motor control proposes that combinations of internal models (Figure 1.1), neural processes that can predict responses of the motor system given certain motor commands, play an integral role in the planning of movement and motor adaptation[69,128,143]. Two types of internal models have been suggested, forward models and inverse models. Forward models predict the motion which would result given a set of motor commands (Figure 1.1b). Conversely, inverse models compute these motor commands given the desired motion (Figure 1.1a). In the case of planning reaching movements, an inverse model would convert a set of inputs about the desired reach, such as the start location (where a movement begins), the goal location (the intended endpoint of the movement), and the intended movement vector (the displacement required to reach the goal location) into motor commands, a sequence of muscle activations of the arm.

In order to achieve accurate movements in new environments, the inverse model needs to learn how to generate motor commands which will produce the desired motion. Recent studies have suggested that the error signal driving motor adaptation is a sensory prediction error, originating from the comparison between sensory feedback of a movement and the forward model's prediction of the motor commands generated by the inverse model[82,131]. Specifically, comparisons are made between the predicted motion, obtained by feeding the output of the inverse model into the forward model, and sensory feedback received regarding the movement (Figure 1.1c). In turn, this prediction error can be used to update both the forward and inverse

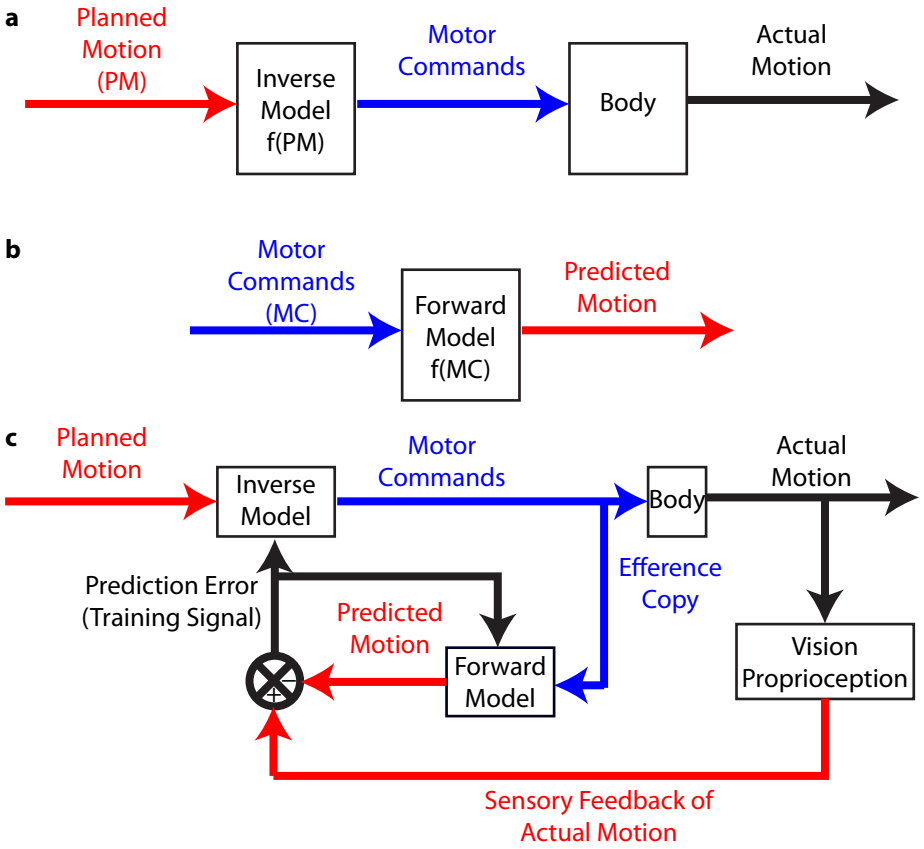

Figure 1.1: Internal models for the control of movement. **a)** The inverse model generates motor commands based on a planned motion; these commands are then sent to the body to generate actual motion. **b)** The forward model predicts the motion states (or the corresponding sensory feedback) that will result from motor commands. **c)** The forward model receives an efference copy of the motor commands generated by the inverse model. Its prediction is compared against the sensory feedback from the actual motion to produce an error signal which can be used as a training signal to update both the forward and inverse models.

model[135]. In support of this hypothesis, studies have found that copies of motor commands are fed back to the cortex[118]. These efference copies, or corollary discharges, can be used for the internal monitoring of movement, presumably as inputs into a forward model.

1.3.2 – Neural processes underlying the planning of visually guided reaching movements

One factor which contributes to the great diversity in the neural coding of movement is the series of coordinate transformations which must occur during the planning of visually guided

reaching movements[4,5,28,64]. These visually guided movements require transformations from the coordinate frame that first encodes visual targets, the extrinsic eye-centered space, to the coordinate frame which is required to produce motion, the intrinsic joint space of the arm. First, movement related representations of start location and movement goal are present in the parietal cortex[4,5,7,13,15,64,70], a region of the brain that integrates both somatosensory[84] and visual information[6,97]. Specifically, an area of the posterior parietal cortex known as the parietal reach region represents the spatial positions of start locations and movement goals primarily in extrinsic eye-centered coordinates[10,16,24,92]. Another region of the parietal cortex, area 5, is involved in coordinate transformations, encoding start and goal locations in multiple reference fames, specifically relative to eye position and intrinsic limb configuration[16,35,46,77,107]. This transformation from extrinsic eye-centered to intrinsic limb based coordinates is essential for generating motor commands and muscle activations. The neural coding of movement vectors first appears prominently in the premotor cortex which is broadly tuned to the preferred direction of movements[17,92]. The ventral premotor cortex primarily codes visual reaching targets in extrinsic arm-centered coordinates[45], while movement vectors are encoded in the dorsal premotor area in hand-centered and eye-centered extrinsic coordinates as well as in intrinsic, joint-based space[17,92,107]. Ultimately, this planning feeds into the primary motor cortex which is the principal area that generates neural impulses that lead to the execution of movement. Here, neurons are largely tuned to a preferred intrinsic movement direction[40], although movement vector and position derivatives are still simultaneously encoded as the position and velocity of ongoing movement[8,88,138].

1.3.3 – The adaptation of visually guided reaching movements

The multiplicity of the overlapping coordinate representations involved in the neural coding of movement indicates that there are several possible mechanisms through which the adaptation of visually guided reaching movements could occur. One popular theory is that the remapping of movement vectors underlies visuomotor adaptation[74,137]. In contrast, another theory proposes that the goal locations of movements are remapped instead[93,98]. But the multitude of internal representations involved in movement planning seem to mandate a complex multi-level remapping of movement features with runs counter to these either/or theories. Unfortunately, although adaptation-specific activity has been found in the human posterior parietal cortex[21], neurophysiology studies have focused on examining adaptive changes in the primary motor cortex and not in planning related areas[90,141].

1. 4 – Scope of this work

The primary goal of this thesis is to examine the principal mechanisms which underlie the adaptability of visually guided reaching movements. I approach this goal by first dividing the adaptability into two distinct components: (1) how motor learning rate can be predicted by motor variability (2) how motor learning affects the mechanisms which underlie movement planning.

In Chapter 2, inspired from previous work in reinforcement learning[62,66,67,86,120,132], we examine the effects of motor output variability on motor learning rate. In combination with the experiments conducted by my fellow graduate student, Yohsuke Miyamoto, our experiments demonstrate how task-relevant motor variability can be used to predict both person-to-person differences in learning rate as well as task-to-task differences. We find that higher levels of task-relevant variability predict faster learning rates in both reward-based learning tasks as well as

error-based learning tasks. Moreover, we find that the motor system harnesses the power of task-relevant variability by specifically increasing it to produce faster learning rates, and that these increases persist overnight. These results indicate that, despite its negative effects on the consistency of performance, variability is an important feature of the motor system which can enhance motor learning when properly directed.

In Chapter 3, we examine how motor adaptation affects the planning of visually guided movements and movement sequences. We specifically design an experimental paradigm which isolates the effects of adaptation on three key movement attributes: the start location of the movement, the goal location of the movement, and the intended movement vector. Creating a model in which movement planning is based on both the movement vector and the goal location of the movement, we find that both features are significantly remapped during motor adaptation. With independent motor plans based on each feature generated in parallel, the amount of remapping of a given feature will only affect the motor plans based on that feature. As a consequence, the effects of each feature's remapping on the executed movement are modulated by the weighting of its associated motor plan when determining the net motor output. These findings demonstrate the complexity in the generalization of visuomotor adaptation to untrained movements and movement sequences. Nevertheless, based on our model and the parameters we determined in the attribute isolating experiments, we are able to predict over 90% of the adaptive changes in movement sequences induced by adaptation to visuomotor rotations.

Chapter 2 – The role of motor output variability in motor learning

Motor output variability is a universal feature in human motor performance, but its role in motor control is a topic of much debate. In one camp, motor control theorists have proposed that motor variability is the result of signal-dependent noise, arising from the stochastic nature of nervous system function[20,49,60,105,119,126]. Thus variability has been seen as a source of error in motor execution, to be mitigated through optimal motor planning[50,85,106,127,128,134]. In the other camp, reinforcement learning theory posits that variability, which underlies action exploration, is essential for learning[62,120]. In humans, variability has largely been treated as noise that is detrimental to motor performance, however recent studies in songbirds have examined variability under the scope of reinforcement learning and provide experimental support for this theory[66,67,86,132]. In this chapter, we rigorously examine the relationship between motor output variability and motor learning ability in a variety of visually guided reaching tasks. We find that the structure of motor variability is coupled with learning ability, so that the amount of variability related to a particular task can predict both person-to-person as well as task-to-task differences in motor learning ability.

2.1 – Summary

Individual differences in motor learning ability are widely acknowledged[1,2,61,133], yet little is known about the factors that underlie them. Reinforcement learning theory states that motor learning requires action exploration, which manifests as movement-to-movement variability, a ubiquitous if often unwanted characteristic of motor performance[62,120]. Here we examine whether individual differences in the temporal structure of motor variability can predict differences in learning ability. We find that higher levels of task-relevant motor variability before training predict faster learning rates both across individuals and across tasks in two different motor learning paradigms: one relying on reward-based learning to shape specific motion trajectories and the other relying on error-based learning to adapt movements in novel physical environments. We proceed to show that extended training can, in turn, reshape motor output variability, aligning it with the trained task to improve learning, and that this realignment persists from one day to the next. These results show that the structure of motor variability predicts learning ability, and that this structure is dynamically regulated by the nervous system to improve learning.

2.2 – Introduction

In 2009, Brendon Todd became the first golfer to hit two consecutive hole-in-ones on the same hole during a professional tournament. Anyone who has swung a golf club would consider the first ace quite a feat, but repeating it was a truly amazing stroke of luck. But why should it be difficult to repeat a hole-in-one or any other action? The ever-present variability in motor

execution, widely thought to be due to the stochastic nature of nervous system function[20,49,60,105,119], makes it virtually impossible to exactly repeat our actions. Indeed, several theories of motor control posit that movements are planned to minimize how inherent motor variability affects performance either alone[50,106,134] or in combination with effort[85,127,128]. Yet motor variability can also be equated with action exploration, an essential component of reinforcement learning[62,120]. Consider the process of learning a golf swing: at first the motion is highly variable, but with practice performance levels and precision increase in parallel. But to what extent does motor variability impede performance early on and to what extent does it enable learning to ensure future success? The idea that motor variability may facilitate learning is supported by recent studies in songbirds, in which inactivations of a cortex-analogue brain area (LMAN) projecting to the song control circuits dramatically reduce both vocal variability and the capacity for song learning[14,66,67,86]. Here we test the idea that movement variability promotes motor learning in humans by examining whether its temporal structure predicts individual learning rates on different motor learning paradigms.

2.3 – Methods

2.3.1 – Participants

All participants gave informed consent for the experimental procedures which were approved by Harvard's Committee on the Use of Human Subjects. In total, we recruited 146 healthy, neurologically intact people to participate in the experiments detailed within this chapter. The age of these people ranged from 18-58 with an average age of 23, of these 146 subjects, 82 were female, and everyone was right handed.

Figure 2.1: Illustration of the experimental setup for Experiments 1 and 2

2.3.2 – Experimental paradigm for the reward-based learning experiments

Eighty-two naïve, neurologically intact subjects (age range 18-55, 46 female, all right handed) participated in the reward-based learning experiments. Twenty subjects participated in Experiment 1, and 62 subjects participated in Experiment 2 (29 subjects in subgroup A and 33 subjects in subgroup B). Subjects performed rapid 200 mm point-to-point reaching movements, while grasping a handle that reported its position for recording to a high-resolution digitizing tablet (Wacom Intuos3) at a sampling rate of 200 Hz. Subjects sat facing a horizontally mounted monitor placed above the tablet, which obstructed vision of the hand (Figure 2.1). On each trial of a 250 trial unscored baseline period, subjects were instructed to move their hand quickly, outward from a starting location to a target while attempting to trace a curve which connected them on the screen. However, during each trial, subjects did not receive visual feedback of their hand position, and saw only the starting location, the target, and the curve, all of which remained the same throughout the entire experiment. Trials that failed to reach the target within 450 ms of movement onset (defined by a velocity threshold of 12.7 mm/s) were discouraged with immediate negative auditory feedback. In order to realign hand position for the next trial, we instructed subjects to move their hand back towards the starting location. We guided this return

motion by displaying visual feedback of hand position when the hand was within 1 cm of the starting location. This feedback was removed before the start of the next trial.

The unscored baseline period was followed by a training period (500 trials for Experiment 1, 1000 trials for Experiment 2), in which conditions were identical to baseline except that subjects were rewarded with a numerical score between 0 and 1000, displayed above the target after each trial. We instructed subjects to maximize their score by more accurately tracing the displayed curve, although, unbeknownst to them, the way the scores were actually calculated was not related to the displayed curve, as described in Section 2.3.3. Since there was also no-visual-feedback on these movements, this eliminated any obvious error signal on which to base motor learning. Answers to a post-experiment questionnaire revealed that the vast majority of subjects were convinced that the scores helped them trace more accurately; thus, in actuality, they misunderstood their reasons for getting high scores and low scores, even though they were, in general, able to learn the underlying task.

During the training period, the threshold movement time was changed from 450 ms to a new value based on each individual subject's baseline movement durations. These new threshold values were set to be two standard deviations above the mean baseline movement duration, and averaged 429 ms with a range of 289 to 529 ms. Movements that failed to reach the target within threshold time during training were again discouraged with negative feedback and scores were not displayed on these trials. Less than 4% of the overall training trials were excluded based on this threshold.

2.3.3 – Scoring scheme for the reward-based learning experiments

The score for each trial was calculated based on the projection of the middle segment of the hand path (from 15 mm to 190 mm) onto one of the shapes shown in Figure 2.2a. We

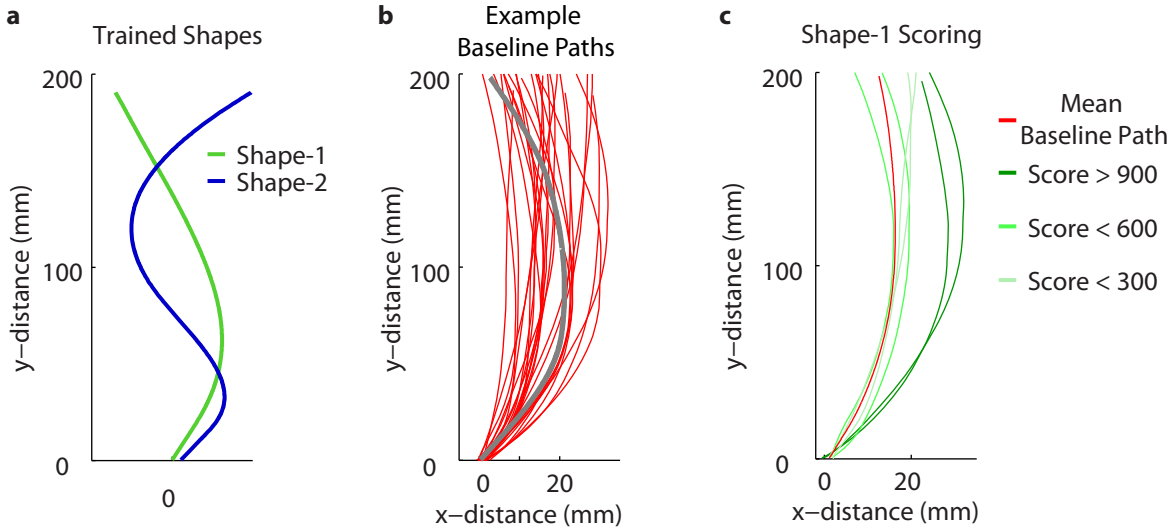

Figure 2.2: Key features of the design of Experiments 1 and 2. **a)** Trajectories of the two shapes which were trained in Experiments 1 and 2 **b)** Example baseline movements from one participant showing the pattern of trial-to-trial variability, compared to the curve subjects saw on the screen and were asked to trace (gray line) **c)** Example movements from a Shape-1 training block in Experiment 2, colored according to score and compared to the mean baseline trajectory (red trace).

linearly interpolated between samples for every 0.25 mm to align the path measurements, facilitating comparison across trials. Thus, each of the baseline paths (Figure 2.2b) were represented as a vector of x-positions measured at specific y-positions. Similarly, Shape-1 and Shape-2 were represented as a function of y-position as well. Since these shapes were chosen to be orthogonal, we can represent each path as a point in a two-dimensional space, the coordinates of which are defined by the magnitude of the projection onto Shape-1 and Shape-2 (Figure 2.3). The units for the projection values are mm root-mean-square (rms), which corresponds to the average contribution of each point within the path to a shape.

Different scores were awarded for different values along the task-relevant axis, which we defined as Shape-1 for Experiment 1, and either Shape-1 or Shape-2 for the two subgroups in Experiment 2. Scores were used to shift subjects' hand paths along the task-relevant axis for each experiment. Ideal scores (score=1000) were awarded 3.6 mm rms away from the baseline

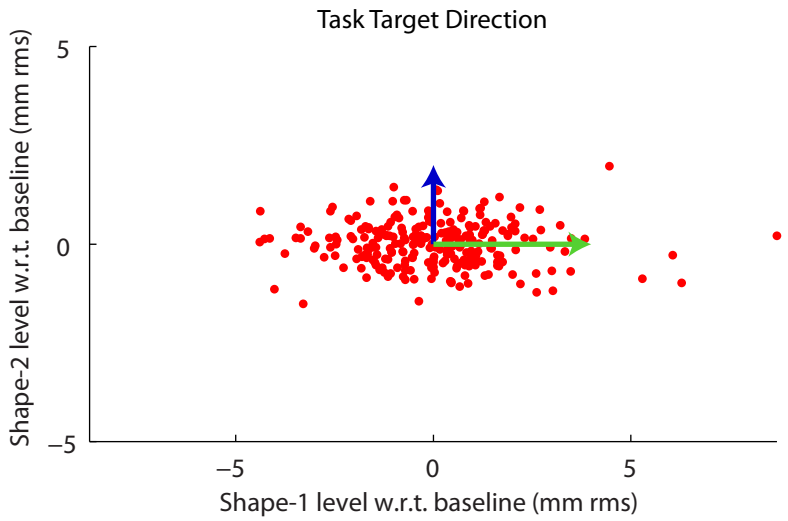

Figure 2.3: The distribution of one subject's baseline movements represented in terms of the magnitude of their projections onto Shape-1 and Shape-2. Note that the variability is higher in the Shape-1 axis than the Shape-2 axis.

mean along the task-relevant axis. About half of the subjects were trained to shift their means in the positive vs negative direction on the task-relevant axis (44 subjects positive, and 38 subjects negative, randomized among subjects). In both Experiments 1 and 2, scores increased monotonically as a function of the difference between the ideal magnitude of the projection and the magnitude of the projection of a trial (Figure 2.4a-b). We chose the ideal distance of 3.6 mm rms based on pilot data indicating robust learning would be achievable within a reasonable duration. This distance covers, on average, about two standard deviations of subjects' baseline variability along the Shape-1 axis. For Experiment 2, we maintained the same ideal distance to facilitate comparison across tasks.

Although the ideal amount of shift on the task-relevant axis was the same for both experiments, the mapping between the amount of shift and the given score differed between Experiments 1 and 2. We employed a dynamic scoring scheme for Experiment 1, which adapted

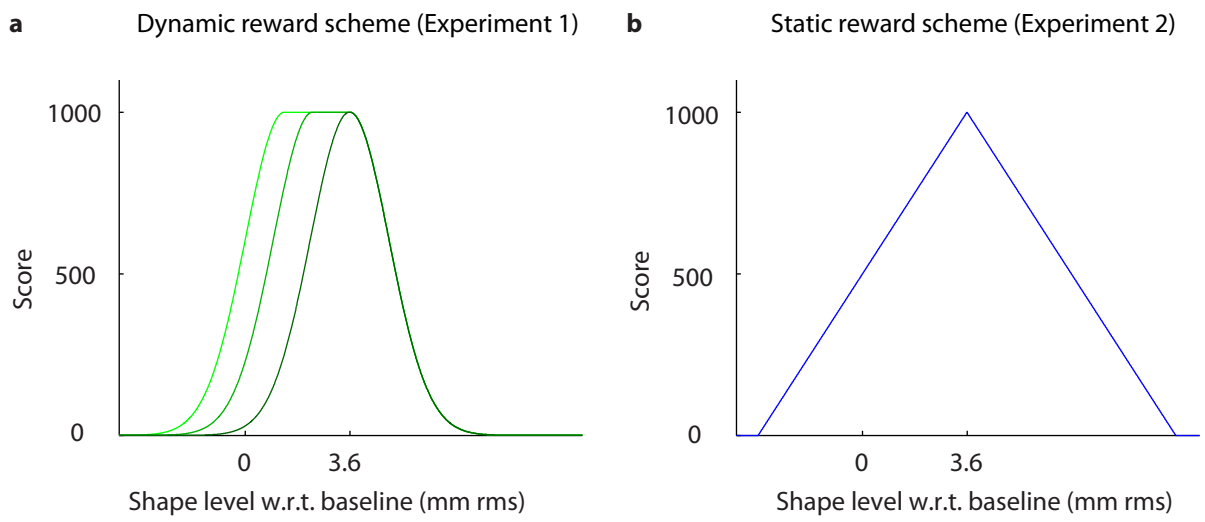

Figure 2.4: Scoring schemes used in the reward-based learning experiments **a)** Illustration of the dynamic reward function used in Experiment 1 in which reward allocation was based on performance relative to the previous 50 trials **b)** Illustration of the static reward function used in Experiment 2 in which the reward allocation was fixed so that reward feedback would be consistent when comparing Shape-1 and Shape-2 learning

from trial-to-trial based on each subject's median and standard deviation during the most recent 50 trials as illustrated in Figure 2.4a. This scoring function is defined by Equation 2.1.

(Equation 2.1)
$$Score\ (x,\eta,\sigma) = \begin{cases} if\ \eta < x^* - \sigma\ AND\ x < x^* & : 1000e^{\frac{-(\min(0,\ x-(\eta+\sigma))^2}{2\sigma^2}} \\ if\ \eta < x^* - \sigma\ AND\ x \geq x^* & : 1000e^{\frac{-(x-x^*)^2}{2\sigma^2}} \\ if\ x^* - \sigma < \eta < x^* + \sigma & : 1000e^{\frac{-(x-x^*)^2}{2\sigma^2}} \\ if\ \eta > x^* + \sigma\ AND\ x \geq x^* & : 1000e^{\frac{-(\max(0,\ x-(\eta-\sigma))^2}{2\sigma^2}} \\ if\ \eta > x^* + \sigma\ AND\ x < x^* & : 1000e^{\frac{-(x-x^*)^2}{2\sigma^2}} \end{cases}$$

Where $\boldsymbol{\eta}$ is the median score of the last 50 trials, $\boldsymbol{\sigma}$ is the standard deviation of the scores from the last 50 trials, x is the magnitude of the projection of the current trial onto the ideal shape, and x^* is the target projection magnitude.

In order to achieve a fair comparison between Shape-1 and Shape-2 learning for the two subgroups in Experiment 2, we employed the same static scoring scheme for both subgroups, illustrated in Figure 2.4b and define by Equation 2.2.

$$\text{(Equation 2.2) } Score(x) = Max\left(0, 1000 - 500\left|\frac{x-x^*}{x^*}\right|\right)$$

Note that this scheme remained constant throughout the experiment, and that it was unaffected by differences in performance, to facilitate comparison between the learning of Shape-1 and Shape-2. A few example paths and corresponding scores from a subject trained to learn Shape-1 are shown in Figure 2.2b.

2.3.4 – Measuring baseline variability and learning rate in the reward-based learning experiments

We quantified task-relevant variability during the baseline period by projecting the hand paths from the last 160 trials during the baseline period (Figure 2.2b) onto the shape which would be trained later (either Shape-1 or Shape2). Taking the standard deviation of the magnitude of these projections yielded the task-relevant baseline variability. Correspondingly, we quantified total baseline variability by taking the square root of the sum of the variances in x-positions for the same 160 trials used to determine task-relevant variability.

We computed the learning level associated with each trial by finding the magnitude of the projection of the hand path onto the trained shapes shown in Figure 2.2a. The learning level was then computed as the baseline subtracted value of this projection normalized by the task's ideal shift of 3.6 mm rms. For example, a baseline-subtracted projection level of 1.8 mm rms would correspond to a learning level of 0.5. To characterize the learning rate of each subject, we used the average learning level during the first 25% of the training period (125 trials) for Experiment

1, and the first 80% of the training period (800 trials) for Experiment 2. We used a longer window in Experiment 2 because the learning curves, particularly those for Shape-2, were slower. Had we used a window for Experiment 2 that was similar to Experiment 1, the slower learning rate for Shape-2 learning would have produced an average learning level not significantly different from zero.

2.3.5 – General procedure for the error-based learning experiments

Sixty-four naïve, neurologically intact subjects (age range 18-58, 36 female, all right handed) participated in the error-based learning experiments. Forty subjects participated in Experiment 3, and 24 subjects participated in Experiment 4. We used a motor adaptation task, force-field learning, which has been extensively used to study error-based learning[43,104,109,111-113].

During these force-field experiments, subjects grasped a handle attached to a lightweight two-joint robotic manipulandum and were instructed to make point-to-point reaching arm movements. Subjects sat facing a monitor and made rapid (500 ms) 10 cm movements toward the torso using the arm configuration displayed in Figure 2.5a while viewing a screen cursor that represented real-time hand position. Subjects were instructed to make a fast, direct movement toward each target that appeared on the monitor, and after each trial subjects moved their hands back to the starting location. Positive auditory feedback was provided on trials completed between 400-600 ms, where movement onset was defined based on a speed threshold of 30 mm/s and movement offset was defined as the first time that the movement speed decreased below 30 mm/s and remained there for 200 ms consecutively. Experiments consisted of three different types of trials (Figure 2.5b-d): null field trials during which no active forces were applied to the subject's arm (Figure 2.5b), error-clamp trials[43,104,111,113,135] to measure the lateral forces produced on a given movement (Figure 2.5d), and force-field perturbation trials during which

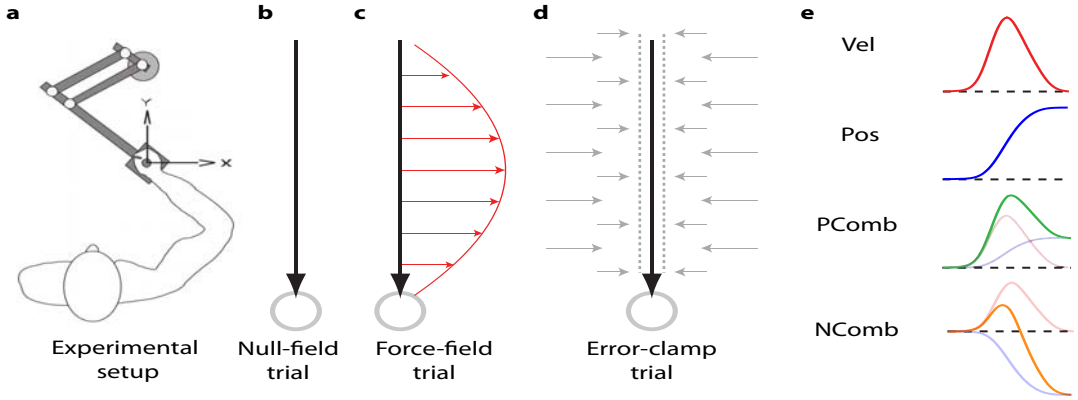

Figure 2.5: Basic experimental protocol for the force-field adaptation experiments **a)** Illustration of the arm configuration subjects had when grasping the robotic arm **b-d)** Illustration of the different types of trials subjects were exposed to in Experiments 3 and 4 **e)** Illustration of four different patterns of dynamics[111]

forces were applied to the arm during the movement based on the instantaneous position and/or velocity of the hand (Figure 2.5c). The position and velocity of the hand as well as the forces generated by the arm were recorded at a sampling rate of 200 Hz.

2.3.6 – Definition of the force-field environments

The force-fields used in the current experiments were composed of a linear combination of position and velocity dependence (Figure 2.5e) with the form:

$$\text{(Equation 2.3)} \quad \begin{bmatrix} F_x \\ F_y \end{bmatrix} = K \cdot \vec{p} + B \cdot \vec{v} = \begin{bmatrix} 0 & -K \\ K & 0 \end{bmatrix} \begin{bmatrix} x \\ y \end{bmatrix} + \begin{bmatrix} 0 & -B \\ B & 0 \end{bmatrix} \begin{bmatrix} \dot{x} \\ \dot{y} \end{bmatrix}$$

Here, x and y denote the x and y position (p) of the hand and $\dot{x}$ and $\dot{y}$ denote the x and y velocities (v) with axes as illustrated in Figure 2.5a. Velocity-dependent (Vel) force-fields shown in Figure 2.5e had values of (K=0 N/m, B=±15 Ns/m), and were used in both Experiments 3 and 4. These force-fields produced forces perturbing the hand that were

proportional in magnitude but perpendicular in direction to the hand's velocity. Position-dependent (Pos) force-field trials had values of (K=±45 N/m, B=0 Ns/m), and the positive-combination (PComb) and negative-combination (NComb) force-field environments had values of (K=±21.2 N/m, B=±13.2 Ns/m) and (K=∓35 N/m, B=±9.4 Ns/m), respectively (Figure 2.5e). To account for biases from biomechanical effects, clockwise and counter-clockwise versions of force-fields were balanced in all experiments, with half the subjects learning each in the data averaged across these conditions.

2.3.7 – Error-clamp trials

Error-clamp trials (Figure 2.5d) were designed to measure the feed-forward motor output produced during a reaching movement. Actions made during reaching movements result from feed-forward motor output and online feedback error correction. Error-clamp trials[104,111,113] restricted the lateral deviations during movement below 1 mm, effectively eliminating the lateral error signal and corresponding feedback responses, thus allowing for isolation of feed-forward motor output. We restricted these deviations by applying a very stiff, damped elastic force (K=6000 N/m, B=250 Ns/m) to counteract lateral forces produced by subjects, while essentially clamping movements into a straight line path. Since we were able to counteract the lateral deviations of the subject's arm with a robot generated force, we estimated the lateral force produced by the subject as the opposite of the robot generated clamping force at each time-point. All force data were smoothed with a second order Butterworth filter with a cutoff frequency of 10 Hz to remove high frequency noise generated by force sensors and motor actuators. Motor output variability and motor adaptation during the force-field experiments were assessed based on these smoothed force profiles.

2.3.8 – Experimental paradigm for Experiment 3

Forty right handed neurologically intact subjects (20 female, ages 18-31, mean age 21) participated in Experiment 3. This experiment was designed to examine the relationship between task-relevant variability during the baseline period and motor learning rates for force-field adaptation across individuals. This required accurate measurements of both baseline variability and learning rates for each subject. To obtain accurate measurements of baseline variability, we designed the experiment with a prolonged baseline period of 200 trials during, which baseline variability was assessed based on 20 error-clamp trials that were randomly interspersed among null-field trials. Prior to this baseline period, subjects performed a 100 trial familiarization period during which variability was not measured. Although movement duration was generally between 500-600 ms, we examined the force output generated in a 860 ms window centered at the peak speed point to ensure that we captured the entire movement (average peak speed=320±5 mm/s, average speed at start of window=0.4±0.1 mm/s, average speed at end of window=2.7±0.6 mm/s).

Following the baseline period, subjects experienced a 150 trial training period during which a velocity-dependent force-field environment was applied. In this training period, 80% of trials were training trials and 20% were error-clamp trials which we intermixed to measure the learning level at various points in training. Subjects were stratified based on the amount of velocity-dependent variability present during baseline error-clamp movements, and average learning curves were calculated for each group. Initial learning rate was calculated by finding the average increase in learning level over the first ten trials of training. This period included two error-clamp trials.

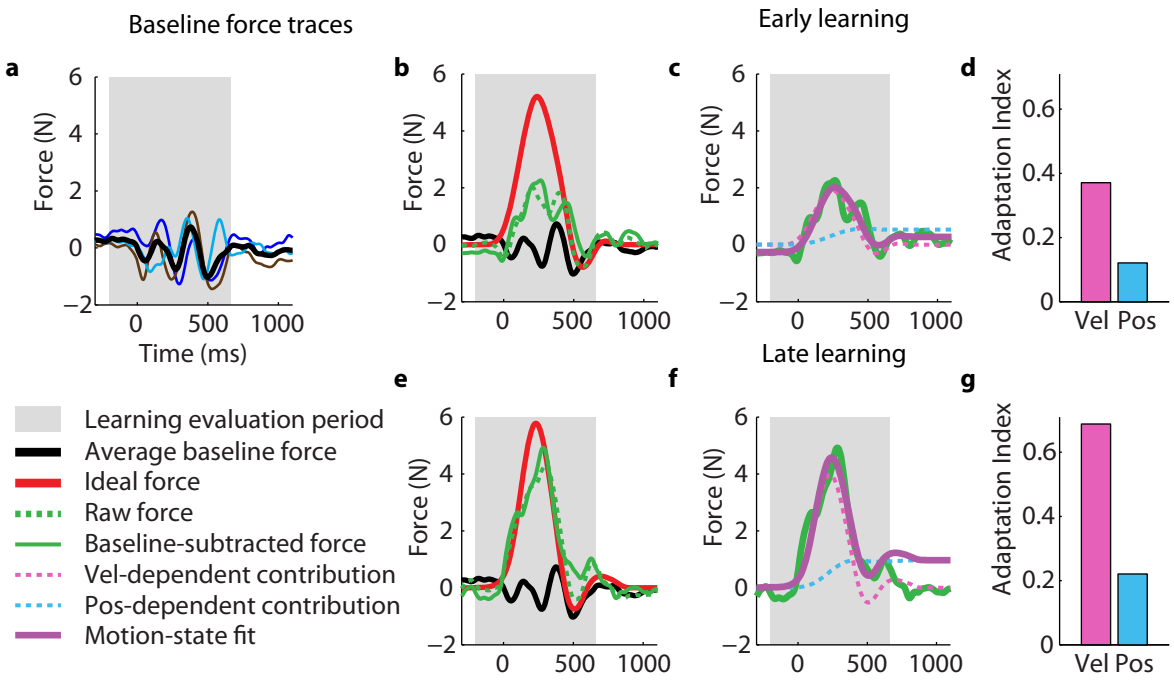

Figure 2.6: Adaptation to a velocity-dependent force-field for one subject. **a)** Lateral force profiles during the baseline period, measured on error-clamp trials. Individual error-clamp measurements are colored, and the subject's average baseline force is shown in black **b-d)** An example force profile measured during an early learning error-clamp trial **b)** Raw (dashed green) and baseline-subtracted (solid green) force profile early in training compared to baseline (black) and full compensation (red) **c)** The baseline-subtracted force profile is regressed onto a linear combination of position (cyan), velocity (pink), and acceleration (not shown) traces **d)** An adaptation index is calculated such that 1 corresponds to full compensation **e-g)** Same as in (**b-d**) but for an example force profile late in learning

2.3.9 – Measuring force-field adaptation

To measure adaptation to the force-field environments, we examined the difference between the force profiles measured during pre-training error-clamp trials (Figure 2.6a) and the error-clamp trials randomly interspersed during the training period. We performed subject-by-subject baseline subtraction to determine the change in motor output induced by exposure to each force-field environment (Figure 2.6b,e). The learning-related changes in the force profiles were then regressed onto a linear combination of the motion states position, velocity, and acceleration during an 860 ms window centered at the peak speed point of each movement (gray box) as

shown in Figure 2.6c,f [58,111]. We measured learning for the pure velocity dependent force-field environment by normalizing the velocity regression coefficient to create an adaptation coefficient for which a value of 1 indicated full compensation for the force-field environment (Figure 2.6d,g). For a force profile that is driven by adaptation to a velocity-dependent force-field, our adaptation coefficient represents the size of the bell-shaped velocity-dependent component of the measured force profile. This velocity-dependent component of the measured force profile specifically corresponds to the force component targeted to counteract the velocity-dependent force-field perturbation. The adaptation coefficients for position-dependent force-fields were calculated in an analogous fashion based on the regression coefficient. Adaptation coefficients for the PComb and NComb environments were obtained by projecting the position and velocity regression coefficients onto the axis of the applied force-field and normalizing the result by the amplitude of the applied force-field[111]. We followed the procedures described in previous work when computing the task-specific and non-task specific adaptation coefficients[111].

2.3.10 – Measuring baseline task-relevant force variability

We found the variance associated with four different force-field environments (described in Section 2.3.6 and illustrated in Figure 2.5e) using the error-clamp trials that were randomly interspersed during the baseline period. We projected each error-clamp force trace onto a normalized trace representative of each force-field environment. Figure 2.7 shows how three example force traces (Figure 2.7a) can be projected onto the four force-field environments shown in Figure 2.5e. We used two measures to characterize task-relevant baseline variability, the amount of baseline variability, and the fraction of variance accounted for by a particular environment. The standard deviation of the magnitudes of the projections was used to determine the amount of task-relevant variability for each subject. We divided the variance of the

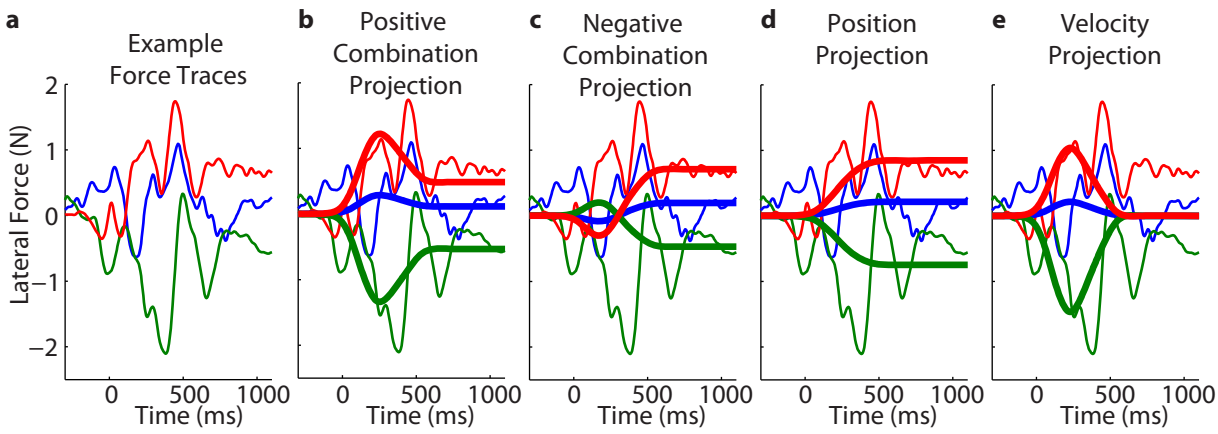

Figure 2.7: Quantifying task-relevant force variability during baseline periods. **a)** Three example force profiles from one subject during the baseline period in the velocity-dependent force-field adaptation experiment (Experiment 3) **b-e)** Projections of the force profiles shown in **a** onto the four different types of visco-elastic dynamics described in Section 2.3.6 and illustrated in Figure 2.5e. Individual force traces are shown as thin lines and the projections are shown as thick lines of the corresponding color.

magnitudes of the projections by the total variance of the force traces to find the fraction of variance accounted for by each environment in the baseline period.

2.3.11 – Analyzing the temporal structure of baseline variability

We used principal components analysis (PCA)[59] on the force traces recorded during baseline error-clamp trials to understand the structure of variability during baseline. To obtain an accurate estimate of the overall structure of variability, we performed PCA on the aggregated baseline force traces for all subjects in Experiment 3. As before, forces were examined in an 860 ms window centered at the peak speed point of each movement. When aggregating the data, we removed the mean baseline force profile produced by each subject so that individual differences in mean behavior would not contribute to our analysis of the structure of trial-to-trial variability. Principal components of the force variability were found by performing eigenvalue decomposition on the covariance matrix of the aggregated force data.

2.3.12 – Single-trial learning rates for different force-field environments

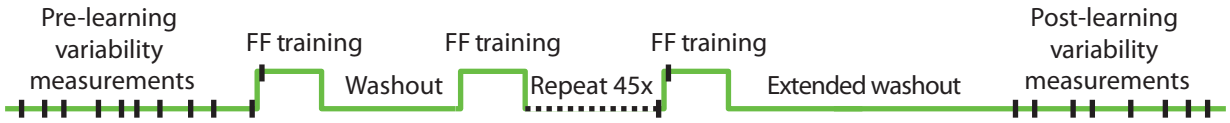

Figure 2.8: Experimental protocol for Experiment 4, in which we assessed changes in learning rate and variability induced by a high consistency environment (HCE)

The single-trial learning rates for each force-field environment were determined using the data reported in a previous publication[111]. In this previous experiment, error-clamp trials were presented before and after a single trial force-field exposure, and the differences in the lateral force output were used to assess single trial learning rates. Since the previous study used a different window size, we recomputed the learning rates in the same 860 ms window used to assess motor output variability, allowing a fair comparison between the variability associated with each type of force-field and the corresponding learning rates of each type of force-field.

2.3.13 – Experimental paradigm for Experiment 4

In Experiment 4, we sought to determine whether the motor system could adaptively reshape the structure of variability to promote learning. Twenty-four naïve neurologically intact right handed individuals (16 female, ages 18-58, average age 23) participated in these experiments which spanned two days. The training paradigm (Figure 2.8) was designed to increase the learning rate for either velocity-dependent or position-dependent force-fields by creating what we refer to as a high consistency environment (HCE). HCEs, where consistency is operationally defined as the correlation between the force-field amplitude on the current trial versus the next trial – i.e. the lag(1) autocorrelation, have been shown to increase a subject's learning rate for the exposed environment[42]. Thus in Experiment 4, a HCE was created by exposing subjects to 48 short blocks of force-field trials (either position-dependent or velocity-dependent) each followed by a block of null-field trials. Each cycle consisted of 7 force-field

trials followed by 8-12 null-field trials. Motor variability was assessed during two epochs on each day: immediately preceding training and after an extended washout period (26-33 null-field trials) following training. Each assessment consisted of 50 error-clamp trials interspersed amongst 150 null-field trials. Half the subjects were trained on the HCE for the position-dependent force-field on day one and for the velocity-dependent force-field on day two. The other half experienced these environments in the opposite order. The initial assessment of variability on day two was also used to probe the degree to which changes in variability induced on day one persisted to the next day. Consequently, variability data from immediately before and after exposure were available for all environmental exposures we studied, whereas next day retention was only available for the day one environment (half the data).

2.3.14 – Measuring changes in the amount and specificity of motor learning

Single-trial learning rate was assessed on 21 of the 48 force-field blocks through the use of an error-clamp triplet[111] centered around the first force-field trial in each of these blocks. On these triplets, subjects performed an error-clamp trial, followed by a force-field trial, and then another error-clamp trial. When present, this triplet was followed by six additional force-field trials to complete the training block. Since previous studies have shown that initial learning of force-field environments results in significant cross-adaptation[111] between position-dependent and velocity-dependent learning, the components of the adaptation that depended on both position and velocity were measured using linear regression using a previous analysis we developed[111]. We examined single-trial learning both before and after exposure to high-consistency training in each environment. For the before-training data, the triplet was experienced on the very first cycle of exposure so that the high-consistency environment itself could have no effect. We supplemented this data with first-exposure single-trial learning data

from other experiments (58 additional velocity learning trials and 12 additional position learning trials) which were essentially identical to the current experiment up to the point of this first exposure, but different thereafter[42,111]. Specifically, the only difference between the experiments which provided the supplemental data and the current one, up to the point of the first exposure, was the number of baseline trials experienced beforehand. The post-exposure single-trial learning data were computed from the averaged learning data from the last 9 of the 48 training cycles - these 9 cycles included 5 measurement triplets for each exposure.

2.3.15 – Measuring changes in the amount and specificity of motor output variability

We also examined the effects of the HCEs on the structure of motor variability. We did this in two ways: 1) by looking at the position- and velocity-dependent changes in the first principal component of variability (PC_1) and 2) by looking at overall changes in position- and velocity-related variability induced by exposure to these environments. After aggregating data across all subjects (as in the analysis of baseline variability in Experiment 3 detailed above in Section 2.3.11), PC_1 was computed in three different epochs: before training, after velocity-training, and after position-training. Another way to determine changes in the structure of motor variability specifically related to an environment is to examine the overall changes in position- and velocity-related variability induced by exposure to position-dependent and velocity-dependent HCEs. To examine these specific changes, we used linear regression to find the position-dependent and velocity-dependent contributions of each force trace before training, after position-training, and after velocity-training. Dividing the variance of these regression coefficients by the total variance in the data allows us to determine the fraction of variance specifically accounted for by velocity and position.

2.3.16 – Statistics

Statistical testing for group learning rates and group variability in Experiments 1-3 were performed by using two sample Student's t-tests. Linear regression analyses were used to determine the association between variability and learning rate (Experiments 1-3) and the fraction of variance accounted for by different force-field environments and their corresponding single-trial learning rate. Since we computed the principal components of the lateral force variability over the population in Experiments 3 and 4, confidence intervals around PC_1 were computed using bootstrap analysis in which the population was resampled 100,000 times to measure the amount of variability in PC_1. In this bootstrap analysis, PC_1 was computed on each iteration using the covariance matrix of the mean subtracted force profiles from the randomly sampled population. A similar 100,000 iteration bootstrap was performed to compute confidence intervals for single-trial learning in Experiment 4 by resampling adaptation force profiles from the population. Correspondingly, statistical testing on the changes in the position and velocity contributions to adaptation and variability were performed with a 100,000 iteration bootstrap as were the changes in position-velocity gain-space angle.

2.4 – Results

2.4.1 – Task-relevant variability predicts individual differences in the rate of reward-based learning

We began by examining the relationship between variability and learning rate in a reward-based motor learning task (Experiment 1, Figure 2.1). Subjects (n=20) learned to produce hand trajectories with specific shapes during 20 cm point-to-point reaching movements through trial-and-error. Participants received no visual feedback of their actual trajectories or the

rewarded shape, ensuring that no error-correcting information was available to guide the learning process. They trained to maximize a numerical performance score given after each trial that was based on the similarity between the movement path and the trained shape (see Section 2.2.2-2.2.3 and Figure 2.4a for details on the paradigm and scoring scheme).

If the variability produced by the motor system is indeed harnessed during trial-and-error learning to improve performance as reinforcement learning theory predicts, we would expect greater task-relevant variability before training to be associated with higher learning rates during training. Each experiment began with a 250 trial unscored baseline period (example data from one subject shown in Figure 2.2b). We computed task-relevant variability during this period by projecting each hand path onto the target shape (Figure 2.2a, Shape-1) to be used during the subsequent shape-specific training.

To look at the effect of baseline motor variability on subsequent learning, we stratified individuals into subgroups based on the amount of Shape-1 variability displayed in the baseline period. Subjects from Experiment 1 were divided into groups with above-mean and below-mean Shape-1 variability, and average learning curves were calculated for each group, as shown in Figure 2.9a. The mean task-relevant baseline variability was 3.47±0.50 mm overall; 2.58±0.16 mm for below-mean subjects and 5.55±1.34 mm for above-mean subjects. For comparison, we also stratified subjects based on the median and quartiles of the data as illustrated in Figure 2.9b (bottom 25%: 1.98±0.11 mm, bottom 50%: 2.29±0.12 mm, top 50%: 4.65±0.86 mm, top 25%: 5.95±1.57 mm). We found that subjects with above-mean task-relevant variability learned considerably faster than below-mean subjects (Figure 2.9a, $p=0.014$). Correspondingly, in the median data, learning curves show a clear early separation between subgroups, with higher variability groups showing higher learning ($p=0.026$ for upper half vs lower half and $p=0.0032$

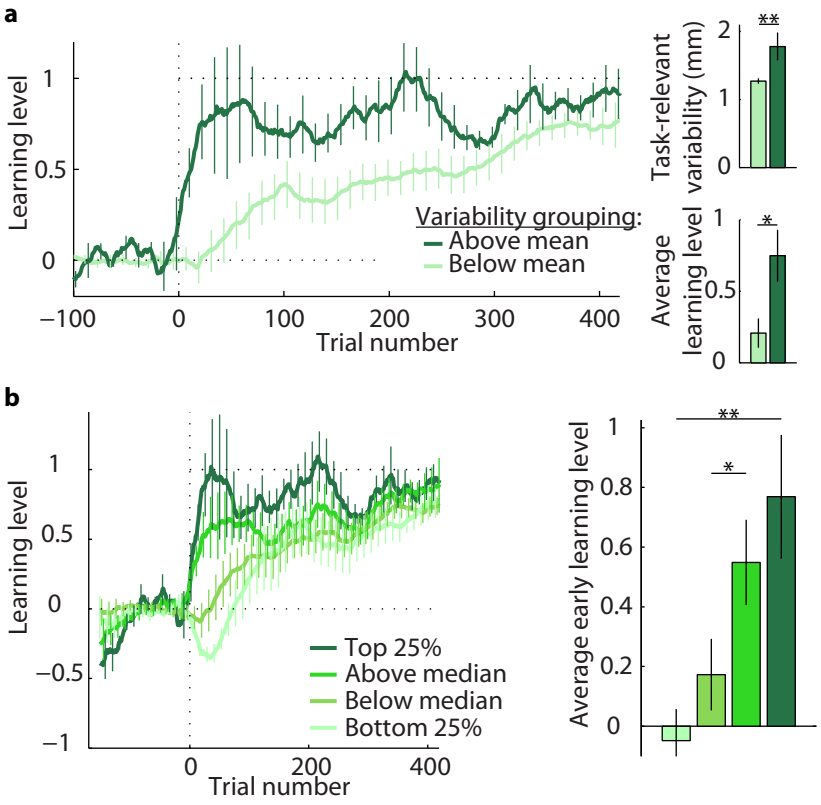

Figure 2.9: Variability grouping analysis of experimental results from Experiment 1. **a)** Participants displaying above-mean amounts of Shape-1 variability during the baseline period exhibited faster learning **b)** Stratifying subjects using percentiles in the baseline variability data show that groups with higher amounts of baseline variability exhibited faster learning. All error bars in figures in this chapter represent s.e.m. Asterisks indicate significance (* $p<0.05$, ** $p<0.001$ in all figures in this chapter)

for upper quartile vs lower quartile, Figure 2.9b). Moreover learning rates calculated for each subgroup in Experiment 1 based on the first 125 trials of training show an increasing monotonic relationship between baseline variability and learning rate across the four subgroups.

We also examined individual differences in task-relevant variability, and found a strong correlation between baseline task-relevant variability and learning rate (Figure 2.10b, $r=0.80$, $p<0.0001$). The subject with the highest task-relevant baseline variability epitomized this relationship by displaying the highest learning rate, but even if this data point is removed, the correlation between task-relevant variability and learning rate remains ($r=0.65$, $p=0.0026$). This

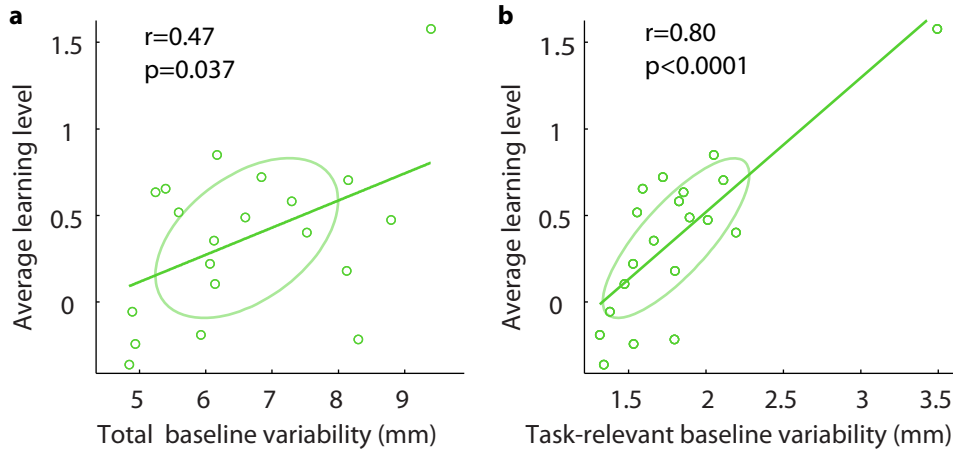

Figure 2.10: Subject-by-subject comparison of learning in Experiment 1 as a function of variability **a)** Average learning rate and total baseline variability are correlated **b)** Average learning rate is more strongly correlated with task-relevant baseline variability

is the first time individual differences in learning rate have been predicted from baseline performance characteristics. However, when we examined the relationship between total variability and learning rate, we also found a significant, albeit weaker, correlation (Figure 2.10a, r=0.47, p=0.037) raising the possibility that it is the amount of total variability rather than its precise temporal structure that matters for learning (in our data set the two are correlated, r=0.63).

2.4.2 – Task-relevant variability predicts across-task differences in the learning rate of two reward-based learning tasks

To determine whether task-relevant variability or total variability drove the differences in learning rate between subjects, we performed a second experiment in which two groups of subjects were trained on two different shapes (Figure 2.2a, n=29 for Shape-1, n=33 for Shape-2), each associated with different amounts of task-relevant variability during the baseline period. Shape-1 was identical to the one used in the first experiment, whereas Shape-2 was chosen to be orthogonal to Shape-1 and to account for a smaller amount of total baseline variability. On

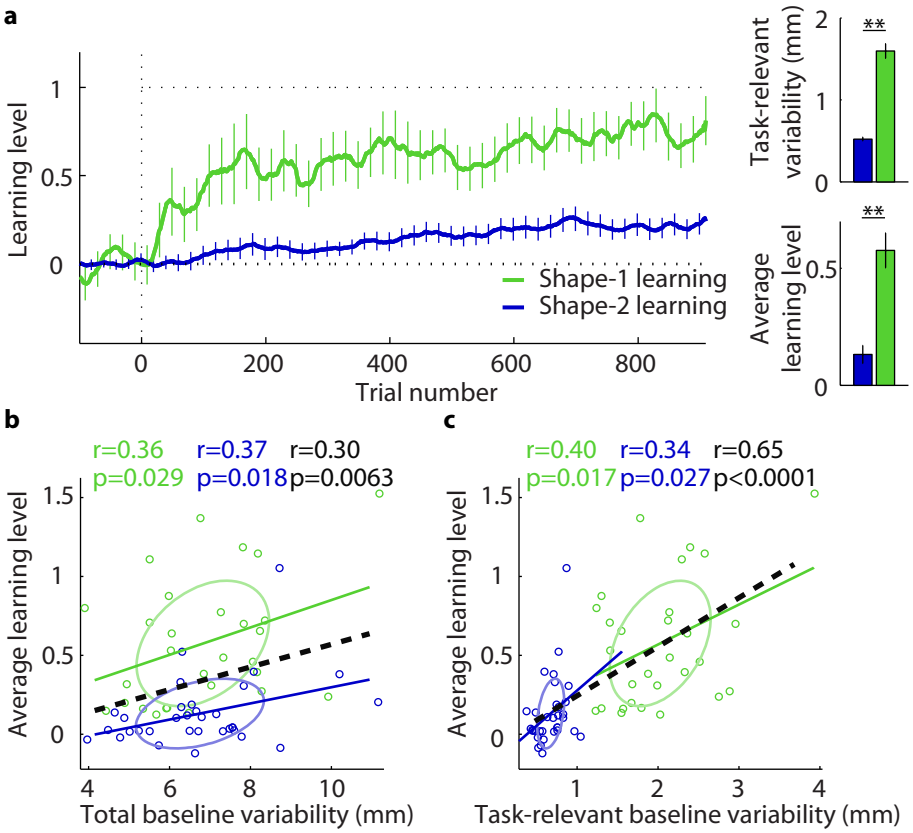

Figure 2.11: Variability grouping and individual subject analysis of experimental results from Experiment 2. **a)** Participants learned Shape-1 significantly faster than Shape-2, in line with the disparity in task-relevant baseline variability. **b)** Total variability predicts individual differences within tasks, but not across tasks. Note that in **b-c**, the colored lines depict regression for each task whereas the dashed black line depicts regression across both tasks. **c)** Task-relevant variability predicts individual differences in learning both within and across tasks. Correspondingly, the bivariate linear regression analysis shows a significant effect of task-relevant, but not total variability.

average, Shape-1 accounted for 9.2±1.1% of the total variability, while Shape-2 accounted for 0.66±0.12% of the total variability during the baseline period. Thus Shape-2 learners should display decreased task-relevant variability but identical total variability compared to Shape-1 learners allowing us to dissociate the effects of these two types of variability on learning rate.

We found that task-relevant variability during baseline was positively correlated with learning rate both within (Figure 2.11c, Shape-1 (green): p=0.017; Shape-2 (blue): p=0.027) and

across groups (dashed black line: $p<0.0001$) with slower learning rates for Shape-2 compared to Shape-1 (Figure 2.11a, $p<0.0001$), suggesting that it may account for the observed differences in learning rates. Moreover, simultaneous regression of learning rate onto both types of variability across groups reveals a significant effect of task-relevant (partial $R^2=0.38$, $p<0.0001$) but not total variability (partial $R^2=0.0090$, $p=0.47$). Correspondingly, a single relationship between task-relevant variability and learning rate (Figure 2.11c, dashed black line) appears to explain the individual differences in learning ability for both groups just as accurately as a composite relationship individualized for each group ($R^2=0.427$ vs $R^2=0.434$, respectively), indicating that task-relevant variability provides a unifying explanation for both inter-individual and inter-task differences in learning rate.

2.4.3 – Task-relevant variability predicts differences in learning rate on an error-based learning task

We next examined the generality of the relationship between motor variability and motor learning rates on a task thought to be learned through error-based learning. Reward-based learning is often associated with slow learning rates due to an absence of error-correcting signals, whereas tasks in which dynamic or kinematic perturbations produce error-correcting signals are learned more rapidly. Reinforcement learning theory posits that motor exploration is essential for reward-based learning algorithms, and although recent studies have suggested that learning on error-based tasks may arise from multiple mechanisms[55,56], error-based adaptation need not be contingent on such exploration.

To examine whether motor variability can also facilitate learning in error-based motor adaptation tasks, subjects (n=40) adapted to an environment with altered physical dynamics

during point-to-point reaching movements (Figure 2.5a). Since these subjects would later be exposed to a velocity-dependent force-field, we analyzed what would become the task-relevant component of the variability before any learning occurred by computing the amount of velocity-dependent variability present in baseline error-clamp trials. We computed the velocity-dependent component of variability by projecting each force trace onto its corresponding velocity profile (Figure 2.7e), and calculating the variance across the magnitude of these projections. Thus, if motor output variability was fully velocity-dependent, the variability in force traces would not change after projection and would be equal to the total variability.

After a 200 trial baseline period, these subjects were exposed to a velocity-dependent force-field environment in which the force vector perturbing the hand was proportional in magnitude and lateral in direction to the hand's velocity[57,104,111,113,125] as shown in Figure 2.5c. Error-clamp trials[104,111,113] (Figure 2.5d) were randomly interspersed in both baseline null-field (Figure 2.5b) and training velocity-dependent force-field (Figure 2.5c) periods to measure the lateral forces produced during these periods. Task-relevant variability at baseline was evaluated for each subject as explained in Section 2.3.10, while velocity-dependent force-field learning during the training period was quantified by regressing the error-clamp force profiles onto the velocity traces associated with each movement (see Section 2.3.9 and Figure 2.6).

We stratified individuals based on the level of velocity-dependent variability displayed during the baseline period (Figure 2.12a), and found that participants with above-mean variability showed faster velocity-dependent force-field learning than those with below-mean variability (Figure 2.12b, $p=0.014$ when comparing the average learning rate over the first ten trials). Moreover, individuals with variability at least one standard deviation above mean had more than twofold higher learning rates than individuals with variability levels one standard

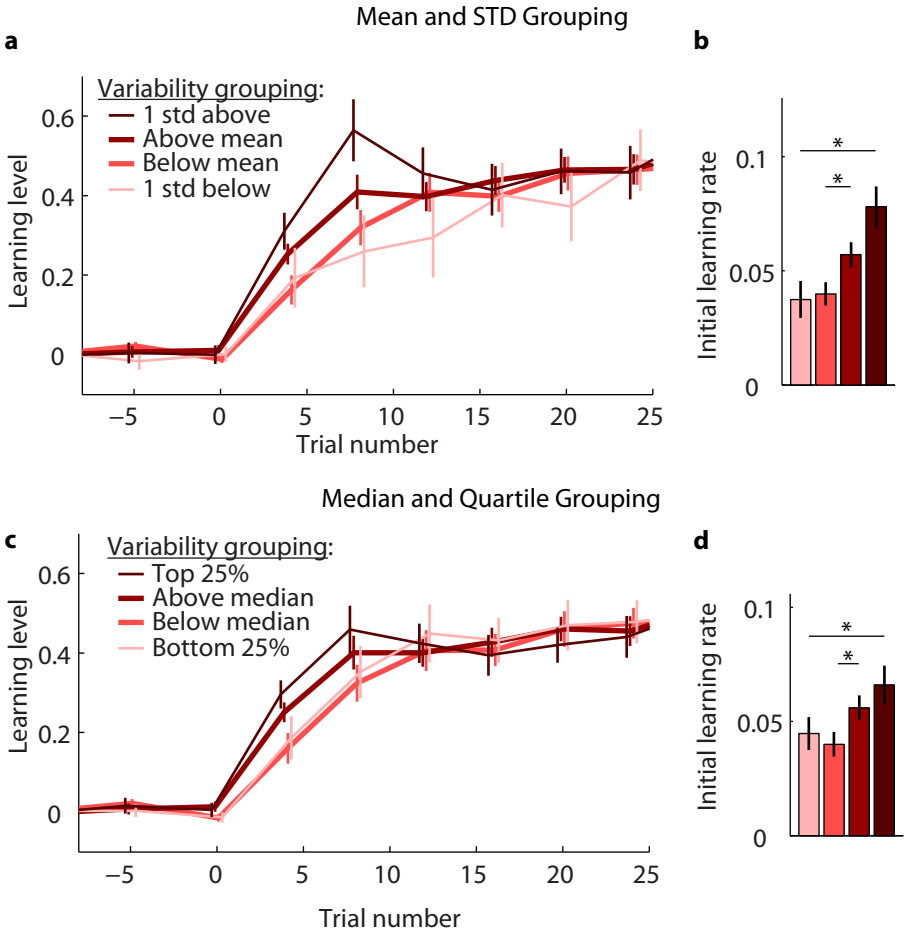

Figure 2.12: Variability grouping analysis of experimental results from Experiment 3. **a-b)** Participants displaying above-average amounts of velocity-dependent variability during the baseline period show faster initial learning. **c-d)** Stratifying subjects using percentiles in the baseline variability data show that groups with higher amounts of variability during the baseline period exhibited faster learning.

deviation below mean (Figure 2.12b, p=0.0047). The mean task-relevant baseline variability was 3.2±1.1 N, there were 21 subjects with variability under mean (mean variability 2.4±0.6 N) and 19 subjects with variability above mean (mean variability 4.1±0.8 N). There were 5 subjects with variability less than 1 STD below mean (mean variability 1.6±0.4 N) and 6 subjects with variability more than 1 STD above mean (mean variability 5.1±0.7 N). For comparison, we also stratified subjects based on the median and quartiles of the data to determine the robustness of the trend we observed (Figure 2.12c-d), and found a similar trend to the mean/STD stratified data

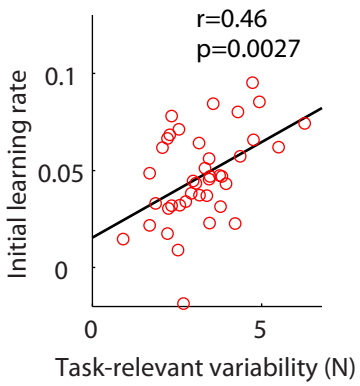

Figure 2.13: The amount of task-relevant variability during the baseline period predicts individual differences in learning rate in Experiment 2

(40% faster learning in upper half vs lower half p=0.020, 68% faster learning in upper quartile vs lower quartile p=0.014).

Interestingly, the relationship between baseline variability and learning rate only persists for 10-15 trials, after which the learning curves converge (Figure 2.12a,c). This early-only relationship may suggest that action exploration contributes to early learning during an error-based learning task, but that this exploration-driven learning becomes overshadowed by error-based learning later on. Another hypothesis is that the task-relevant variability may continue to predict learning rate, but that task-relevant variability changes over the course of learning so that a relationship between learning rate and current variability is maintained although the relationship between learning and baseline variability disappears.

When we examined the individual differences in initial learning rate and variability, we found a significant positive correlation between the amount of velocity-dependent baseline variability and initial learning rate (r=0.46, p=0.0027) as shown in Figure 2.13. Combining these results with those found in Experiments 1 and 2 indicates that individuals with higher levels of task-relevant variability learn faster in both error-based and reward-based motor learning tasks.

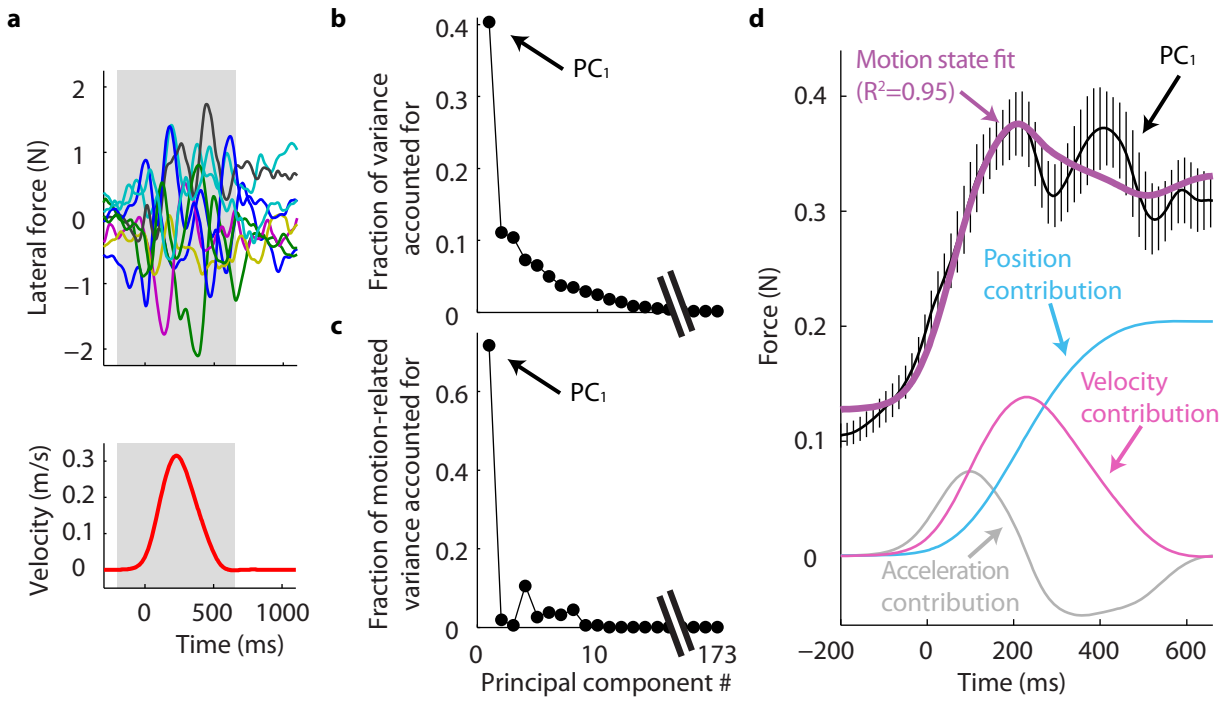

Figure 2.14: The structure of motor output variability. **a)** Example lateral force profiles from one participant aligned to the corresponding movement's peak speed point. The mean velocity profile is plotted below as a timeline reference. **b-d)** Principal components (PC) analysis of the structure of the baseline lateral force variability. **b-c)** Fraction of total and motion-related variance accounted for by each PC. Note that PC_1 accounts for over 40% of the total variance and over 70% of the motion-related variance. **d)** The shape of PC_1 is highly dependent on motion state (R^2=0.95) and closely corresponds to a positive linear combination of the mean position and velocity traces.

This suggests that the relationship between motor variability and learning may reflect a general principle of motor learning, rather than one that is specific for particular types of tasks.

2.4.4 – The largest single component of motor variability exhibits motion state dependence

If indeed there is a general relationship between the structure of motor variability and learning ability, variability in force production during movements may explain why some types of force dynamics are learned more quickly than others[11,111]. However, little is known about movement-related force variability, as force production is usually studied under isometric

conditions[49,60,105]. We thus examined whether the temporal structure of baseline motor variability might explain the ability to learn different types of dynamics.

Although subjects were asked to repeat the same reaching movement, the baseline lateral force profiles showed considerable trial-to-trial variability (Figure 2.14a). We performed principal components analysis on the structure of this variability (described in Section 2.3.11), a data-driven method which identifies the temporal patterns that contribute most to the total variance. We found that the first principal component (PC_1), the force pattern which best characterizes the total motor variability, by itself accounted for 40±2% of the total variance – over three times as much as any other component (Figure 2.14b). Inspired by previous work showing that novel dynamics are learned as a function of motion state rather than time[22,23,39,108], we examined the extent to which each principal component explained motion-related variability (Figure 2.14c). PC_1 accounted for 72±2% of the variability associated with motion state – more than twice as much as all the other components combined. This suggests that PC_1 may account for a large fraction of learning-related variability. PC_1's shape was itself strongly motion-related, being well approximated (R^2=0.95) by a linear combination of the position, velocity, and acceleration of the hand (Figure 2.14d). Interestingly, the position and velocity contributions which account for the majority of PC_1's shape (R^2=0.85) are in positive combination, closely resembling the pattern of visco-elastic dynamics which have been found to be learned the fastest[111].

The fraction of overall variance (Figure 2.14b) directly corresponded to the eigenvalues determined in the eigenvector decomposition of the covariance matrix. In particular, this fraction corresponds to the ratio of the eigenvalue for a particular principal component to the sum of the eigenvalues for all principal components. Correspondingly, the fraction of motion-

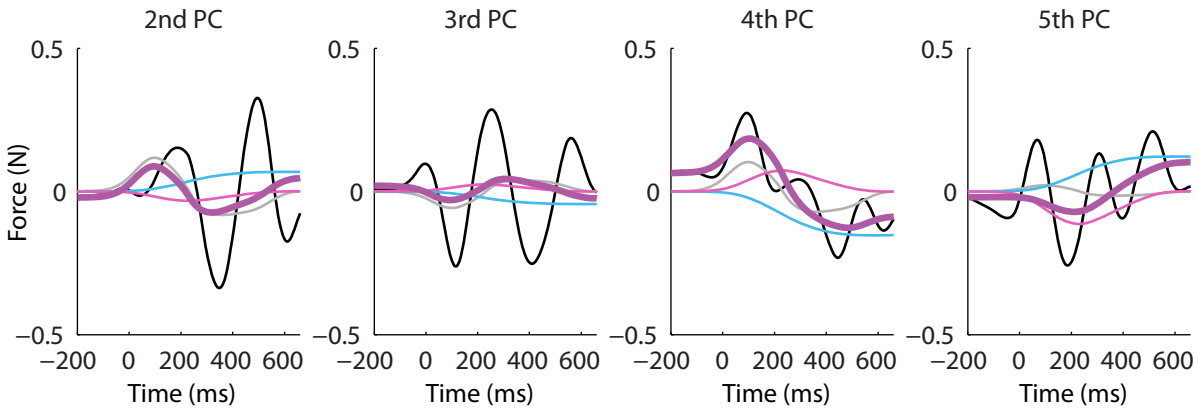

Figure 2.15: The shapes of PC_2-PC_5. Colors correspond to those used in Figure 2.14d.

related variance (Figure 2.14c) can be computed based on a scaling of each eigenvalue, where the scale factor is the fraction of the corresponding eigenvector's variance accounted for by motion state (for example, 0.95 for PC_1 shown in Figure 2.14d). Note that we operationally define motion related variance (Figure 2.14c) as variance that can be explained by a linear combination of position, velocity, and acceleration.

Of the 173 principal components, the first five components accounted for over 75% of the total variance and over 85% of the motion-related variance. Figure 2.15 presents the shapes of the next four principal components. Note that the shape of PC_1 (Figure 2.14d) is almost entirely motion related (R^2=0.95), while PC_2, PC_3, and PC_5 have shapes which are barely motion related. Interestingly, PC_4 has a shape which is almost as strongly motion related as PC_1 (R^2_{PC4}=0.77 vs R^2_{PC1}=0.95), but the position and velocity contributions are in negative combination, and it accounts for far less total variance than PC_1. Note that the eigenvector associated with each principal component is scaled by the square root of its eigenvalue for display in Figure 2.15 in order to take into account the amount of variability explained by it. This same scaling is applied to each principal component displayed in this chapter.

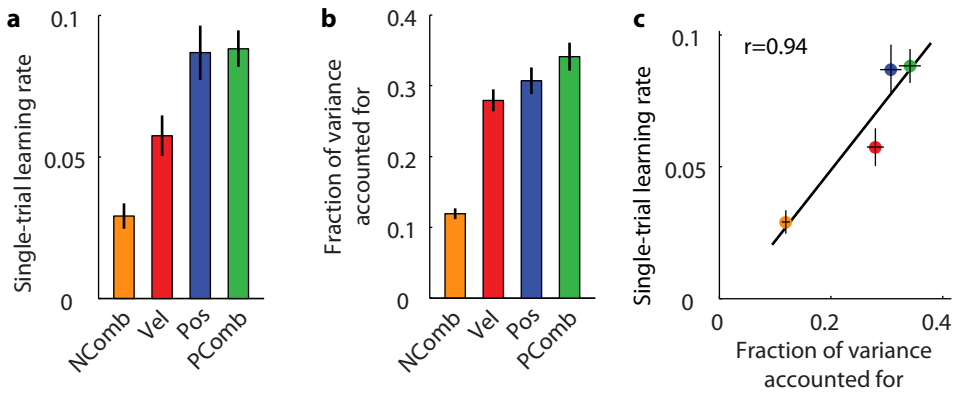

Figure 2.16: The amount of task-relevant variability correlates strongly with the single-trial learning rate for different force-field environments **a)** Single-trial learning rates for four different force-field environments **b)** Fraction of variance accounted for by each type of force-field environment **c)** Larger amounts of task-relevant variability during the baseline period predicts faster learning of a force-field environment

2.4.5 – Task-relevant variability predicts the initial learning rate of different error-dependent tasks

The resemblance between the temporal pattern that accounts for the greatest fraction of the baseline variability (PC_1) and the most rapidly learn dynamic force-field environment[111], suggests a link between motor output variability and motor learning ability across different force-field environments, analogous to what we found for different reward-based learning tasks (Figure 2.11). To explore the nature of this connection, we examined the relationship between baseline motor variability and learning rates for four different dynamics, each with a different combination of position and velocity contributions (diagrammed in Figure 2.5e). Projecting the overall baseline variability onto the force patterns associated with each of the perturbations revealed that the negative combination dynamics, which is the most difficult to learn (Figure 2.16a), accounted for the smallest portion (12±1%) of the baseline variability (Figure 2.16b). In contrast, the positive combination dynamics, which is the easiest to learn, accounted for the largest portion (34±2%). Across all four force-fields, we find that the amount of task-relevant

variability during baseline accurately predicts single-trial learning rates (Figure 2.16c, r=0.94), similar to what we observed across the reward-based learning tasks (Figure 2.11). These results show that task-relevant variability can predict motor learning ability both across individuals and across tasks in both reward-based and error-based learning.

2.4.6 – The structure of motor output variability can be reshaped to promote faster learning

Having established a relationship between variability and learning ability, we wondered if the motor system could capitalize on this relationship to improve learning by modulating variability. Recent work in songbirds suggests that the circuits generating motor variability can promote learning by directing exploration towards more rewarding regions of motor output space[3,139]. But can the motor system do more to promote efficient exploration than adaptively re-centering the motor output[3,114,130,139]? We considered the possibility that the structure of motor variability could be reshaped around its mean, allowing for more efficient exploration to improve learning. Such an adaptive reshaping would specifically increase variability along the task-relevant dimension of motor output space.

To explore this hypothesis, we measured motor variability before and after a training paradigm designed to increase motor learning ability. Increases in learning rates for position-dependent or velocity-dependent force-fields were induced in two different groups by repeatedly exposing subjects to the force-fields in short blocks of seven trials, interleaved with longer blocks of null trials (Figure 2.8). This created environments that were highly consistent from one trial to the next[42]. We first examined how these high-consistency environments (HCEs) affected learning ability and then determined whether they reshaped motor variability.

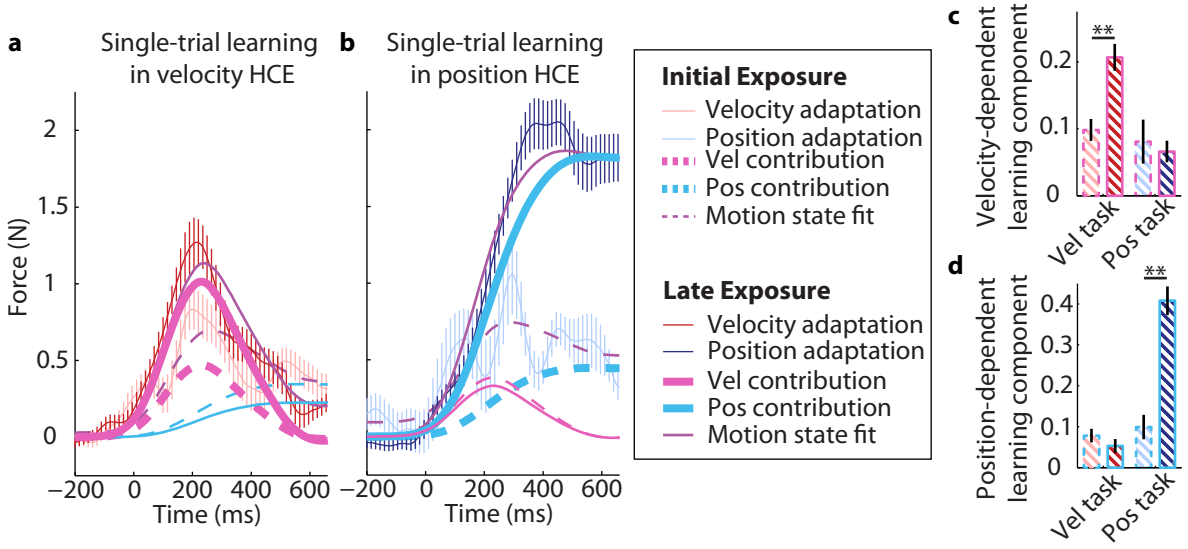

Figure 2.17: Change in single-trial learning. **a-b)** Specific increases in single-trial force adaptation result following exposure to the corresponding high consistency environment (HCE), indicating specific upregulation of learning. **c-d)** The velocity (Vel) component of learning increases only with exposure to the Vel HCE while the position (Pos) component of learning increases only with exposure to the Pos HCE.

We found that prolonged exposure to these environments resulted in single-trial learning that was not only larger in amplitude, but also more specific to the given environmental perturbation as compared to early exposures to the force-field, in which learning was small in amplitude and largely non-specific in shape[42,111]. This was true for both velocity- and position-dependent force-field groups (Figure 2.17a-b, note the dark red and blue traces based on late exposures (blocks 40-48) in the velocity- and position-dependent HCEs respectively compared to the lighter traces based on initial exposure (block 1)). To quantify these effects, we used linear regression to determine the components of the single-trial adaptive responses associated with hand velocity and position. We found a more than twofold increase in the velocity-dependent component of learning ($p=0.00051$) and a more than fourfold increase in the position-dependent component ($p<0.0001$) following exposure to the corresponding HCEs with no significant

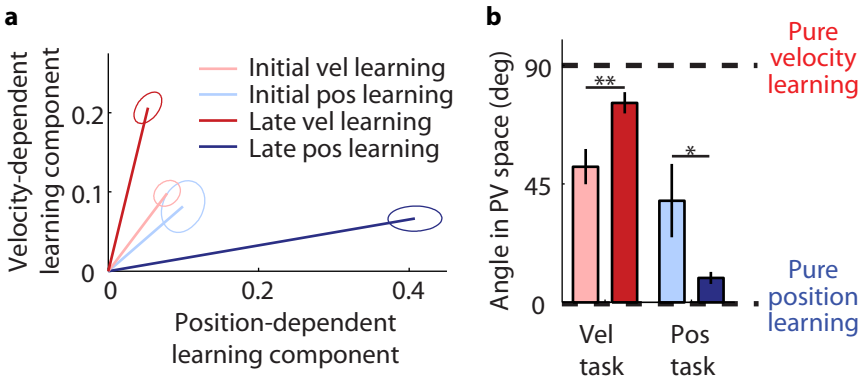

Figure 2.18: Specificity of the changes in single-trial learning. **a)** Plotting adaptation in a position-velocity (PV) gain-space reveals similar initial learning, but late exposure single-trial learning becomes specific to the trained HCE force-field. **b)** The angle of single-trial learning reveals significantly increased specificity following HCE training.

changes in the untrained components (Figure 2.17c-d, p=0.35 and p=0.21 and for position and velocity respectively).

We quantified the specificity of single-trial learning in this data set using a position-velocity (PV) gain-space analysis (Figure 2.18). The velocity-dependent learning component is shown on the vertical axis while the position-dependent learning component is shown on the horizontal axis. In this gain-space, positive-combinations of position and velocity dependence appear in the first quadrant while negative combinations would appear in the second or fourth quadrants. Non-specific learning for either a position- or velocity- dependent environment would correspond to equal sized position and velocity components of the learning resulting in a 45° angle in the PV gain-space. In contrast, specific learning for a velocity-dependent force-field would correspond to a 90° angle in PV gain-space whereas specific learning for a position-dependent force-field would correspond to a 0° angle (Figure 2.18b). Note that initial (first-cycle) learning displays PV gain-space angles near 45° for both velocity- and position- dependent force-fields, indicating highly non-specific pre-exposure learning as shown in Figure 2.18. In

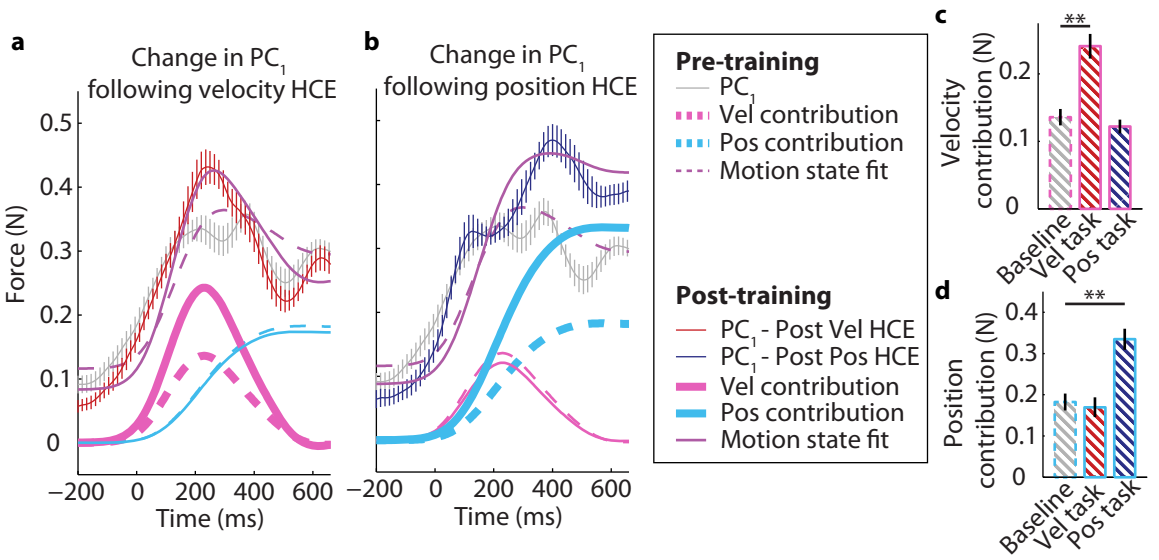

Figure 2.19: Change in PC_1. **a-b)** Specific increases in the velocity- and position-dependent components of PC_1 result following exposure to the HCEs indicating specific reshaping of variability. **c-d)** The velocity component of PC_1 increases only with exposure to the velocity HCE while the position component of PC_1 increases only with exposure to the position HCE.

contrast, post-exposure single-trial learning (last 9 cycles) has PV gain-space angles much closer to 90° for velocity- and 0° for position-dependent HCEs indicating that these environments induced increased specificity in single-trial learning. Thus, the adaptive response to the velocity-dependent HCE displays increased velocity-specificity ($p<0.0001$) whereas the position response shows increased position-specificity (Figure 2.18, $p=0.016$).

We next examined whether these experience-dependent changes in learning ability were paralleled by changes in the temporal structure of motor variability. To quantify changes in the amplitude and structure of movement-related force variability, we scaled the unit vector characterizing the main axis of variability (i.e. the direction of PC_1) by the amount of variability it explained (Figs 2.19a-b). Figure 2.19a presents a comparison of the scaled first principal component of motor output variability before and after exposure to the velocity-dependent HCE, and Figure 2.19b presents the analogous data for the position-dependent HCE. The shape of PC_1

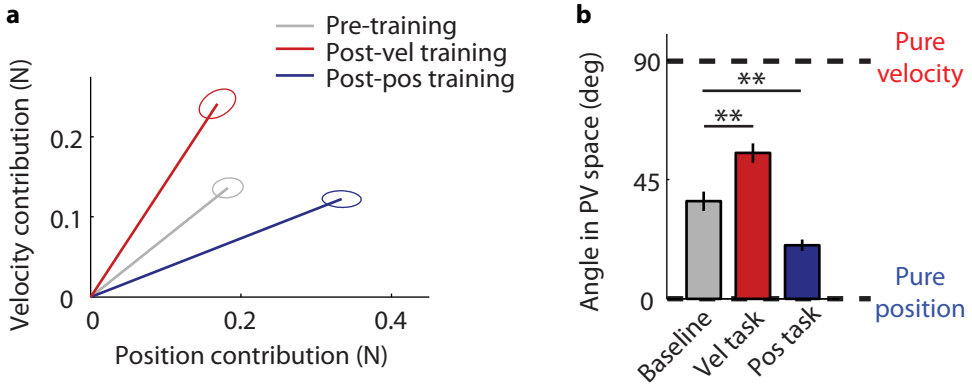

Figure 2.20: Specificity of the changes in PC_1. **a)** Plotting PC_1 in a PV gain-space reveals that exposure to HCEs reshape motor variability so that PC_1 becomes aligned to the trained HCE force-field. **b)** The angle of PC_1 in the PV gain-space reveals significantly increased specificity following HCE training

was, both before and after exposure to the HCEs, well characterized by a linear combination of position, velocity, and acceleration (similar to what we saw for an independent data set in Figure 2.14d: $R^2_{Fig2.14d}$=0.95, R^2_{pre} = 0.94, $R^2_{post\text{-}vel}$=0.96, $R^2_{post\text{-}pos}$= 0.94).

We thus focused on changes in the sizes of the position and velocity contributions to PC_1 as shown in Figure 2.19c-d, which were computed using linear regression. Training in the velocity-dependent HCE induced a 78±21% increase in the velocity-dependent component of PC_1 ($p<0.0001$) without affecting the position-component ($p=0.34$). In contrast, exposure to position-dependent HCE led to an 82±26% increase in the amplitude of the position-dependent component of PC_1 ($p<0.0001$) without affecting the velocity-component ($p=0.19$). Similar to the changes in single-trial force-field adaptation, we can examine the changes in PC_1 using a PV gain-space analysis (Figure 2.20). The PV gain-space projections of these principal components show that, similar to the motor adaptation, motor output variability changes in an environment-specific fashion (Figure 2.20a), with both velocity- and position-dependent HCEs leading to increased task-specific motor variability (Figure 2.20b, $p<0.0001$ in both cases). We also

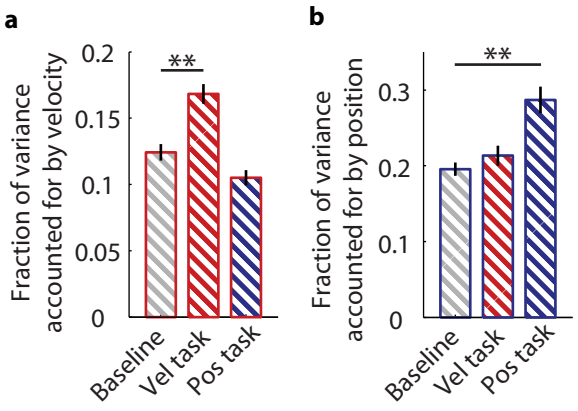

Figure 2.21: Specific increases in overall position- and velocity-dependent variability following HCE training **a)** Velocity-dependent variability specifically increases following exposure to a velocity-dependent HCE. **b)** Position-dependent variability specifically increases following exposure to a position-dependent HCE.

performed an alternative analysis which examined the overall changes in position- and velocity-related variability by regressing each force profile collected during the baseline period onto temporal traces of position and velocity. Taking the variance of these regression coefficients and dividing by the total variance of the force profiles reveals analogous environment-specific reshaping of the structure of motor variability (Figure 2.21).

2.4.7 – Retention of changes in motor output variability on the subsequent day

For environments presented on day one, the baseline period on the second day provided an opportunity to examine the overnight retention of the changes in motor output variability induced by exposure to an HCE on the first day. Thus we used these measurements to examine the retention of the changes in motor variability for the 12 subjects who experienced velocity training and the 12 subjects who experienced position training on day one. This resulted in a data set that was half the size of the ones presented above (Figures 2.19-2.20). Despite the increased noise inherent in computing principal components based on smaller data sets, we found that the PC_1 consistently displayed strong motion dependence, with a position, velocity, and

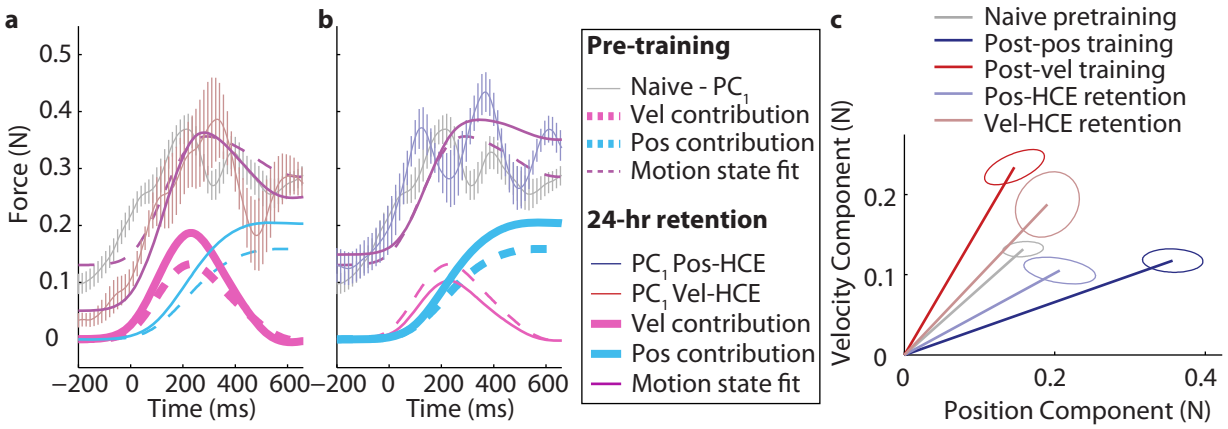

Figure 2.22: Retention of the specific reshaping of variability induced by HCE training **a)** Velocity-specific reshaping of PC_1 following velocity-dependent HCE training is retained after 24 hours. **b)** Position-specific reshaping of PC_1 following position-dependent HCE training is retained after 24 hours. **c)** The PC1s 24 hours after velocity-dependent or position-dependent HCE exposure are significantly different from each other (p=0.047).

acceleration fit producing an average R^2 value of 0.77 compared to 0.92 for PC_1 calculated from all pre-training data. Furthermore, in 90% of cases, with 12 subjects per group, and each group measured in 2 conditions, the R^2 values were above 0.54. A small group of outliers which were reducing the overall R^2 values were found. These outliers had R^2 values less than 0.35 and included just 2.5% of the cases. Thus when we determined the gain space angles by comparing the relative sizes of the position and velocity coefficients in the motion state fit, we eliminated these 2.5% of cases in which PC_1 was not well described by motion states. This should not produce a bias in the estimates of the PV gain-space angles because elimination was based on the degree to which the gain-space vector characterized the shape of PC_1 rather than the location of this vector. The resulting PC_1's and the position and velocity contributions are shown in Figure 2.22. To assess whether the specific reshaping of variability was retained on the subsequent day, we compared the change in PV angle for the position-dependent HCE retention to that for the velocity-dependent HCE retention. Interestingly, over half of the specificity increases induced during the 90-minute training sessions in the HCEs persist to the following day (Figure 2.22c,

faded red and blue traces, p=0.047). These findings indicate that the motor system can effectively reshape the temporal structure of motor output variability in a way that can persist from one day to the next.

2.5 – Discussion

In summary, we demonstrate an intriguing link between task-relevant motor variability and motor learning ability. In line with predictions from reinforcement learning theory, we show that higher levels of task-relevant variability predict faster learning rates both across individuals within a task and across different tasks. We further show that the structure of motor output variability can be reshaped to promote faster learning. Previous studies have identified genetic[37], structural[27,129], or neural activity markers[12,100,122] which correlate with learning rate, however our findings are the first demonstration of the ability to predict task-specific differences in learning ability from baseline performance characteristics. Moreover, our findings provide a mechanistic explanation for why an individual may be better than average at learning some tasks, but worse than average on others.

Our results support the view that motor variability, rather than being an unwanted consequence of noisy nervous system function, is an essential feature of reinforcement learning[62,67,86,120,132] that is centrally-driven[19,20,86,117] and actively regulated[66-68,80] by the nervous system. This view emerged from work in songbirds where motor variability and learning ability are coupled[67,86,132], and is further supported by experimental evidence in both songbirds[66,68,71,144] and primates[80,121] showing that motor variability is actively reduced when motor precision is crucial, such as when a reward is at stake[67,71,121,144], and that motor variability is increased during

learning[66-68,80,87]. The current findings extend these observations by demonstrating that: (1) in humans, learning ability is linked to motor variability, (2) variability can predict individual differences in learning ability, and (3) the motor system does not merely modulate the overall amount of motor variability, but rather actively reshapes the structure of motor variability to direct exploration for more efficient learning. Elucidating the relationship between variability and learning not only enhances our basic understanding of learning in the motor system, but also provides a potential avenue for the rational design of novel training procedures for improving motor learning and rehabilitation.

Chapter 3 – The generalization of visuomotor adaptation to untrained movements and movement sequences

In the previous chapter we demonstrated that the motor system utilizes variability to direct the adaptation of visually guided reaching movements, and further that this variability can be reshaped to increase the rate of learning. However, we did not look into the specific mechanisms which underlie the adaptation of these movements. It is difficult to identify these neural mechanisms because of the redundancy and complexity in the neural representations of movement planning. Many of these representations, at least partially, reflect the internal remappings which could produce accurate movements in novel perturbing environments. Thus it is difficult to localize where these remappings actually occur. In this chapter, we seek to identify the fundamental mechanisms which underlie the adaptability of visually guided reaching movements by performing a series of behavioral experiments that examine the generalization of motor adaptation to several conditions.

When determining the mechanisms underlying visuomotor adaptation, behavioral experiments are encumbered because simply observing adaptation does not provide insight into how this adaptation is occurring. Thus in this chapter, we rely on generalization experiments, quantitatively observing both the adaptation of the reaching movement and the transfer of adaptation to untrained movements and movement sequences. Proposing a simple model for

motor planning based on two movement features, we design experimental paradigms in which motor adaptation would affect the motor plans associated with each feature in isolation. We then rigorously test the ability of this model to characterize more complex situations where adaptation simultaneously affects multiple factors of movement planning.

3.1 – Summary

The planning of visually guided movements is highly adaptable; however, the basic mechanisms underlying this adaptability are not well understood. Even the features of movement that drive adaptation are hotly debated. Some studies suggest that visuomotor adaptation occurs through the remapping of goal locations while others credit the remapping of the movement vectors which lead to the goal locations. However, several recent motor learning studies and the multiplicity of the neural coding underlying visually guided movements stand in contrast to this either/or debate on the modes of motor planning and adaptation. Based on a novel model for combining movement vector and goal location remapping, we examine the transfer of visuomotor adaptation to visually guided movements and movement sequences throughout the workspace and demonstrate, for the first time, the ability to predict how motor adaptation affects the planning of movement sequences. By dissociating the effects of remapping goal location and movement vector, we show that (1) motor adaptation differentially remaps these two features, and (2) these features contribute to motor planning with weightings that modulate the extent to which each remapping generalizes. We then show that, without any free parameters, a computational model based on the differential weighting and the remapping of these features predicts over 90% of the variance in novel movement sequences, even when

multiple movement attributes are simultaneously adapted. These findings indicate that the effects of motor adaptation on movements and movement sequences can be accurately predicted by accounting for the differential weighting and remapping of goal locations and movement vectors during motor planning.

3.2 – Introduction

Although every voluntary movement is shaped by motor learning, the mechanisms underlying this adaptability remain unclear. Applying a reductionist approach would entail identifying the features used for motor planning, then subsequently examining how those features adapt. Along these lines, a central theory in motor control posits that the key feature of motor planning is the movement vector. That is, the plans for point-to-point reaching movements are internally represented as movement vectors from start locations to movement goals, and the adaptive changes in motor planning are driven by remapping of movement vectors[17,40,44,74,99,109,115,116,123,137]. In line with this theory, neurophysiological and behavioral studies have shown that adaptive changes in motor planning can often be explained by the remapping of movement vectors[74,89,123,137,141]. The movement vector planning hypothesis is further supported by the generalization of sensorimotor learning to movements with similar movement vectors even when other attributes, such as start or goal locations, are altered[74,137].

However, several recent studies have shown that adaptation to visuomotor transformations is not limited to movement vector learning[25,56,79,101,110]. These studies have found a small but significant proprioceptive recalibration of hand position following adaptation to visuomotor transformations which directly affect movement planning because the motor

system weighs visual and proprioceptive sensory information to estimate the start location of movements[99,115,116]. Moreover, it would be surprising if visuomotor adaptation was based entirely on the remapping of a single feature, either movement vectors or goal locations, given what we know about the richness and diversity in the neural coding of movement representations. In particular, movement vectors, start locations, and goal locations are all represented in motor planning areas and any of these features could be remapped during motor adaptation[9,10,15,33,45,77,92]. In line with this idea, recent findings have suggested that location-based and movement-vector-based control may be distinct processes that are differentially remapped by motor adaptation[32,41,75,76,103,110]. However, the way in which these features are combined during motor planning is not yet well understood.

In this chapter, we hypothesize that, during motor adaptation, the target location and movement vector are differentially remapped, and that these features contribute to motor planning with weightings independent of the amount of remapping. If this were the case, motor adaptation would depend on three distinct factors: the amount of movement vector remapping, the amount of goal location remapping, and the differential weighting of movement-vector-based planning and goal-location-based planning. We begin by designing a series of experiments that dissociate the effects of motor adaptation on movement-vector-based and goal-location-based planning allowing us to quantify the contributions of these three factors for both individual movements and movement sequences. Then, we test the idea that these three factors can be used to characterize the planning of goal-directed movement sequences by building a combined remapped feature model which quantitatively predicts the effects of motor adaptation based on these factors. We find that this model predicts over 90% of the variance introduced by the effects of motor adaptation on novel movement sequences.

3.3 – Methods

3.3.1 – Subjects

Ninety-three naïve neurologically intact adults (53 female, 3 left-handed) between the ages of 18 to 59 participated in this study. Data from three subjects were not included because they could not perform the task consistently. One could not consistently move with the requested rapidity, one was unable to consistently perform movement sequences, and one subject failed to show consistent adaptation to the trained visuomotor rotations. All experimental procedures were approved by Harvard's Committee on the Use of Human Subjects, and all subjects provided informed written consent before the experiment began.

3.3.2 – Apparatus

The same apparatus was used in all three experiments in this study. Subjects sat at a desk facing a horizontal LCD monitor (BENQ V2400W, 1920 x 1200 pixels, 75 Hz refresh rate, Taipei, Taiwan). The height of the chair was adjusted at the start of each experiment so that the subject was in a comfortable position for viewing and reaching under the LCD monitor (Figure 3.1). Underneath the monitor, subjects grasped and moved a stylus-embedded foam handle on top of a digitizing tablet that recorded hand position (12 inches by 19 inches, 100 Hz refresh rate, WaCom Intuos3, WaCom Corporation, Saitama, Japan). The subject's midline was aligned with the center of the digitizing tablet which corresponded to the center of the workspace and the LCD monitor. Vision of the digitizing tablet and the subject's arm were obstructed by the LCD monitor for the duration of the experiment.

Figure 3.1: Illustration of the experimental setup

3.3.3 – General experimental protocol

This study included three different experiments in which subjects made arm reaching movements while grasping a foam handle with their dominant hand. During each experiment, the digitizing tablet recorded hand position, and a 0.25 cm diameter cursor represented this position on the monitor. A +30% visual magnification was applied to the cursor such that a 1.0 cm hand movement resulted in a 1.3 cm cursor movement; this magnification was present from the very first movement throughout the duration of the experiment, independent of applied visuomotor rotations and should not affect rotation learning or its transfer. Figure 3.2 illustrates the location of the six targets (T1-T6) and center circle (C), drawn to scale, and sample movements collected from subjects in the baseline period. The center circle and all six peripheral target circles were 1.2 cm in diameter in hand space. Subjects were instructed to perform two types of visually-guided movements: individual point-to-point movements 9.0 cm in length (Figure 3.2a-b) and movement sequences which consisted of two submovements, each 9.0 cm in length (Figure 3.2c). Individual point-to-point movements were either performed from the center circle to one of the six peripheral targets (Figure 3.2a), or between two adjacent peripheral targets (Figure 3.2b). On movement sequences, the first submovement began at the center circle

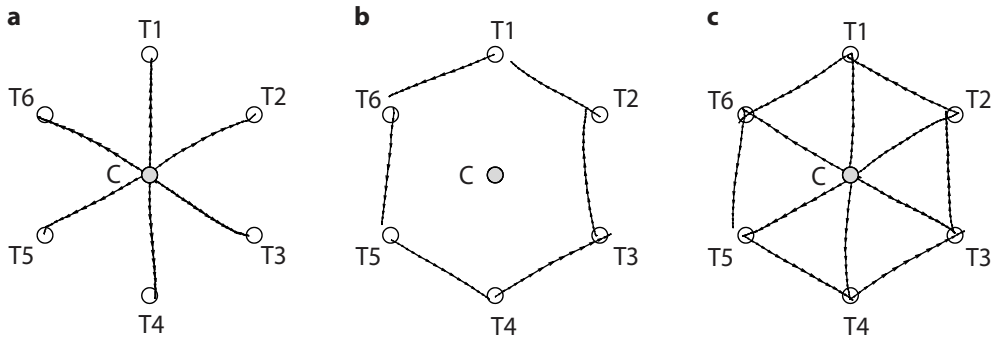

Figure 3.2: Illustration of target locations and sample movements from subjects collected during baseline. **a)** Point-to-point movements from the center circle to a peripheral target **b)** Point-to-point movements from one peripheral target to an adjacent target **c)** Movement sequences

and was directed at one of the six peripheral targets, and the second submovement started at the end of the first submovement and was directed towards one of the two adjacent peripheral targets (Figure 3.2c).

At the start of each trial, a target was displayed for 250 ms before the go cue. During this waiting interval, the center circle was colored yellow, and subjects were instructed to continue holding the cursor inside the center circle. After 250 ms, center circle was recolored to purple, cueing subjects to move to the displayed target. Auditory rewards were provided following individual movement trials based on two criteria, movement duration and movement endpoint. Movement duration was defined as the amount of time during which hand velocity exceeded 5.0 cm/s. The time of movement onset was determined as the time at which hand velocity first exceeded and remained above 5.0 cm/s for 100 ms, while the time of the movement endpoint was defined as the beginning of the period in which hand velocity had remained below 5.0 cm/s for 300 ms. Subjects received auditory reward following movements with 200-400 ms duration with locations of movement endpoints inside the presented target. Movement direction was

computed 100 ms after movement onset, and deviations were measured with respect to the line segment connecting the center circle to the center of the target.

Following each trial, the subject returned the cursor to the center circle. We assessed the feed-forward movement plan by removing visual feedback of the cursor on selected individual movement trials, which we refer to as probe or test trials, and on all movement sequence trials. Movements from the center circle to each of the peripheral targets were administered with visual feedback on ~50% of the trials during the baseline and testing periods. In contrast, individual movements between peripheral target locations and movement sequences used to probe the effects of adaptation were never administered with visual feedback. Visual feedback was restored prior to the start of the following trial when the cursor was within 2.0 cm of the center circle so that subjects could position their hands for the next trial.

All experiments followed the same general paradigm which consisted of 1950 trials spread over four experimental periods. First, subjects were administered a 300 trial familiarization period which consisted entirely of individual movements with visual feedback so that they could become accustomed to the task instructions and learn the required movement speed. Following the familiarization period, subjects performed a 300 trial baseline period during which movement sequences and no visual feedback trials were intermixed with continuous visual feedback trials to gauge the baseline performance of the feed-forward motor system, before the onset of visuomotor rotation learning.

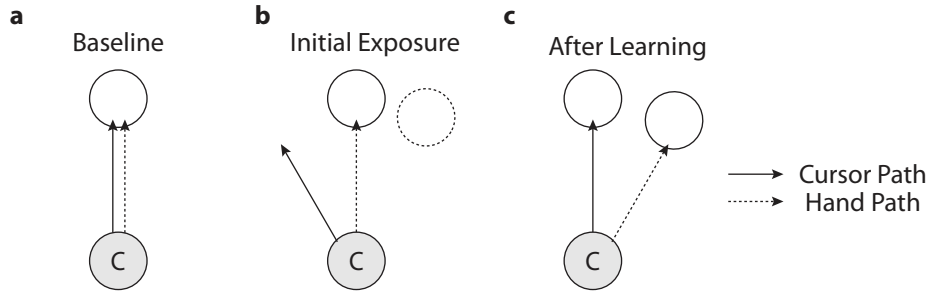

Figure 3.3: Illustration of adaptation to visuomotor rotation. **a)** During the baseline period, the cursor path matches the hand path. **b)** On initial exposure to a visuomotor rotation, the subject's hand movements continue as in baseline, but the cursor movements are rotated. **c)** The subject learns to rotate his hand movements so that the cursor moves straight to the target

The training period, which followed the baseline period, consisted of 450 continuous visual feedback trials during which subjects were exposed to one of several possible patterns of visuomotor rotations[25,41,56,73,74,82,103,137]. The visuomotor rotations that we used in this study were either +30° (counter-clockwise), -30° (clockwise), or 0° (no rotation). On initial exposure to a (non-zero) visuomotor rotation, subjects make a hand movement directly to the target, resulting in a cursor movement that is rotated off course around the center circle by ±30° (Figure 3.3b). However, with practice, subjects reduce the errors in the cursor movements by performing hand movements that are rotated in the opposite direction of the applied visual rotation (Figure 3.3c). In Experiments 1-2, non-zero rotations were trained to two of the six peripheral target locations, and in Experiment 3, non-zero rotations were trained in four of the six peripheral target locations.

The testing period, which followed the training period, consisted of 900 trials of which about half were no visual feedback movement sequence, probe, or test trials used to assess the transfer of motor adaptation. The remaining trials were pseudorandomly intermixed continuous visual feedback trials used to reinforce the visual rotations that were trained for each target location. In each experiment, the same visuomotor rotation pattern was applied during the training and testing periods, the specifics of these patterns will be described later. Each

experiment was performed in 150 trial blocks with rest breaks of 1-5 minutes between blocks. Thus there was always a rest break at the end of each period and a single rest break was provided in the first two periods, whereas two breaks were provided in the training period, and five in the testing period.

3.3.4 – Design of Experiments 1 and 2: Attribute isolating experiments

We designed Experiments 1 and 2 to characterize the effects of adapting three different movement attributes: start location (SL), movement vector (MV), and goal location (GL) on the planning of individual movements (Experiment 1, n=15 subjects) and movement sequences (Experiment 2, n=35). Typically, learning simultaneously affects multiple movement attributes, and it is difficult to dissociate the effects of adapting each attribute. To address this issue, we designed these two experiments to utilize test movements (Experiment 1) and test sequences (Experiment 2) in which the adaptation of these movement attributes could be examined independently of one another, so that motor adaptation would affect one attribute of a test movement or test sequence, but not the other two.

Although both Experiments 1 and 2 examined the effects of adapting three movement attributes (SL, MV, and GL), Experiment 1 utilized test movements to examine these effects in individual movements, whereas Experiment 2 utilized test sequences to examine these effects in movement sequences. In Experiment 1, test movements proceeded as follows: subjects first moved from the center circle (C) to a displayed target with continuous visual feedback, but as the cursor approached this target, a second target appeared, adjacent to the first. Subjects completed the initial movement and held the cursor within the first target for an additional 300 ms. After this period, subjects moved towards the second target, while visual feedback of the cursor was removed at movement onset. In contrast, in Experiment 2, subjects made a movement sequence

by performing two submovements in rapid succession, without any additional delay. Visual feedback was withheld at the onset of the first submovement for the duration of the entire movement sequence, and was only restored when subjects returned to C for the start of the next trial.

Since Experiments 1 and 2 were both designed to examine the effects of adapting each movement attribute independently, and only differed in the types of test trials being used (individual movements vs movement sequences), we used the same rotation pattern for both experiments. Specifically, we applied a +30° (counter-clockwise) rotation on movements from C to the peripheral targets T2 and T5, while movements from C to the other four targets (T1, T3, T4, and T6) were trained with zero rotation. We designed our test movements and test sequences so that this rotation pattern would adapt one movement attribute at a time.

3.3.5 – Measuring the effects of movement vector, goal location, and start location adaptation

The amount of adaptation associated with each movement attribute (SL, MV, and GL) of a test movement or test sequence was assessed by examining the differences between baseline and adapted attribute-matched probe movements. The MV-matched movement (MVM) has a movement vector that matches the test movement in Experiment 1, or the second submovement of the test sequence in Experiment 2. The vector differences in the endpoints of the baseline and adapted MVM define the MV-adaptation vector ($\Delta\overrightarrow{MV}$). Similarly, the GL-matched movement (GLM) has an endpoint that matches the goal location and the SL-matched movement (SLM) has an endpoint that matches the start location of the test movement or test sequence. Correspondingly, vector differences in the endpoints of the baseline and adapted GLM and SLM define the GL-adaptation vector ($\Delta\overrightarrow{GL}$) and SL-adaptation vector ($\Delta\overrightarrow{SL}$), respectively.

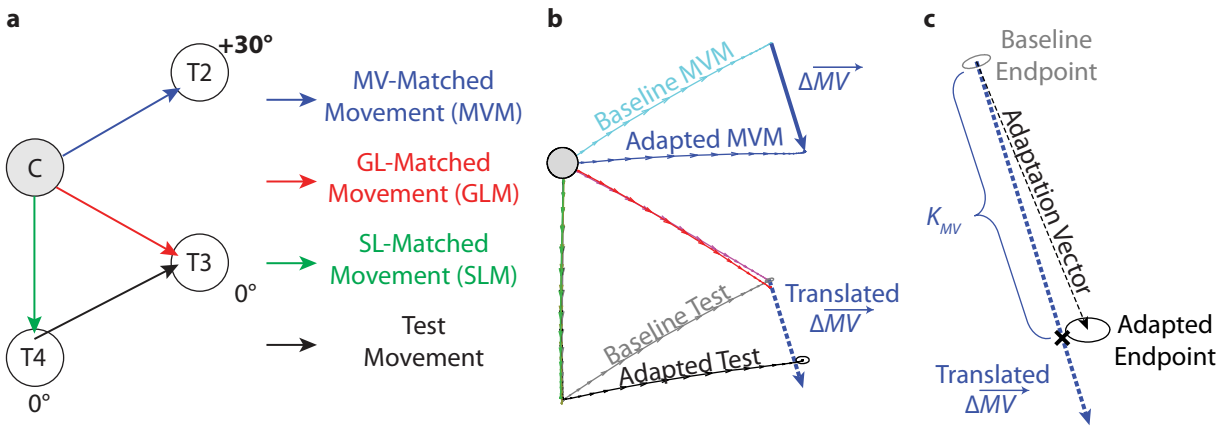

Figure 3.4: Example of a test movement with isolated movement vector adaptation. **a)** We isolate the effects of MV adaptation using the test movement (T4 to T3) because the MV-matched movement (C to T2) was trained with rotation, while the GL-matched (C to T3) and SL-matched (C to T4) movements were trained with zero rotation. **b)** The difference in endpoints of the baseline and adapted attribute-matched movements define the attribute adaptation vectors. However, since only the MV-matched movement was trained with rotation, both $\Delta\overrightarrow{GL}$ and $\Delta\overrightarrow{SL}$ are near zero while $\Delta\overrightarrow{MV}$ is non-zero and defined by the difference in endpoints of the baseline and adapted MV-matched movement. Translating $\Delta\overrightarrow{MV}$ to the baseline test movement endpoint generates a prediction for a test movement exhibiting full transfer of the effects of MV adaptation. **c)** The Adaptation Vector is defined as the difference in endpoints between the baseline and adapted test movements. $\Delta\overrightarrow{MV}$'s gain coefficient ($K_{MV}$) can be computed as the dot product of the adaptation vector and $\Delta\overrightarrow{MV}$.

The effect of MV adaptation was assessed by examining test movements and test sequences with MVs that were adapted during the training period, while the SL and GL of the test movement were unadapted ($\Delta\overrightarrow{SL} = 0$ *and* $\Delta\overrightarrow{GL} = 0$). Since movements from C to T2 and C to T5 were rotated during the training period, the 30° and -150° MVs were adapted. The movements from T3 to T4 and T1 to T6 shared a MV with the adapted C to T5 movement, while the movements from T4 to T3 and T6 to T1 shared a MV with the adapted C to T2 movement, thus these movements (T3 to T4, T1 to T6, T4 to T3, and T6 to T1) served as test movements for evaluating the effect of MV adaptation. Figure 3.4 shows an example test movement that measures the effect of MV adaptation. In Figure 3.4a, we examine the test movement from T4 to

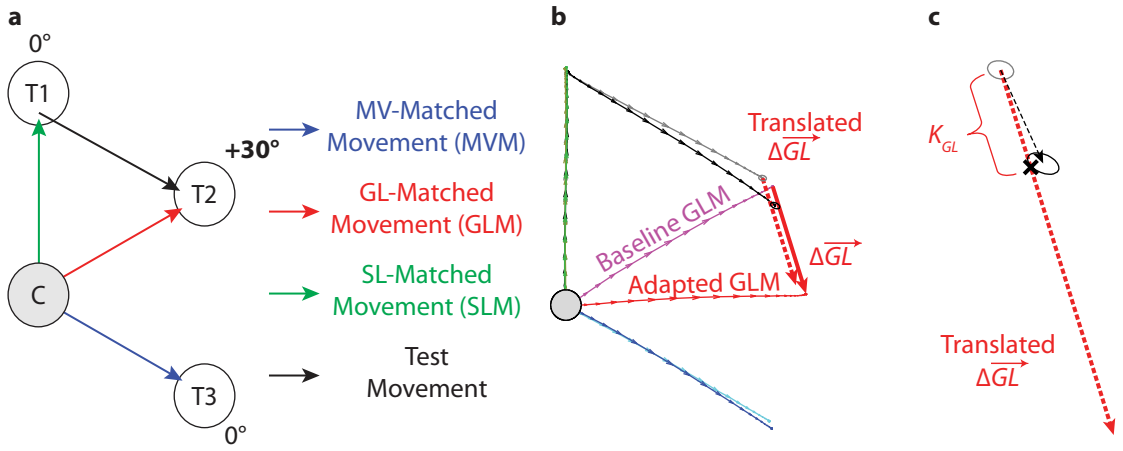

Figure 3.5: Similar to 3.4 but for a test movement (T1 to T2) with isolated goal location adaptation. **a)** GL-matched movement (C to T2) was trained with rotation, while the MV-matched (C to T3) and SL-matched (C to T1) movements were trained with zero rotation. **b)** Both $\Delta\overrightarrow{MV}$ and $\Delta\overrightarrow{SL}$ are near zero, but not $\Delta\overrightarrow{GL}$. **c)** $\Delta\overrightarrow{GL}$'s gain coefficient ($K_{GL}$) can be computed as the dot product of the adaptation vector and $\Delta\overrightarrow{GL}$.

T3 (black arrow), with an MVM (blue arrow) of C to T2, GLM (red arrow) of C to T3, and SLM (green arrow) of C to T4. Note that in Figure 3.4b, the adapted MVM (blue trace) is rotated relative to the baseline MVM (cyan trace), while the baseline and adapted GLM (magenta/red traces) lie on top of each other as do the baseline and adapted SLM (yellow/green traces), hence $\Delta\overrightarrow{MV} \neq 0, while\, \Delta\overrightarrow{SL} = 0\ and\ \Delta\overrightarrow{GL} = 0$. The difference between the endpoints of the adapted and baseline MVMs define $\Delta\overrightarrow{MV}$, and is represented as the solid blue arrow in Figure 3.4b.

If the movement vector adaptation of the MVM fully transfers to the test trial, we would expect the adapted test endpoint to be shifted by $\Delta\overrightarrow{MV}$ relative to the baseline endpoint (dashed blue arrow). Since only the MV was adapted, changes in the test trial must be due to the adaptation of MV ($\Delta\overrightarrow{MV}$), and the effects of movement vector adaptation can be evaluated in isolation. In other words, movement vector adaptation of the test trial induced changes in its endpoint (black ellipse and black dashed test adaptation vector arrow Figure 3.4c), and the coefficient, K_{MV}, represents the gain on $\Delta\overrightarrow{MV}$ that best approximates this change. We computed

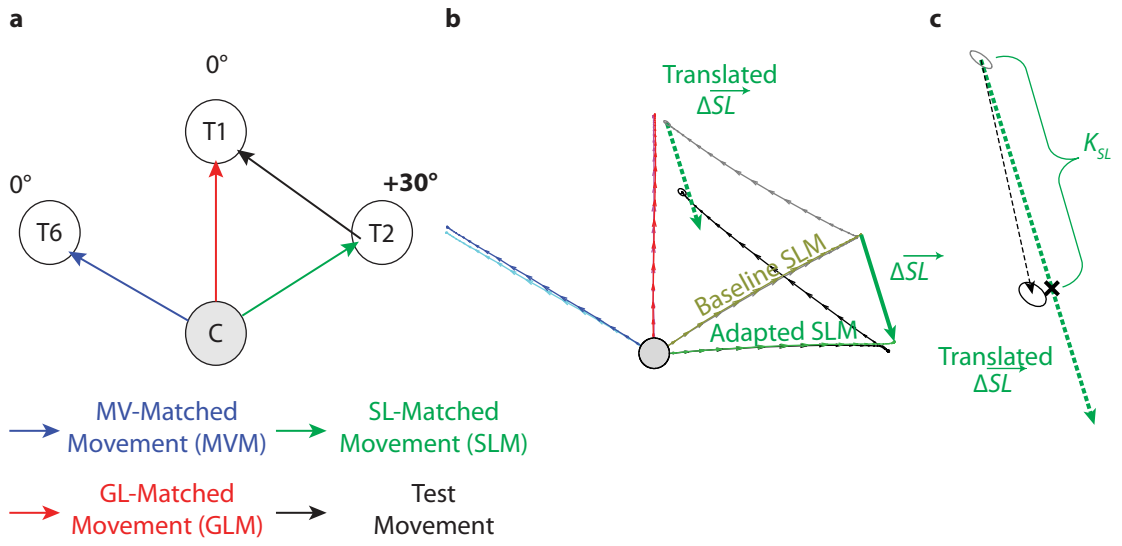

Figure 3.6: Similar to 3.4 but for a test movement (T2 to T1) with isolated start location adaptation. **a)** SL-matched movement (C to T2) was trained with rotation, while the MV-matched (C to T6) and GL-matched (C to T1) movements were trained with zero rotation. **b)** Both $\Delta\overrightarrow{MV}$ and $\Delta\overrightarrow{GL}$ are near zero, but not $\Delta\overrightarrow{SL}$. **c)** $\Delta\overrightarrow{SL}$'s gain coefficient ($K_{SL}$) can be computed as the dot product of the adaptation vector and $\Delta\overrightarrow{SL}$.

K_{MV} by finding the magnitude of the scalar projection of the test adaptation vector onto $\Delta\overrightarrow{MV}$ (black cross). The same analysis was conducted for each of the four test trials with an adapted movement vector. Corresponding analyses were conducted to determine the effects of GL-adaptation (Figure 3.5) and SL-adaptation (Figure 3.6). In the GL-adaptation cases $\Delta\overrightarrow{GL} \neq 0, while\, \Delta\overrightarrow{MV} = 0\ and\ \Delta\overrightarrow{SL} = 0$, thus changes in the test trials must be attributed to $\Delta\overrightarrow{GL}$. Whereas changes in the test trials must be attributed to $\Delta\overrightarrow{SL}$ in the SL-adaptation cases because $\Delta\overrightarrow{SL} \neq 0, while\, \Delta\overrightarrow{MV} = 0\ and\ \Delta\overrightarrow{GL} = 0$. We also computed the gains (K_{GL} and K_{SL}) on $\Delta\overrightarrow{GL}$ and $\Delta\overrightarrow{SL}$ that best approximate the difference in baseline and adapted test endpoints in each of the GL-isolating and SL-isolating test trials.

3.3.6 – Experiment 3: Movement sequences following the adaptation of multiple attributes

Experiment 3 (n=40) investigated how movement sequences were affected by simultaneous adaptation of MV, GL, and SL in contrast to Experiments 1-2 which examined the effects of adapting only one of these attributes at a time. This experiment allowed us to compare the effectiveness of pure MV-based, pure GL-based, and combined MV-GL-based models. In Experiment 3a (n=20), we examined the effects of adapting two movement attributes on movement sequences, either SL and GL or SL and MV. Movements from C to the peripheral targets T2, T3, T5, and T6 were trained with the same rotation (11 subjects trained +30° rotations while 9 subjects trained -30° rotations) while movements from C to T1 and T4 were trained with zero rotation. On movement sequences during the testing period, subjects made a first submovement to one of the targets trained with rotation (T2, T3, T5, T6) followed by a second submovement to an adjacent target. SL adaptation affected each movement sequence because the first target in each sequence was always trained with rotation. In addition to the SLs, GLs were adapted on half of the sequences (submovements made from T2 to T3, T5 to T6, T3 to T2, and T6 to T5), while MVs were adapted on the other half (submovements made from T2 or T6 to T1 or from T3 or T5 to T4).

Experiment 3b (n=20) investigated the effects of simultaneously adapting all three movement attributes. The training paradigm was similar to Experiment 3a, however there was no training given on movements from C to T1 and from C to T4 because visual feedback of the cursor was withheld on all movements made to T1 and T4. Again, 11 subjects trained +30° rotations to T2, T3, T5, and T6 while 9 subjects trained -30° rotations to those targets. We expected partial adaptation of the C to T1 and C to T4 MVs and target locations due to the generalization from training rotations on movements to the other four targets, similar to the results observed in a previous study[74]. Experiment 3b had the same movement sequences as

Experiment 3a, but all three attributes were adapted on each sequence. Since the first target (T2, T3, T5, or T6) had been trained with rotation, full SL adaptation affected each movement sequence. When the location of the second target was also adapted (submovements from T2 to T3, T5 to T6, T3 to T2, and T6 to T5), the GL of the test sequence was fully adapted while the MV was only partially adapted. However, when the second target was T1 or T4, the GL was only partially adapted, while the MV of the submovement was fully adapted.

3.3.7 – Data analysis

The adaptation vectors associated with each movement attribute ($\Delta\overrightarrow{MV}$, $\Delta\overrightarrow{GL}$, and $\Delta\overrightarrow{SL}$) were determined by examining the adaptive changes of attribute-matched movements (see examples in Figures 3.4-3.7). We focused our analysis on the endpoints of these attribute-matched movements because, compared to analysis of movement direction, this allowed for two-dimensional information about adaptive changes in movement planning. The adaptive change in movement vector ($\Delta\overrightarrow{MV}$) was computed as the difference in endpoints between the baseline and adapted MV-matched no-feedback probe trials. These probe trials began at the center location (C) and had the same visual displacement as the test trial. Similarly, the adaptive change in start location ($\Delta\overrightarrow{SL}$) was defined as the difference in endpoints between the average baseline and average adapted SL-matched probe trials, and the adaptive change in goal location ($\Delta\overrightarrow{GL}$) was defined as the difference in endpoints between the average baseline and average adapted GL-matched probe trials. The SL-matched probe trials were no visual feedback movements from C to the first target, whereas the GL-matched probe trials were no visual feedback movements from C to the second target.

In Experiments 1 and 2, four different movement configurations were used to probe each of the gains that we estimated (K_{MV}, K_{GL}, and K_{SL}). On average, each subject repeated each configuration 25 times during the testing period and 10 times during the baseline period. To compute $\Delta\overrightarrow{MV}$, $\Delta\overrightarrow{GL}$, and $\Delta\overrightarrow{SL}$ for each individual, we determined the gains based on the average movements for each configuration and then averaged the gains across the four configurations. Note that the confidence ellipses for movement endpoints in Figures 4-8 represent standard errors across subjects.

In Experiment 3, we evaluated the goodness of fit for MV-based, GL-based, and Combined MV-GL-based models on movement sequences with multiple simultaneously adapted movement attributes. Since a value of W_{VL}=1 produces pure MV-based planning, the MV-based model constrained W_{VL}=1 and had one free parameter, R_{MV}. This corresponded to fitting K_{MV} as a free parameter with K_{SL}=1 and K_{GL}=0. Similarly, since a value of W_{VL}=0 produces pure GL-based planning, the GL-based model constrained W_{VL}=0 and had one free parameter, R_{GL}. This corresponded to fitting K_{GL} as a free parameter with K_{SL}=0 and K_{MV}=0. For the combined MV-GL-based model, all three parameters (W_{VL}, R_{GL}, and R_{MV} or K_{SL}, K_{MV}, and K_{GL}) had nontrivial values. These parameters were either fit on the Experiment 3 data ('CRF - Best Fit Model' with three free parameters) or predetermined based on the across-subject averages from Experiment 2 ('CRF - Predetermined Model' with no free parameters). The ability of these models to account for the data observed in Experiment 3 was quantified by computing the prediction error defined as the mean Euclidean distance between the endpoint data and the model prediction.

We performed two types of cross-validation to calculate prediction error and R^2 for each of the models. Leave-one-out cross-validation was performed by determining the model parameters on the group average data from all but one of the subjects, then applying a model

with those parameters to the remaining subject. Significance levels associated with leave-one-out cross-validation were computed by performing a paired t-test comparing the fraction of variance accounted for by each type of model. This form of cross-validation assesses the goodness of fit of the model for each individual subject, but is prone to the noise inherent within single subject data. Thus we also performed repeated two-fold cross-validation to reduce the effect of noise originating from each subject. To perform this kind of cross-validation, we recursively divided each of the four subgroups (±30° training in Experiment 3a and ±30° training in Experiment 3b) in half and determined the model parameters by fitting on the average data from one half of the subjects, and then evaluating the resulting model on the average data from the other half of the subjects. This analysis was then repeated after swapping the fitting and testing groups, and iterated 1000 times based on different randomly chosen subject groupings with the two resulting error and R^2 values being averaged on each iteration. This generated a distribution from which the mean and standard error plotted in Figures 8E-F can be determined. Significance levels associated with repeated two-fold cross-validation were computed by totaling the number of iterations on which one model outperformed the other. Note that since each of the subgroups in Experiment 3 had an odd number of subjects, either nine or eleven, the fitting and testing groupings were not exactly equal in size. Instead they contained four or five subjects in the case of nine person subgroups and five or six subjects in the case of eleven person subgroups. We can think of the variance associated with each subject's data as arising from two components: one reflecting how the entire population of neurologically intact participants would hypothetically perform, and one reflecting individual subject-specific noise. The latter component should average out if data from multiple subjects are combined. Since the average data from ~5 subjects was used to evaluate the goodness of fit for the cross-validated model,

repeated two-fold cross-validation would be expected to eliminate ~80% of the noise variance, thus allowing us to backcalculate an estimate of the total inter-subject variance present during the leave-one-out cross-validation. Subtracting this inter-subject variance from the residual of the leave-one-out cross-validation produces an estimate of the 'true' R^2 values for each of the models in the absence of inter-subject noise.

3.4 – Results

A series of experiments were performed to determine how motor adaptation affects the planning of untrained visually guided movements and movement sequences, focusing on how the effects of motor adaptation could be accounted for by planning movements in terms of two key features: the goal location (GL) and the movement vector (MV). We began by developing a computational framework for understanding how these two features affect the adaptive planning of goal-directed reaching movements. We then experimentally characterized the simple cases in which motor adaptation affected only one movement attribute at a time, in order to isolate the specific effect that each attribute had on movement planning for both individual movements and movement sequences. Using these results, we were able to parameterize the computational model we developed so that it could make specific predictions for the endpoints of movement sequences. We then proceeded to test these predictions on complex movement sequences for which multiple attributes were simultaneously adapted.

3.4.1 – Computational framework

We hypothesized that motor plans based on movement vector ($\overrightarrow{X}_{MV}$) and goal location ($\overrightarrow{X}_{GL}$) are averaged, and that the weighting of these two features (W_{VL}) determines the extent to which the remapping of each feature affects the net motor output ($\overrightarrow{X}_{TOT}$):

$$\text{(Equation 3.1)}\quad \overrightarrow{X}_{TOT} = W_{VL} \cdot \overrightarrow{X}_{MV} + (1 - W_{VL}) \cdot \overrightarrow{X}_{GL}$$

Note that W_{VL} is the weighting of the vector versus the location plan, such that when W_{VL}=1, the motor output depends only on the MV-based plan, whereas when W_{VL}=0, the motor output depends only on the GL-based plan.

We next considered the effects of motor adaptation on $\overrightarrow{X}_{TOT}$ given the relationship expressed in Equation 3.1. In particular, we examined how three different effects of adaptation might alter $\overrightarrow{X}_{MV}$ and $\overrightarrow{X}_{GL}$. As illustrated in Figure 3.7b-d, motor adaptation may affect three movement attributes: the movement vector, start location (SL), and goal location associated with a particular movement. Figure 3.7b shows the geometry of these three adaptations whereas Figure 3.7c-d shows how they might affect motor planning. Note that $\Delta\overrightarrow{GL}$, $\Delta\overrightarrow{MV}$, and $\Delta\overrightarrow{SL}$ are the overall adaptation vectors affecting goal location, movement vector, and start location, respectively.

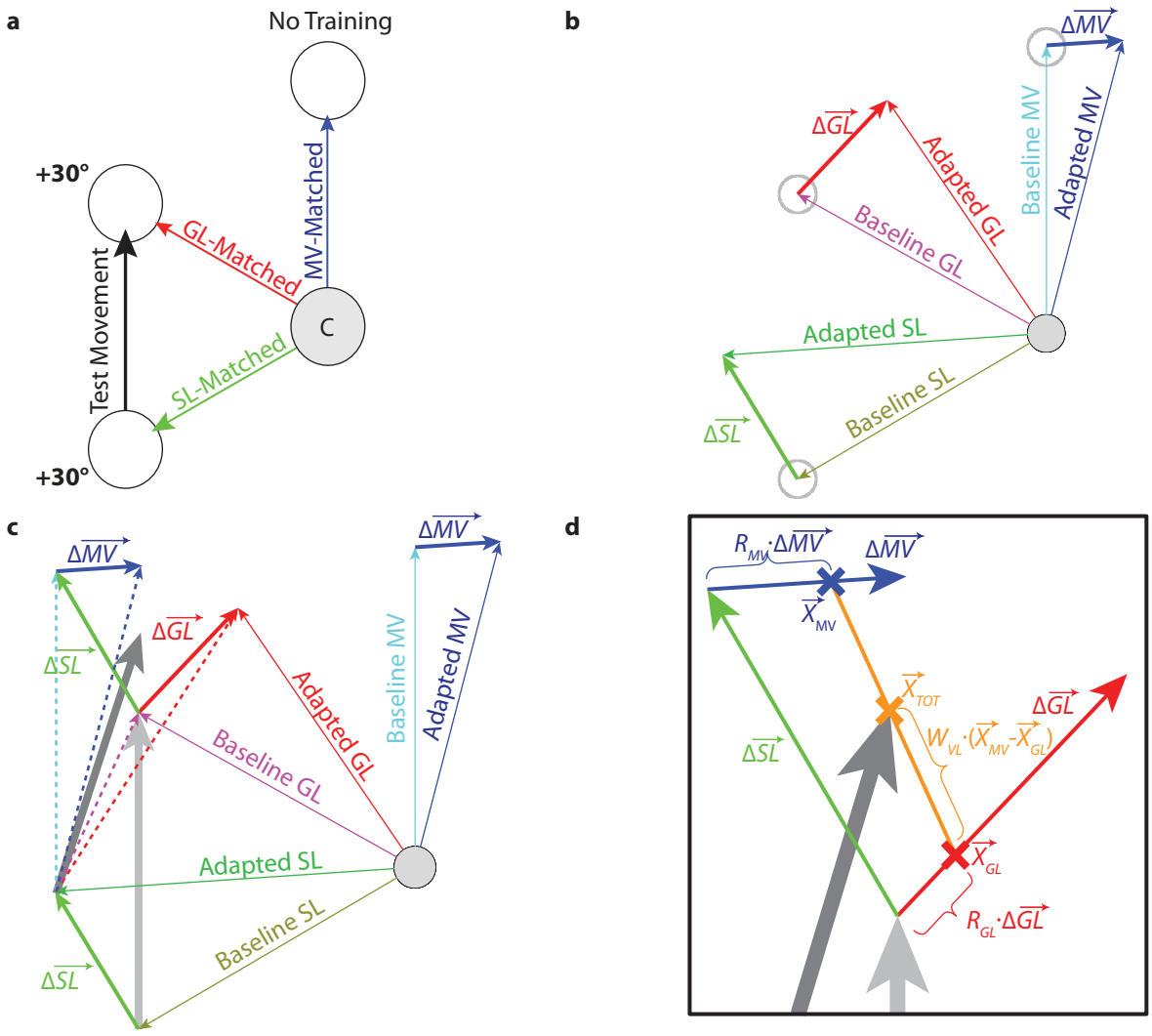

Figure 3.7: Illustration of how the Combined Remapped Feature (CRF) model predicts the effects of adaptation on movement planning. **a)** Illustration of an example test movement that is affected by visuomotor adaptation. The test movement has three attribute-matched movements. The movement-vector-matched movement (MV-Matched) has the same visual displacement on the LCD monitor as the test movement. The goal-location-matched movement (GL-Matched) is directed at the same goal location as the test movement. The start-location-matched movement (SL-Matched) is directed at the start location of the test movement. **b)** Motor adaptation produces changes in each attribute-matched movement which can be represented as the attribute adaptation vectors ($\Delta\overrightarrow{MV}$, $\Delta\overrightarrow{GL}$, and $\Delta\overrightarrow{SL}$) which are the differences between the baseline and adapted attribute-matched movements. **c)** MV-based and GL-based motor planning can occur based on either baseline, fully remapped, or partially remapped features. $\Delta\overrightarrow{GL}$ runs from the Baseline GL (magenta arrow) to the Adapted GL (red arrow). Note that GL-based planning predicts endpoints at a particular position, specifically the locus of points defined by $\Delta\overrightarrow{GL}$. In contrast, MV-based planning predicts displacements originating from the adapted start location (green arrow, end of the adapted SL-Matched movement), these displacement predictions are bounded by the baseline and adapted MV (dashed light blue and dashed dark blue arrows, respectively) and lie on the translated $\Delta\overrightarrow{MV}$ (solid dark blue arrow). **d)** Remapping could affect both the MV-based and GL-based plans, partially shifting both feature-based plans along $\Delta\overrightarrow{MV}$ and $\Delta\overrightarrow{GL}$ with the amount of shift dependent on the amount of remapping of both movement vector (R_{MV}) and goal location (R_{GL}). However, the net motor output ($\overrightarrow{X}_{TOT}$, orange cross) depends on a weighting (W_{VL}) between the motor output associated with MV-based plan ($\overrightarrow{X}_{MV}$, blue cross) and that associated with the GL-based plan ($\overrightarrow{X}_{GL}$, red cross) with W_{VL}=0 yielding fully GL-based plans and W_{VL}=1 yielding fully MV-based plans.

As illustrated in Figure 3.7c, if full goal location remapping were to occur, the GL-based motor plan (red dashed arrow) would be directed at the adapted GL. In contrast, if no GL remapping were to occur, the GL-based motor plan (magenta dashed arrow) would be directed at the baseline GL. Note that the adaptation vector associated with the goal location ($\Delta\overrightarrow{GL}$) spans the locus of endpoints between these two extremal GL-based motor plans. Thus we can define a remapping gain, R_{GL}, with a value between 0 and 1 that describes the amount of goal location remapping ($\Delta\overrightarrow{X}_{GL}$) that occurs in terms of $\Delta\overrightarrow{GL}$:

$$\text{(Equation 3.2)}\quad \Delta\overrightarrow{X}_{GL} = R_{GL} \cdot \Delta\overrightarrow{GL}$$

We also hypothesized that, during motor adaptation, movement vector and goal location are remapped independently of one another. If full movement vector remapping were to occur, the MV-based motor plan (dashed dark blue arrow) would match the displacement of an adapted movement with the same MV (arrow labeled "Adapted MV"). In contrast, if no MV remapping were to occur, the MV-based motor plan (dashed light blue arrow) would match the displacement of a baseline movement with the same MV (arrow labeled "Baseline MV"). Note that the adaptation vector associated with the movement vector ($\Delta\overrightarrow{MV}$) spans the locus of endpoints between these two extremal MV-based motor plans but is offset from the baseline movement endpoint by the adaptation vector associated with the start location ($\Delta\overrightarrow{SL}$). This offset specifically affects the MV-based plan ($\overrightarrow{X}_{MV}$) because this plan is based on a displacement relative to the (adapted) start location whereas the GL-based plan ($\overrightarrow{X}_{GL}$) is based on the intended endpoint independent of the start location. Therefore, the adaptive change in the movement vector ($\Delta\overrightarrow{X}_{MV}$) depends on both $\Delta\overrightarrow{SL}$ and $\Delta\overrightarrow{MV}$ modulated by a remapping gain, R_{MV} and can be expressed as follows:

(Equation 3.3) $\Delta\overrightarrow{X}_{MV} = \Delta\overrightarrow{SL} + R_{MV} \cdot \Delta\overrightarrow{MV}$

Based on Equations 3.1-3.3, the adaptive change in the net motor output ($\Delta\overrightarrow{X}_{TOT}$) depends on both the weighting coefficient (W_{VL}) and the remapping coefficients (R_{MV} and R_{GL}) for movement vector and goal location, as follows:

(Equation 3.4)

$$\Delta\overrightarrow{X}_{TOT} = W_{VL} \cdot \Delta\overrightarrow{X}_{MV} + (1 - W_{VL}) \cdot \Delta\overrightarrow{X}_{GL} = W_{VL} \cdot \Delta\overrightarrow{SL} + W_{VL} \cdot R_{MV} \cdot \Delta\overrightarrow{MV} + (1 - W_{VL}) \cdot R_{GL} \cdot \Delta\overrightarrow{GL}$$

Correspondingly, when a single movement is adapted, the learned adaptation could result from remapping of the movement vector (R_{MV}) or the goal location (R_{GL}) associated with this movement or a combination of the two. However, it is difficult to dissect the contributions of these two features by focusing on trained movements, because the effects of these features are intrinsically coupled in all trained movements. Wang and Sainburg offered a key insight into dissociating the effects of adaptation on goal location and movement vector[137]. The idea is that the effects of adaptation on these features can be uncoupled by adapting one movement and examining how this adaptation affects another – a test movement. In particular, Wang and Sainburg designed an experiment to put the effects of movement vector remapping and goal location remapping in opposition for individual test movements.

Here, we refined this approach by training adaptation to a single target (i.e. a single combination of movement vector and goal location) as opposed to a range of targets so that the remapping of these features could be examined independently of one another, thus isolating the effects of R_{MV} and R_{GL} rather than oppositely coupling them. We also designed test movements to examine the extent to which goal location and movement vector influence the planning of movements, independently of the extent to which these features are remapped, allowing us to

determine W_{VL}. This weighting coefficient, W_{VL}, effectively modulates the contribution of each feature to the planning of untrained movements so that, in conjunction with R_{MV} and R_{GL}, these three factors collectively determine the effect of motor adaptation on untrained movements. We predict that if W_{VL}, R_{MV}, and R_{GL} are identified, the effect of adaptation on untrained movements and movement sequences can be quantitatively determined from Equation 3.4.

3.4.2 – Design of Experiment 1: Attribute isolating experiments

We designed Experiment 1 to characterize the three factors that determine the effects of motor adaptation on the planning of an untrained movement: the amount of MV remapping (R_{MV}), the amount of GL remapping (R_{GL}), and the weighting between an MV-based plan and a GL-based plan (W_{VL}). We can use Equation 3.4 as a guide to show how this can be accomplished. Note that this equation describes the adaptive change in the motor output ($\Delta\overrightarrow{X}_{TOT}$) as a linear combination of the adaptation vectors for three movement attributes, the start location ($\Delta\overrightarrow{SL}$), the movement vector ($\Delta\overrightarrow{MV}$), and the goal location ($\Delta\overrightarrow{GL}$) where their gains are based on W_{VL}, R_{MV}, and R_{GL} and should not change from one movement to the next. This can be made explicit by rewriting Equation 3.4 in terms of these gains as follows:

$$\text{(Equation 3.5)}\quad \Delta\overrightarrow{X}_{TOT} = K_{SL}\cdot\Delta\overrightarrow{SL} + K_{MV}\cdot\Delta\overrightarrow{MV} + K_{GL}\cdot\Delta\overrightarrow{GL}$$

where the gains are $K_{SL} = W_{VL}$, $K_{MV} = W_{VL}\cdot R_{MV}$, and $K_{GL} = (1-W_{VL})\cdot R_{GL}$. The form presented in Equation 3.5 makes it clear that, if the effects of each adaptation vector ($\Delta\overrightarrow{SL}$, $\Delta\overrightarrow{MV}$, and $\Delta\overrightarrow{GL}$) can be isolated, the corresponding gains can be uniquely determined as follows:

$$\text{(Equation 3.6)}\quad K_{SL} = \frac{\Delta\overrightarrow{X}_{TOT}}{\Delta\overrightarrow{SL}} \;\; \textit{if}\;\; \Delta\overrightarrow{MV} = 0 \;\textit{and}\; \Delta\overrightarrow{GL} = 0$$

(Equation 3.7) $K_{MV} = \frac{\Delta \overrightarrow{X}_{TOT}}{\Delta \overrightarrow{MV}}$ *if* $\Delta \overrightarrow{SL} = 0$ *and* $\Delta \overrightarrow{GL} = 0$

(Equation 3.8) $K_{GL} = \frac{\Delta \overrightarrow{X}_{TOT}}{\Delta \overrightarrow{GL}}$ *if* $\Delta \overrightarrow{MV} = 0$ *and* $\Delta \overrightarrow{SL} = 0$

We thus designed Experiment 1 to determine each of these gains by independently controlling the magnitudes of the three attribute adaptation vectors, as illustrated in Figures 3.4-3.6. Once these gains (K_{MV}, K_{GL}, K_{SL}) are measured, the weighting and remapping coefficients can be determined from these three gains.

(Equation 3.9) $W_{VL} = K_{SL}$

(Equation 3.10) $R_{MV} = \frac{K_{MV}}{K_{SL}}$

(Equation 3.11) $R_{GL} = \frac{K_{GL}}{1 - K_{SL}}$

As shown in Figure 3.8, subjects were trained on movements from a center circle (C) to six peripheral targets (T1-T6). We trained subjects with +30º visuomotor rotations on movements from C to T2 and T5, while movements from C to the other peripheral targets (T1, T3, T4, and T6) were trained with no rotation (i.e. 0° rotation). We then examined test movements in which only one of the three movement attributes was adapted during training. For each test movement, the start location was one of the peripheral targets (T1-T6), and the goal location was one of the two peripheral targets adjacent to the SL (Figure 3.4). For example, a test movement from T4 to T3 was affected by only MV adaptation because it shared a MV with the movement from C to T2 which was trained with +30º rotation, while its SL (T4) and GL (T3) were not adapted during the training period because 0° rotation was trained from C to T3 and

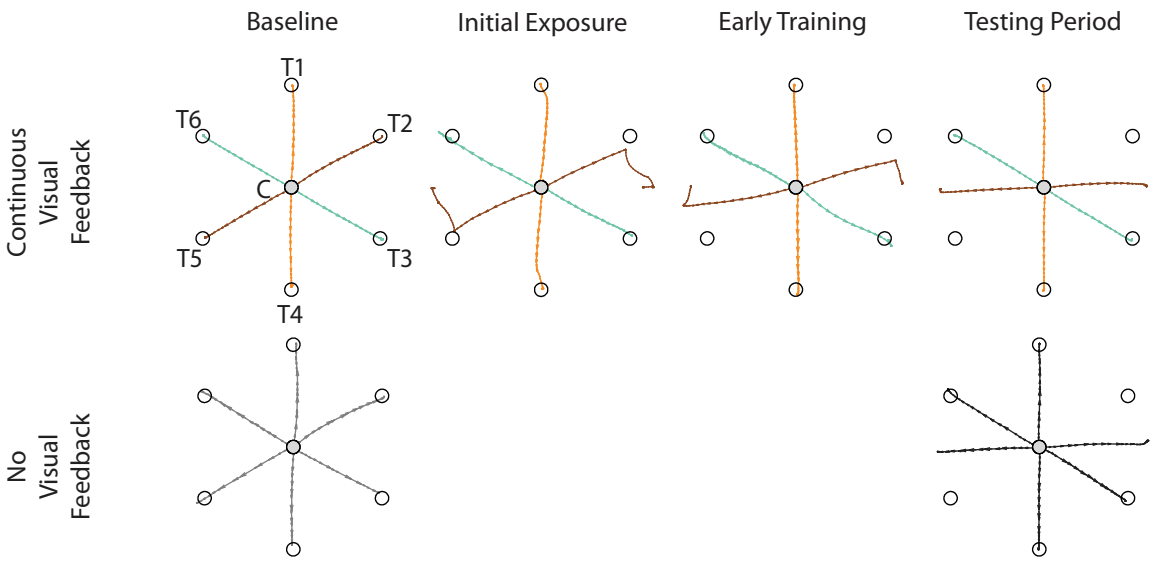

Figure 3.8: Hand paths of point-to-point movements in Experiment 1. +30° rotations were applied on movements from C to T2 and C to T5 during the training and testing periods. Across subject average movement traces are shown in the Baseline and Testing period, while individual movements are shown for Initial Exposure and Early Training

from C to T4 as illustrated in Figure 3.4. Before the test movement, subjects moved to the SL from C and waited an additional 300 ms for the go cue before moving to the GL. In actuality, subjects waited 752±27 ms (mean±S.E.M. are provided throughout this chapter unless otherwise noted) between the end of the first movement and the start of the test movement. Visual feedback of the cursor was removed at the onset of the test movement and was only restored when the subject returned to C after the test movement. Note that because of the regular hexagonal layout of the peripheral targets, the target displacements for the training (center-out) and test (edge-traversing) movements were identical, as shown in Figure 3.2.

3.4.3 – Adaptation to visuomotor rotations during the training period in Experiment 1

Before examining how learning visuomotor rotations transferred to untrained movements, we examined the data from the baseline and training periods. During the baseline period, subjects made quick movements (movement duration = 425±3 ms, peak speed = 48.44±0.28

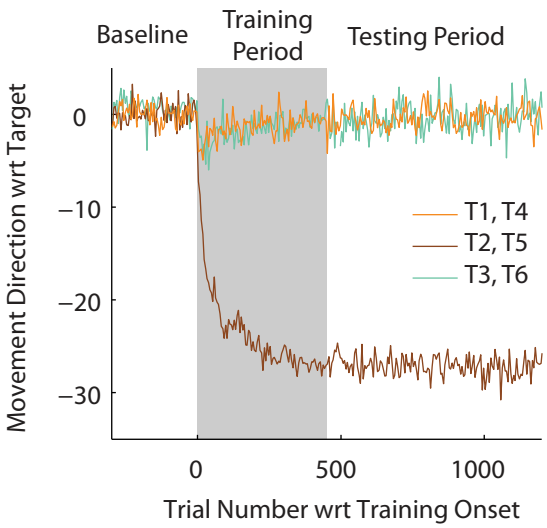

Figure 3.9: Average movement direction measured 100 ms after movement onset over the course of Experiment 1. Note that rotation was imposed starting from Trial 0, and the testing period started from Trial 450. Trace colors match the movement colors in Figure 3.8.

cm/s) from C to each of the six peripheral targets. These movements were essentially straight and aimed directly at the targets (first column of Figure 3.8), with no visual feedback probe movements and continuous visual feedback movements to the same targets essentially identical to one another (compare the colored and gray traces in the first column of Figure 3.8). When a visuomotor rotation was applied during the training period, hand movements were initially directed towards the baseline position associated with the target with an error correction at the end due to visual feedback of the cursor missing the target (second column of Figure 3.8). But gradually, subjects adapted to the visuomotor rotation, and hand movements rotated away from the visual target (third column of Figure 3.8). Ultimately, by the end of the training period and during the testing period, subjects made cursor movements straight to the intended targets with rotated hand paths (fourth column of Figure 3.8). Thus, during the testing period, movements to a given target were essentially identical regardless of the availability of visual feedback on cursor position (compare the colored and black traces in the fourth column of Figure 3.8). Similar to

previous visuomotor rotation studies[41,56,73,74,103,137], we found nearly full adaptation on movements trained with rotation (90±1% adaptation), while movements trained with zero rotation showed minimal changes following the training period (3±1% adaptation) as shown in Figure 3.9.

3.4.4 – Isolating the effects of movement vector, goal location, and start location adaptation

To study the effects of movement vector adaptation independently of SL adaptation and GL adaptation, subjects performed a test movement in which the MV-matched movement (MVM) was trained with a +30º rotation, while the GL-matched movement (GLM) and SL-matched movement (SLM) were trained with 0º rotation. In the example shown in Figure 3.4, the test movement (T4 to T3) has a MVM (C to T2) which was trained with a +30º visuomotor rotation. In contrast, the GLM (C to T3) and the SLM (C to T4) were both trained with a 0º rotation. Since neither the GL nor the SL of the test movement is adapted, this manipulation isolates the effect of MV adaptation. This effect can be observed by comparing the difference between the adapted and baseline test movements (black vs gray movements in Figure 3.4b). If the rotation learned in the MVM (C to T2) movement vector fully transfers to the test movement (T4 to T3), the change in MV observed in the test movement would match the change in movement vector ($\Delta\overrightarrow{MV}$) of the MVM (C to T2). However, the example given in Figure 3.4 shows about 21° of rotation (black vs gray data) for the test movement compared to about 28° of rotation for the MVM (blue vs cyan data). The gain on this transfer (K_{MV}) can be quantified as a fraction of the learned change in movement vector ($\Delta\overrightarrow{MV}$) by projecting the test-movement adaptation vector (dashed black arrow) onto the trained adaptation vector ($\Delta\overrightarrow{MV}$) as shown in Figure 3.4c. For each subject, we applied this analysis to the four types of MV-isolating test

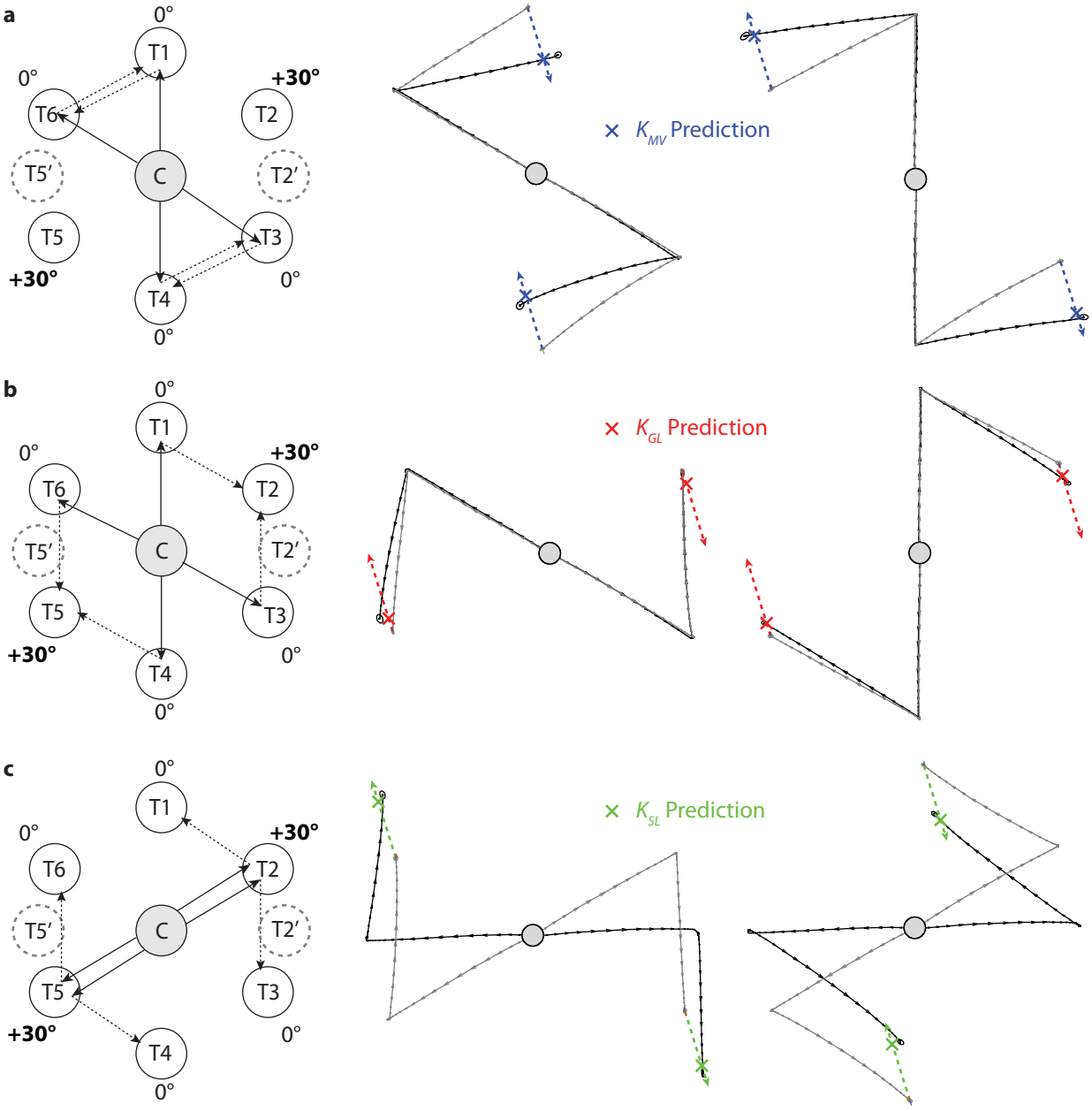

Figure 3.10: Results from the attribute isolating experiment using individual movements (Experiment 1). **a)** Test movements with isolated MV-adaptation. Dashed blue arrows indicate the shifted $\Delta\overrightarrow{MV}$, as shown in Figure 3.4b-c and 3.7. All hand paths display across subject average movements with standard error ellipse at the endpoint. The blue cross indicates the best fit location of K_{MV} over all four movements. **b)** Test movements with isolated GL-adaptation. Dashed red arrows indicate the shifted $\Delta\overrightarrow{GL}$. **c)** Test movements with isolated SL-adaptation. Dashed green arrows indicated the shifted $\Delta\overrightarrow{SL}$.

movements in Experiment 1 (Figure 3.10a) to estimate K_{MV} from our data and found similar gains for all participants (K_{MV} = 0.69±0.03).

Analogously, to study the effects of goal location adaptation independently of MV adaptation and SL adaptation, subjects performed test movements in which the GLM was trained with a +30º rotation while the MVM and SLM were trained with no rotation. In the example shown in Figure 3.5, the test movement (T1 to T2) has a GLM (C to T2) which was trained with a +30º rotation, while the MVM (C to T3) and SLM (C to T1) were trained with 0º rotation. This particular manipulation isolated the effect of GL adaptation from the effects of MV adaptation and SL adaptation, and this effect can be observed by comparing the difference between the adapted and baseline test movements (black vs gray movements in Figure 3.5b). The example in Figure 3.5 shows about 1.1 cm of shift for the adapted test movement endpoint compared to 4.2 cm of shift for the adapted GLM. We quantified the gain of this transfer (K_{GL}) by projecting the test-movement adaptation vector (dashed black arrow) onto the trained adaptation vector ($\Delta\overrightarrow{GL}$) as shown in Figure 3.5c. To estimate K_{GL} from our data, we applied this analysis to each of the four types of GL-isolating test movements (Figure 3.10b) in each subject, finding a significant transfer of goal location adaptation to the untrained test movements in all participants (K_{GL} = 0.17±0.01).

We also isolated the effects of start location adaptation by having subjects perform test movements in which the SLM was trained with a +30° rotation while the MVM and GLM were trained with zero rotation. In the example shown in Figure 3.6, the test movement (T2 to T1) has a SLM (C to T2) which was trained with a +30º rotation, while zero rotation was trained on the MVM (C to T6) and GLM (C to T1), thus isolating the effect of SL adaptation. Similarly to the MV and GL examples, the difference between the adapted and baseline test movements shows

the effect of SL adaptation (black vs gray movements in Figure 3.6b). Again, we quantified the gain of this transfer (K_{SL}) by projecting the test-movement adaptation vector (dashed black arrow) onto the trained adaptation vector ($\Delta\overrightarrow{SL}$) as shown in Figure 3.6c. We applied this analysis to each of the four types of SL-isolating test movements (Figure 3.10c) in each subject, to estimate K_{SL} from our data and found significantly positive gains in all participants (K_{SL} = 0.72±0.01). Note that in Figures 3.4-3.6, all adaptive changes were measured from the same C to T2 movement thus $\Delta\overrightarrow{MV} = \Delta\overrightarrow{GL} = \Delta\overrightarrow{SL}$ for different test movements, illustrating that adaptation of a single movement can affect different movement attributes of untrained test movements.

3.4.5 – Experiment 2: Attribute isolating experiment for movement sequences

In Experiment 2, we studied the transfer of visuomotor adaptation to the planning of movement sequences. As in Experiment 1, we examined the effects of adaptation for movement vector, goal location, and start location in isolation from one another. In this experiment there were two subgroups of subjects, neither of which participated in Experiment 1. One subgroup performed the MV- and GL-isolating trials while the other group performed the SL-isolating trials. In contrast to the individual test movements of Experiment 1, during the movement sequences in Experiment 2, subjects were trained to proceed to the second target immediately after completing the first submovement. The dwell time between the end of the first submovement and the onset of the second submovement was thus substantially shorter than in Experiment 1 (311±16 ms vs 752±27 ms, $p<0.00001$). During these movement sequences, visual feedback was removed at the onset of the first submovement of the sequence and remained off for the entire duration of the movement sequence.

Similarly to Experiment 1, we designed Experiment 2 so that the visuomotor adaptation affected only one of the second submovement's three attributes at a time, with the affected

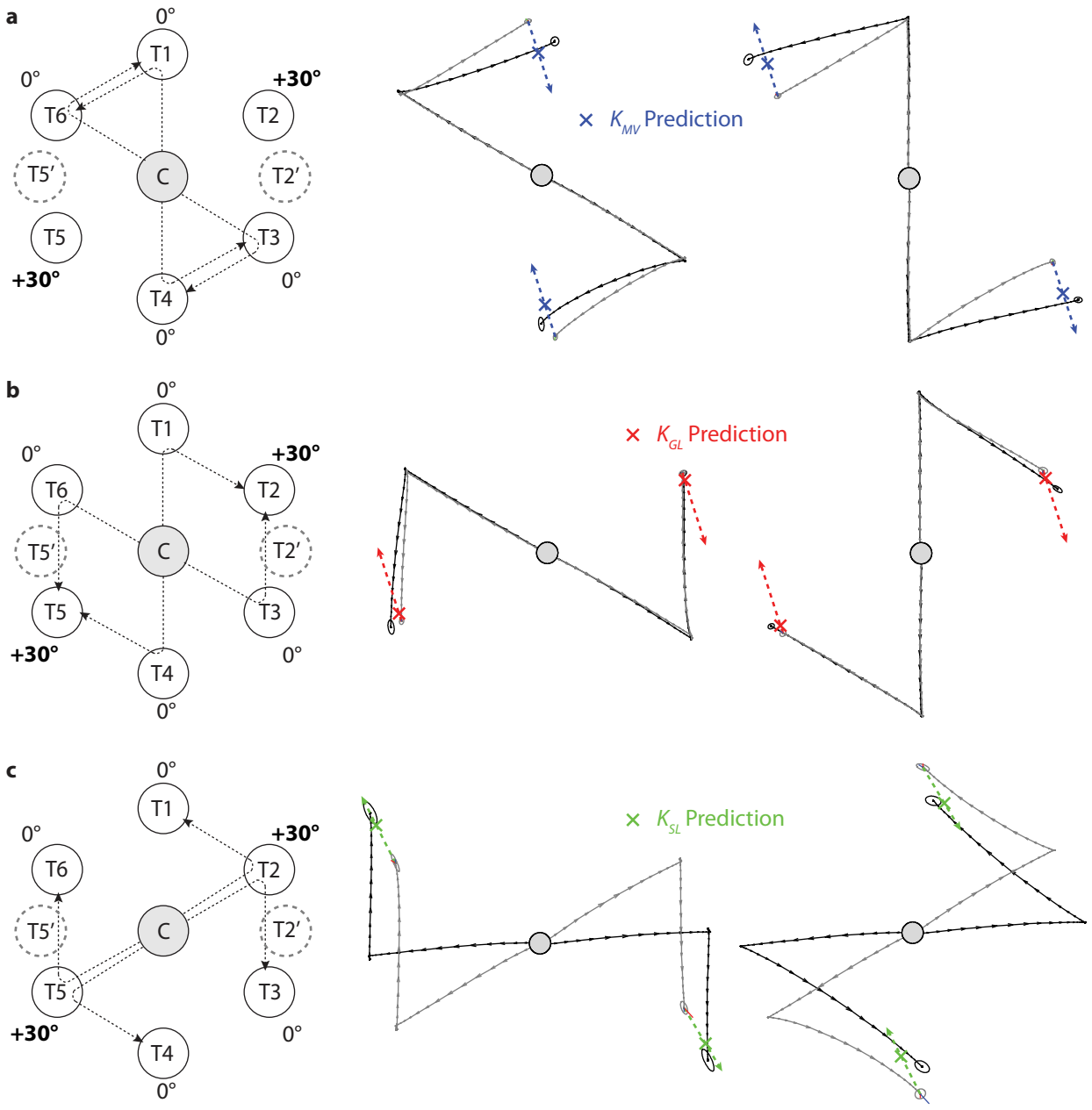

Figure 3.11: Results from the attribute isolating experiment using movement sequences (Experiment 2). Same as in Figure 3.10, but for the movement sequences in Experiment 2.

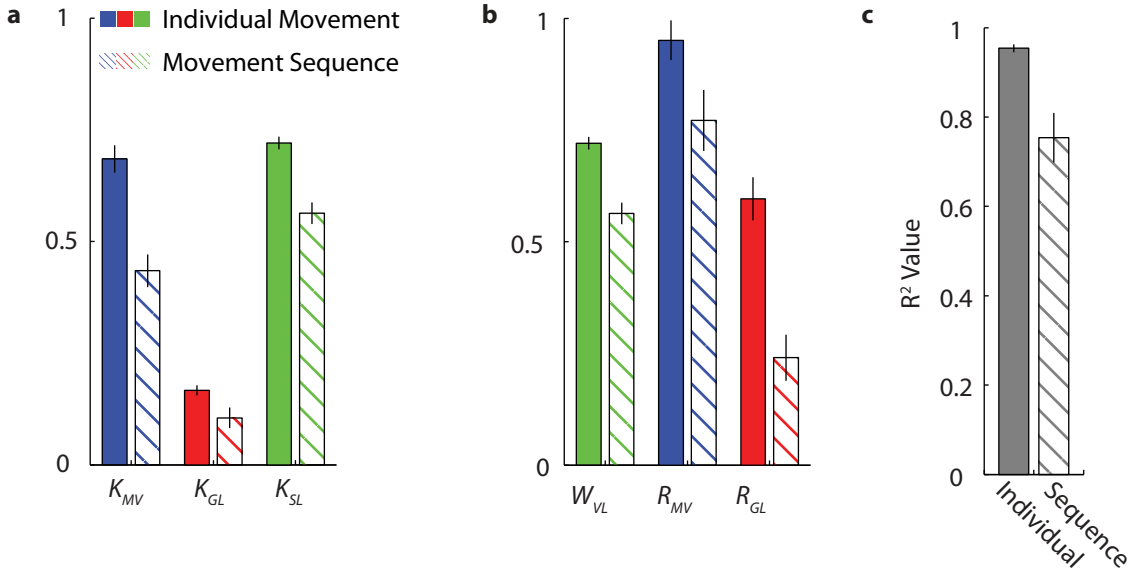

Figure 3.12: Comparison of results from Experiment 1 and 2. **a)** Mean and S.E.M. for K_{MV}, K_{GL}, and K_{SL} found in Experiments 1 and 2. **b)** Mean and S.E.M. for W_{VL}, R_{MV}, and R_{GL} found in Experiments 1 and 2. c) Mean and S.E.M. for the variance accounted for by the Combined Remapped Feature model in Experiments 1 and 2.

attribute depending on the specifics of the movement sequence. As in Experiment 1, we found significant transfer of adaptation in all three movement attributes (Figure 3.11), but the adaptation gains were reduced for each of the three attributes (K_{MV}=0.43±0.04, K_{GL}=0.11±0.02, K_{SL}=0.56±0.02 for Experiment 2, compared to K_{MV}=0.69±0.03, K_{GL}=0.17±0.01, K_{SL}=0.72±0.01 for Experiment 1, $p<0.05$ for all three), as shown in Figure 3.12a. One key difference between Experiments 1 and 2 is the lack of visual feedback at the start location of the test movement. Without visual feedback of hand position, the internal estimate of start location becomes more dependent on proprioceptive information[116], which results in reduced transfer of the visuomotor adaptation to the test sequence. A second important difference is that the reduced dwell times between submovements that occur in movement sequences are known to result in altered motor planning compared to individual movements[54].

3.4.6 – Differential weighting and remapping of movement vectors and goal locations

Using Equations 3.9-3.11, we can compute the differential weighting (W_{VL}) and remapping of goal locations (R_{GL}) and movement vectors (R_{MV}) from the contributions of each attribute's adaptation vectors to the net motor output (K_{SL}, K_{MV}, K_{GL}) determined in Experiments 1 and 2. We find that, in combination, these factors can accurately characterize the planning of both individual movements and movement sequences when movement attributes are adapted in isolation (R^2=0.95±0.01 for individual movements, R^2=0.75±0.06 for movement sequences) as shown in Figure 3.12c. However, in both cases, movement vectors displayed significantly more remapping than goal location (R_{MV}=0.95±0.04, R_{GL}=0.60±0.05 for individual movements $p<0.0001$, R_{MV}=0.77±0.07, R_{GL}=0.24±0.05 for movement sequences $p<0.0001$) as shown in Figure 3.12b. On the other hand, individual movements appear to be predominantly planned based on movement vectors while movement sequences weigh GL-based plans more evenly with MV-based plans (W_{VL}=0.72±0.01 for individual movements, indicating a ratio between MV-based planning (W_{VL}) and GL-based planning (1-W_{VL}) of about 2.6:1 as compared to, W_{VL}=0.56±0.02 for movement sequences, indicating a ratio between MV-based planning and GL-based planning of about 1.3:1, see Figure 3.12b).

3.4.7 – Experiment 3: Predicting the planning of movement sequences with multiple adapted attributes

In Experiment 3, we tested the ability of the model presented in Equations 3.4-3.5 to accurately predict the complex effects of motor adaptation on movement sequences with multiple simultaneously adapted attributes. We refer to this model as the Combined Remapped Feature (CRF) model because it incorporates the multiple effects of motor adaptation associated with the remapping both movement vectors and goal locations. As described in Equation 3.4, the CRF model accounts for the differential remapping of movement vectors (R_{MV}) and goal locations

(R_{GL}), and modulates the MV-based and the GL-based plans based on a weighting (W_{VL}). However, this model may also be expressed in terms of the gains (K_{SL}, K_{MV}, and K_{GL}) used to linearly combine the effects of three attribute adaptation vectors ($\Delta\overrightarrow{SL}$, $\Delta\overrightarrow{MV}$, and $\Delta\overrightarrow{GL}$) as shown in Equation 3.5. Since we have demonstrated that K_{SL}, K_{MV}, and K_{GL} are determined by W_{VL}, R_{MV}, and R_{GL}, both formulations are mathematically equivalent. Critically, because the parameters of the CRF model for movement sequences were individually determined in Experiment 2, we can, without any free parameters, test the ability of this model to predict more complex movement sequences with multiple adapted attributes.

We therefore designed experiments in which subjects performed movement sequences which were affected by the adaptation of either two (Experiment 3a) or three (Experiment 3b) attributes simultaneously. This is in contrast to the attribute isolating experiments (Experiments 1 and 2) discussed above in which only a single attribute was affected for each individual movement or movement sequence. Separate groups of subjects were recruited for Experiment 3a (n=20) and 3b (n=20), and in each of these experiments, subjects performed eight different types of movement sequences in which multiple attributes were simultaneously adapted. Because approximately half of the subjects in each group learned counter-clockwise (+30°) versus clockwise (-30°) visuomotor rotations that affected the planning of these sequences (see section 3.36 and Figure 3.15a and 3.16a), we studied a total of 32 adaptation-sequence combinations, 16 each in Experiment 3a and 3b.

3.4.8 – Predictions of the Combined Remapped Feature (CRF) model

Figure 3.13 illustrates how the CRF model predicts changes in motor planning in an example movement sequence with two-attribute adaptation. In this example, the second submovement (T3 to T4) is simultaneously affected by start location and movement vector

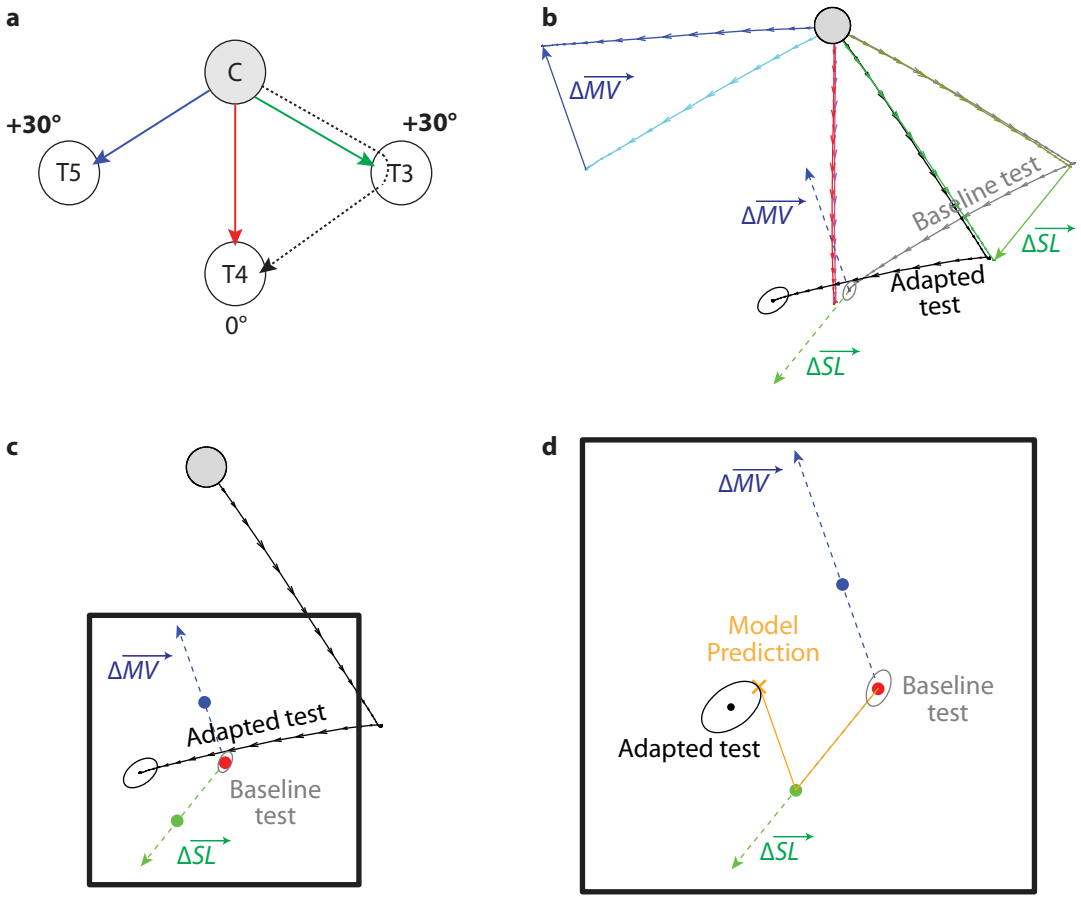

Figure 3.13: Example of the CRF Model prediction for a movement sequence with two simultaneously adapted movement attributes. **a)** Experimental paradigm for a C to T3 to T4 test sequence in Experiment 3a. **b)** Baseline and adapted attribute-matched movements define the attribute adaptation vectors, color scheme is the same as in Figures 3.4-3.7. Two attributes, MV and SL, are adapted during the training period while $\Delta\overrightarrow{GL}$ is near zero because the GL-matched movement was trained with zero rotation. **c)** Test movement sequence with $\Delta\overrightarrow{MV}$ and $\Delta\overrightarrow{SL}$ translated to the baseline endpoint. Colored dots indicate the contributions of $\Delta\overrightarrow{MV}$, $\Delta\overrightarrow{SL}$, and $\Delta\overrightarrow{GL}$ as predicted by the CRF model. **d)** The model prediction (orange cross) is generated by the addition of the $\Delta\overrightarrow{MV}$ and $\Delta\overrightarrow{SL}$ contributions. Average attribute-matched movements and average test sequences are shown with standard error ellipse shown around test sequence endpoints.

adaptation because both the SLM (C to T3) and the MVM (C to T5) received +30º rotation training, whereas the GLM (C to T4) was trained with 0° rotation (Figure 3.13b). Here we used the predetermined values for K_{MV} and K_{SL} from Experiment 2 to compute the contributions of MV and SL adaptation to this test sequence (Figure 3.13c). Figure 3.13d illustrates how a linear combination of $\Delta\overrightarrow{MV}$ and $\Delta\overrightarrow{SL}$ can predict the adaptation-induced change in test sequence endpoint. Note that the blue, red and green dots represent the individual contributions of MV, GL, and SL to the model prediction, respectively (Figure 3.13c-d). In this two-attribute adaptation example, there was no adaptation of the GL of the test sequence and thus no contribution from $\Delta\overrightarrow{GL}$ to the model prediction (red dot). The CRF model predicts that the adapted test endpoint (black dot and error ellipse) will be deviated from the baseline test endpoint (gray error ellipse) by the vector sum of the $\Delta\overrightarrow{SL}$ (green dot) and $\Delta\overrightarrow{MV}$ (blue dot) contributions (orange cross) as shown in Figure 3.13d.

An example of a three-attribute adaptation movement sequence is shown in Figure 3.14. In this example, all three attributes of the test sequence's second submovement (T3 to T2) are adapted. In addition to the +30° training of the SLM (C to T3) and GLM (C to T2), rotation learning generalized to the MVM (C to T1) so that it was also partially rotated, as illustrated in Figure 3.14b. Consequently, as shown in Figure 3.14c, parameterizing the CRF model with the predetermined weights from Experiment 2 generates non-trivial contributions (blue, red, and green dots) from each of the three attributes ($\Delta\overrightarrow{MV}$, $\Delta\overrightarrow{GL}$, and $\Delta\overrightarrow{SL}$). Taking the vector sum of these contributions (orange cross) predicts the endpoint of the adapted test sequence (black dot and error ellipse) relative to the baseline test sequence (gray ellipse) as shown in Figure 3.14d. Note that this view of the CRF model prediction is analogous to that presented in Figure 3.7 based on the weighting and remapping of movement vectors and goal locations.

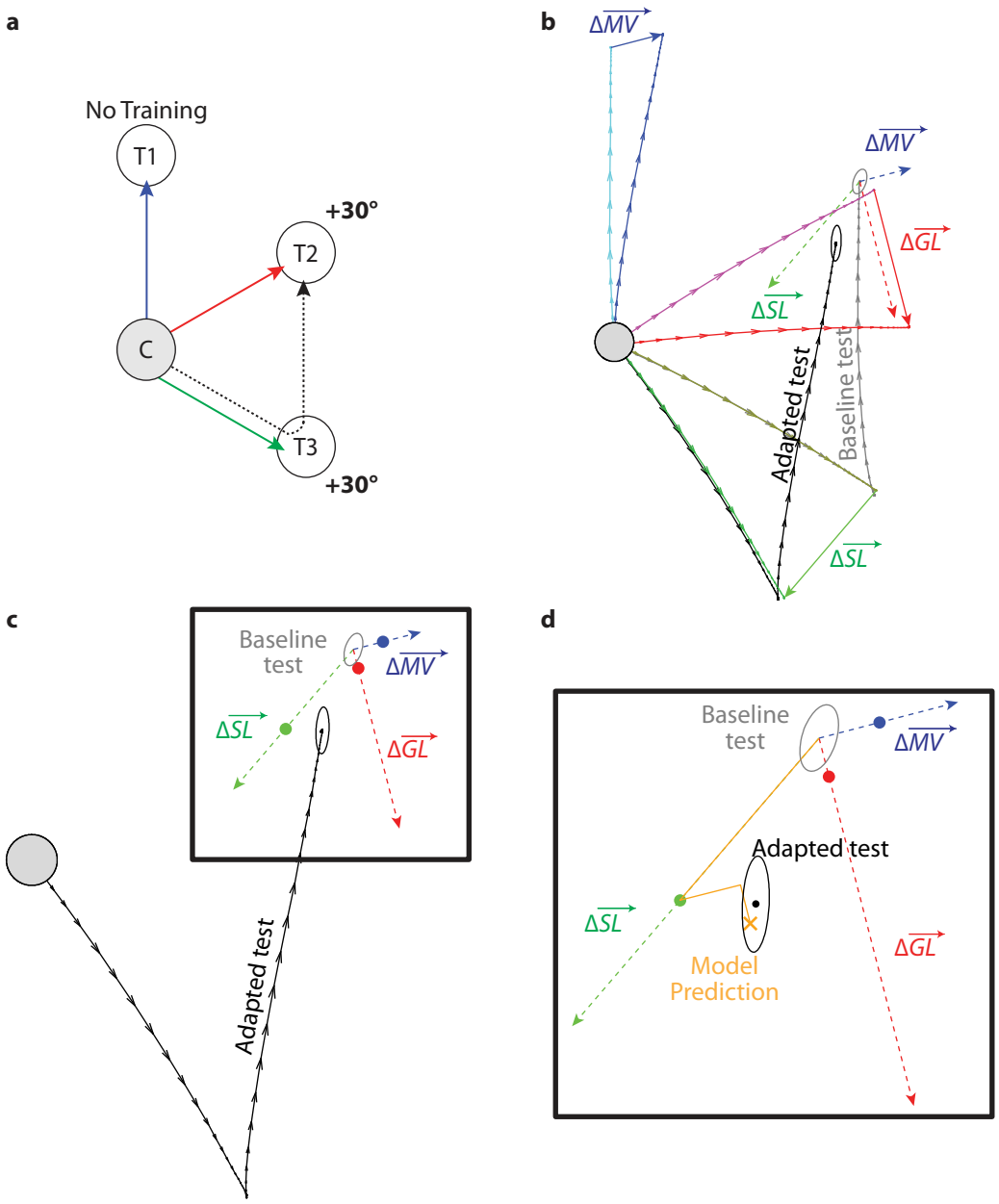

Figure 3.14: Example of the CRF Model prediction for a movement sequences with three simultaneously adapted movement attributes. **a)** Experimental paradigm for C to T3 to T2 test sequence in Experiment 3b. **b)** Baseline and adapted attribute-matched movements define the attribute adaptation vectors, color scheme is the same as in Figures 3.4-3.7. All three attributes, MV, GL, and SL, are adapted during the training period. **c)** Test movement sequence with each attribute adaptation vector translated to the baseline endpoint. Colored dots indicate the contributions of each adaptation vector as predicted by the CRF model. **d)** The model prediction (orange cross) is generated by the addition of all three contributions. Average attribute-matched movements and average test sequences are shown with standard error ellipse around test sequence endpoints.

3.4.9 – Specifics of the design of the two-attribute and three-attribute adaptation experiments

In Experiment 3a, two movement attributes were adapted simultaneously: either start location and goal location or start location and movement vector. To accomplish this, movements from C to the peripheral targets T2, T3, T5, and T6 were trained with ±30° rotations, while movements to from C to T1 and T4 were trained with 0° rotation (Figure 3.15a,d). This training affected the start and goal locations for the four submovements between T2 and T3 and between T5 and T6 but held the movement vectors unchanged (Figure 3.15b,e). In contrast, this training affected the start locations and movement vectors for the four test sequences terminating at T1 or T4, but held the goal locations unchanged (Figure 3.15c,f). Figure 3.15 shows the predictions of the CRF model (orange and lavender crosses) as well as the contributions from $\Delta\overrightarrow{MV}$, $\Delta\overrightarrow{GL}$, and $\Delta\overrightarrow{SL}$ (blue, red, and green dots) for all 16 two-attribute adapted sequences examined in Experiment 3a. The predictions of the CRF model with the parameters predetermined from Experiment 2 are shown as the orange crosses, while the predictions from the CRF model with parameters fit to the Experiment 3 data are shown as the lavender crosses (Figure 3.15). Note the close similarity between these predictions.

Experiment 3b was similar to Experiment 3a except that T1 and T4 were untrained rather trained with zero rotation during the training period. This resulted in noticeable generalization of motor learning to T1 and T4 from the trained movements to T2, T3, T5, and T6. This generalization is roughly in line with the findings of previous work which has shown that when two movement directions, 90° apart, are trained with the same visuomotor rotation, about 55% generalization can be observed midway between[74]. Since the nearest trained targets to T1 and T4 are 120° apart from each other, we would expect less generalization. In line with these

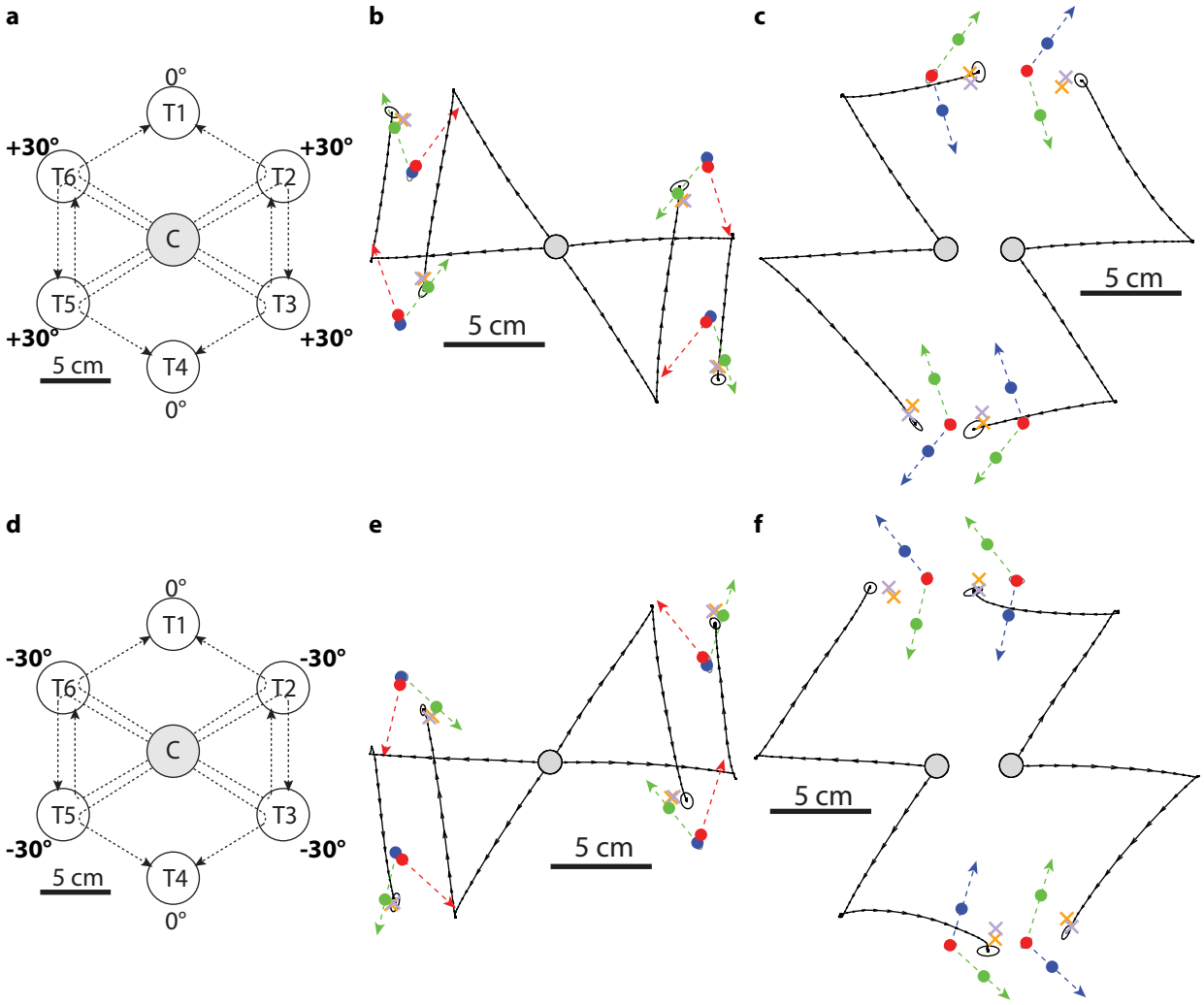

Figure 3.15: Movement sequences with two simultaneously adapted movement attributes (Experiment 3a). **a)** Experimental paradigm for Experiment 3a with +30° (counter-clockwise) rotation training. **b)** Test movement sequences with start location and goal location adaptation. **c)** Test movement sequences with start location and movement vector adaptation. **d)** Experimental paradigm for Experiment 3a with -30° (clockwise) rotation training. **e-f**) Same as **b-c**, but with -30° (clockwise) rotation training. Colored dots indicate the contributions of $\Delta\overrightarrow{MV}$, $\Delta\overrightarrow{GL}$, and $\Delta\overrightarrow{SL}$ as predicted by the coefficients predetermined in Experiment 2. Orange crosses indicate the predictions of the Predetermined CRF Model to Experiment 3 data. Lavender crosses indicate the prediction of the Best Fit CRF model. Average movements are shown with standard error ellipses around sequence endpoints.

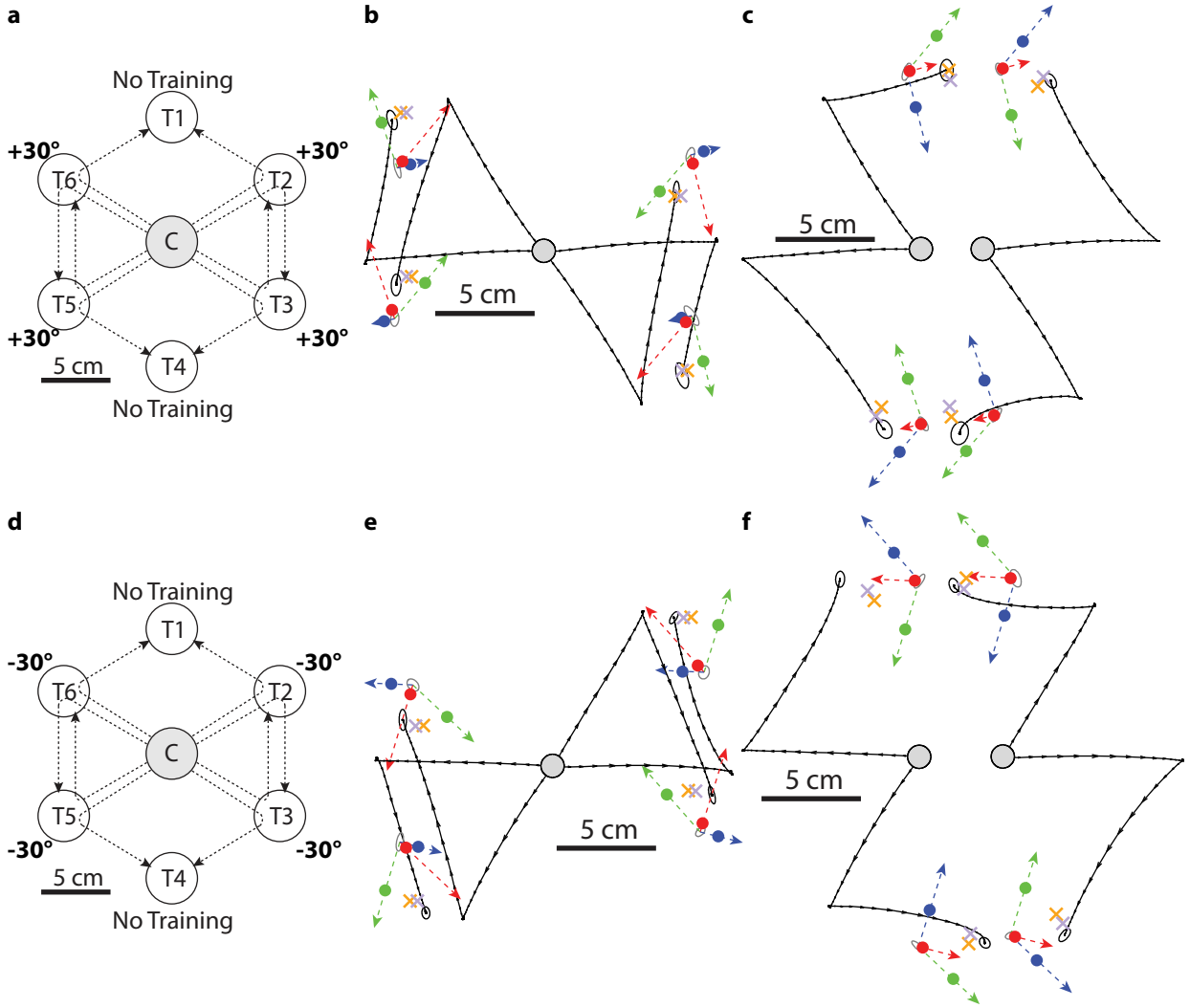

Figure 3.16: Movement sequences with three simultaneously adapted movement attributes (Experiment 3b). **a)** Experimental paradigm for Experiment 3b with +30° (counter-clockwise) rotation training. **b)** Test movement sequences with full start location and goal location adaptation, and partial movement vector adaptation. **c)** Test movement sequences with full start location and movement vector adaptation, and partial goal location adaptation. **d)** Experimental paradigm for Experiment 3b with -30° (clockwise) rotation training. **e-f**) Same as **b-c**, but with -30° (clockwise) rotation training. Colored dots indicate the contributions of $\Delta\overrightarrow{MV}$, $\Delta\overrightarrow{GL}$, and $\Delta\overrightarrow{SL}$ as predicted by the coefficients predetermined in Experiment 2. Orange crosses indicate the predictions of the Predetermined CRF Model. Lavender crosses indicate the prediction of the Best Fit CRF model to Experiment 3 data. Average movement sequences are shown with standard error ellipses around sequence endpoints.

predictions, we found 36±4% generalization on probe trials to T1 and T4 during the testing period. As a result, movements between targets with adapted start and goal locations now had an adapted movement vector as well (blue arrows in Figure 3.16b,e), and test sequences ending at T1 and T4 had a partially adapted goal location (red arrows in Figure 3.16c,f). This partial generalization allowed us to examine how test sequences were affected by simultaneously adapting all three attributes of the second submovement – as in the example documented in Figure 3.14. The predictions of the CRF model with the parameters predetermined from Experiment 2 are shown as the orange crosses, while the predictions from a CRF model which best characterized the data in Experiment 3 are shown as the lavender crosses (Figure 3.16).

3.4.10 – Comparison the predictions of the Combined Remapped Features (CRF) model to single-feature-based models

We find that the CRF model with predetermined coefficients from Experiment 2 predicts the movement sequences studied in Experiment 3 significantly better than models which assume pure GL-based or pure MV-based planning ($p<0.0001$ for both, Figure 3.17) even when these single-feature-based models are fit to the data with free parameters. The net motor output for the pure MV-based plan would entail full weighting for the MV-based plan versus the GL-based plan (W_{VL}=1) so that only movement vector remapping (R_{MV}) would be relevant. In contrast, a pure GL-based plan would entail full weighting for the GL-based plan versus the MV-based plan (W_{VL}=0) so that only goal location remapping (R_{GL}) would be relevant. Correspondingly, each of these models contains one free parameter: R_{MV} or R_{GL}, respectively in the Equation 3.4 version or K_{MV} or K_{GL}, respectively in the Equation 3.5 version.

We compared the pure GL-based and pure MV-based models to a version of the CRF model in which the coefficients were predetermined from Experiment 2, and a version in which

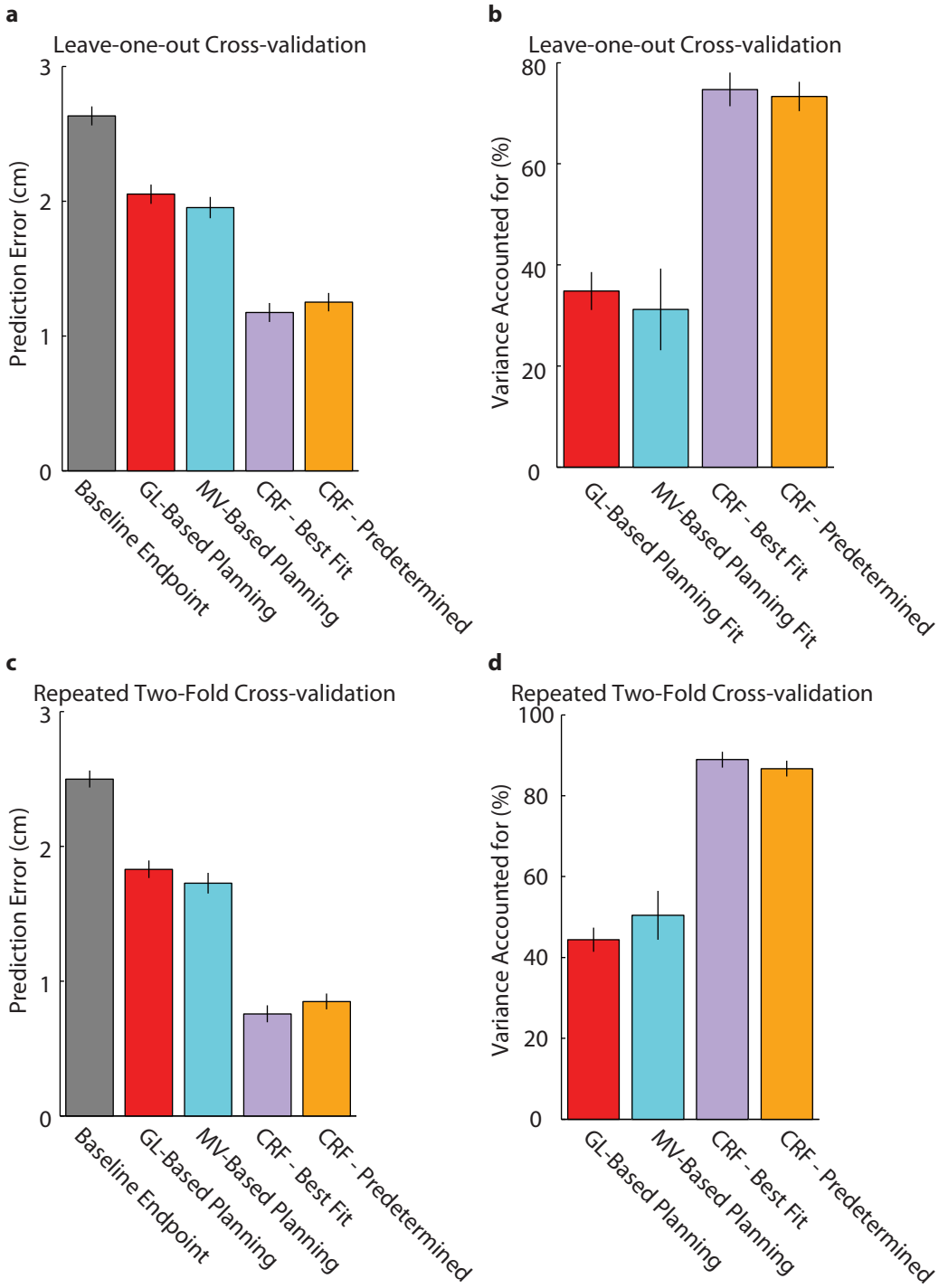

Figure 3.17: Comparison of the Combined Remapped Feature (CRF) model to pure MV-based and pure GL-based planning. **a)** The prediction error of GL-based, MV-based, Best-Fit CRF, and predetermined CRF models computed using leave-one-out cross-validation. **b)** The amount of variance accounted for by each model shown in C relative to the baseline test sequence endpoint **c-d)** The same as in **a-b,** but for repeated two-fold cross-validation to reduce noise across subjects.

the coefficients were fit to the Experiment 3 data. We used leave-one-out cross-validation to characterize the ability of the different model fits to explain individual subject data. This entailed repeatedly fitting the free parameters in each model to the data from all but one of the subjects, and testing this fit on the remaining subject. Because cross-validation entails testing each model on data which was not used in fitting it, the number of free parameters in each model does not bias the assessment of goodness of fit. Thus models with different numbers of free parameters can be compared without specifically accounting for the model complexity or degrees of freedom. Note that there was no fitting in the predetermined CRF model because the same coefficients were used each time.

We found that the pure MV-based and pure GL-based planning models provide similar quality fits, accounting for 31.2±8.1% and 34.8±3.8% of the total variance, respectively. In contrast, the predetermined CRF model explains the adaptive changes in the movement sequence endpoints considerably better, accounting for 73.3±2.9% of the total variance (Figure 3.17b, $p<0.0001$ for the predetermined CRF vs pure MV-based model and for the predetermined CRF vs pure GL-based model). Moreover, when the parameters of the CRF model are chosen to best fit the data in Experiment 3 (lavender crosses in Figure 3.15-3.16), this model accounts for essentially the same fraction of variance (74.7±3.3%) as when the parameters were predetermined with 27/40 of the subjects better characterized by the best-fit CRF model and 13/40 subjects better characterized by the predetermined CRF model ($p=0.12$, paired t-test). This close match between the goodness of fit for the predetermined and best-fit CRF models underscore the predictive power of the results from Experiment 2. Interestingly, if the predetermined values from Experiment 1 are used instead of those from Experiment 2, the quality of the fit deteriorates noticeably, accounting for only 62.2±5.4% of the total variance

($p<0.005$ for the predetermined parameters from Experiment 2 vs Experiment 1, not shown in Figure 3.17).

We designed Experiment 3 to test the CRF model over a wide variety of different movement sequences, rather than to maximize the precision of our endpoint estimate for each movement sequence. Correspondingly, the movement sequence test data for each subject was divided into eight different types of movement sequences, thus reducing by a factor of eight the number of trials we could average together in order to estimate each endpoint position. This resulted in confidence ellipses for each subject's data that were often comparable in size to the errors between each subject's mean data and the CRF model predictions, suggesting that a large fraction of the error in the cross-validated model predictions may be due to noise in estimating the mean data for each subject. If this is the case, the 'true' R^2 values characterizing the ability of the CRF model to explain the effects of motor adaptation on movement sequence planning may be substantially higher than the single subject R^2 estimates made above which are based on noisy data.

One approach to reducing the noise in the mean estimate is to average data across subjects. Thus to make a better estimate of the 'true' R^2 value of the CRF models, we performed repeated two-fold cross-validation in which the data from a randomly chosen half of the subjects were repeatedly used to fit the model, and the mean data from the other half were used to assess the goodness of the model (Figure 3.17c-d). With this approach, we find that the CRF model with predetermined coefficients accounts for 86.7±1.9% of the variance while the best fit CRF model accounts for 89.0±1.9% of the variance (Figure 3.17d). Because there were about 10 subjects in each of the four subgroups in Experiment 3, the repeated two-fold cross-validation allowed us to average across an average of five subjects, thus reducing the mean variability by a

factor of about 5 (~80%). Extrapolation of this reduction in variability yields estimates for the 'true' R^2 values of the predetermined and best-fit CRF models of 90.1% and 91.3%, respectively. This suggests that only 9%-10% of the total variance in movement sequences with multiple adapted movement attributes arises from factors unrelated to GL-based and MV-based planning, such as biomechanical factors not accounted for by the Combined Remapped Feature model.

3.5 – Discussion

We examined the adaptive control of individual movements and movement sequences by characterizing how goal location and movement vector contribute to motor planning and how these features are remapped during visuomotor rotation learning. We began by demonstrating that these factors can be represented in terms of scalar gains on the adaptation vectors ($\Delta\overrightarrow{SL}$, $\Delta\overrightarrow{MV}$, $\Delta\overrightarrow{GL}$) of three movement attributes: the start location, movement vector, and goal location (see Equations 3.1-3.5). By performing a series of experiments to independently adapt each of these attributes (Experiments 1-2), we were able to directly measure the corresponding gains (K_{SL}, K_{MV}, K_{GL}), thus allowing us to determine the weighting and remapping of movement-vector-based and goal-location-based motor plans. Interestingly, we found that these factors accurately characterized the adaptive changes in motor output for both individual movements (R^2=0.95) and movement sequences (R^2=0.75), with the latter showing increased weighting of goal location compared to movement vector but decreased remapping of both goal location and movement vector. We then used the coefficients from the attribute isolating experiment to parameterize a model that combined remapped features (the CRF model) to predict how movement sequences would be affected when multiple movement attributes are adapted in

combination. Remarkably, we found that this model accounted for over 90% of the variance associated with this motor adaptation, significantly more than a best-fit pure movement-vector model (partial R^2=0.73, p<0.00001) and a best-fit pure goal-location model (partial R^2=0.76, p<0.00001). Our results show that multiple features contribute to the planning of both point-to-point and sequential reaching arm movements and that a computational model which takes the remapping of multiple features into account accurately predicts how visuomotor adaptation affects the planning of movement sequences.

3.5.1 – Implications for the neurophysiological representation of the CRF model

As noted in the derivation of Equation 3.5 from Equation 3.4, the CRF model we propose can be expressed in two distinct forms. One form of the CRF model (Equation 3.5) expresses the adaptive changes in the control of movement in terms of adaptive responses to alterations of the start location, movement vector, and goal location. In Experiments 1 and 2, we take advantage of this form by directly measuring these adaptive responses to determine the gains associated with each altered movement attribute (K_{SL}, K_{MV}, K_{GL}). This allowed us to directly test the CRF model by comparing experimental data to quantitative predictions about the effects of simultaneously adapting multiple movement attributes (Experiment 3). Another form of this model (Equation 3.4) casts the adaptive control of motor planning in terms of the weighting (W_{VL}) and remapping (R_{GL} and R_{MV}) of a goal-location-based plan and a movement-vector-based plan. If interpreted literally, Equation 3.4 suggests that the motor system makes multiple plans in parallel before weighting them against one another in order to generate motor output.

Intriguingly, multiple simultaneous representations of motor plans arise during the planning of a goal-directed arm reaching movement[4,5,28,64]. A likely source for goal-location based planning is the parietal cortex, the hub that integrates both somatosensory[84] and visual

information [6,97] for the control of movement[4,5,7,13,15,64]. In primates, one area of the posterior parietal cortex, known as the parietal reach region primarily encodes the goal location of visually-guided movements in eye-centered coordinates[10,16,24,92]. Another region of the parietal cortex, area 5, encodes target locations relative to both eye position and limb configuration[16,77,107]. The representation of target locations in an intrinsic, limb-based coordinate frame is essential for generating goal-location-based motor commands and muscle activations. On the other hand, movement-vector-based planning may originate in the premotor cortex. The ventral premotor cortex primarily codes visual reaching targets[45], while movement vectors are encoded in the dorsal premotor area[92,107]. Even in primary motor cortex, where neural responses are less related to motor planning and more strongly related to motor execution, both the position and velocity of ongoing movement are simultaneously encoded[8,88,138], perhaps providing a mechanism for implementing these motor plans in parallel. Here, hand position could be associated with goal-location-based planning whereas hand velocity with movement-vector-based planning. Future work examining how the neural representation associated with motor planning change during visuomotor adaptation will give further insight into the mechanisms underlying the remapping of movement vector and goal location representations.

3.5.2 – Comparison to sequences of eye movements

The adaptive planning of eye movement sequences has been studied more extensively than arm movement sequences[38,95,124,136,146] and the neural mechanisms for the planning and control of eye saccades are much better understood than for reaching arm movements[28,78,96]. The adaptive control of saccades is highly complex, with learning that is specific to both the kinematic and behavioral context[29,30,34,52,53,91]. The prevailing theory on the planning of saccadic eye movements states that locations of visual targets are specified by a difference vector in the

retinotopic reference frame, this vector is then transformed into a desired eye displacement vector (i.e. a movement vector), leading to a specific pattern of muscle activations that foveates the target[18,78,81,95,145]. However, studies examining the adaptive control of saccade sequences have revealed both movement-vector-based and goal-location-based remapping[38,95,124,136,146], with different results depending on the details of the paradigm and the types of saccade sequences elicited.

These results are in line with the findings of this chapter demonstrating the remapping of both movement vectors and goal locations during motor adaptation. One study focused on adaptation of the start location[124], one on goal location adaptation[146], another compared one condition with goal location adaptation to another condition where goal location and movement vector adapted together[38], and two others dissociated goal location from movement vector adaptation[95,136]. However, none of these studies compared the effects of start location, movement vector, and goal location adaptation as in the current study allowing for the dissociation of the weighting versus the remapping of the movement vectors and goal locations. Thus, even in the two studies that specifically dissociated adaptation of these features[95,136], it is unclear whether the differences in goal location and movement vector adaptation are due to differences in the weighting of these two features, the remapping of them, or both. This may be an exciting path for future investigation.

3.5.3 – Remapping of movement vectors or positions?

The results in this chapter challenge the conclusions of a recent study that argued for the existence of movement vector remapping without goal location remapping during visuomotor learning[137]. Interestingly, the basic methodology in that study is very similar to the current work in that the authors looked specifically at the effects of visuomotor rotation learning on untrained

test movements. However, instead of fully dissociating movement vector and goal location remapping as in our attribute isolating experiments, the experimental design placed movement vector and goal location remapping in conflict. Although post-adaptation movements were not fully aligned with predictions from either type of remapping, the data were clearly better characterized by the movement vector prediction, and the authors concluded that visuomotor adaptation remaps movement vectors but not goal locations.

However, the Wang and Sainburg results preclude the possibility of goal location remapping in lieu of movement vector remapping, rather than rule out the coexistence of both factors. In line with this idea, the $\Delta\overrightarrow{GL}$-isolation experiment we perform, with an example illustrated in Figure 3.5, shows that goal location remapping clearly contributes to motor planning ($p<0.0001$). In fact, the Wang and Sainburg data appear to be well explained by the dual remapping of both movement vectors and goal locations predicted by the CRF model: The coefficients determined in Experiment 1 for the planning of individual movements indicate a substantially larger effect of movement vector (68%) than goal location (17%), thus predicting the Wang and Sainburg data to fall in between the pure movement vector and pure goal location predictions, but much closer to the movement vector prediction, which is indeed what they found.

3.5.4 – Multisensory integration during motor planning

In the current chapter, movement start location was altered by motor adaptation to dissociate GL-based motor plans from MV-based motor plans and dissect the differential contributions of these two features toward movement planning. Several previous studies have also altered movement start locations, but surreptitiously, thereby creating a mismatch between proprioceptive and visual sensory information[99,115,116]. As in the current results, these studies found that the change in start location was not fully reflected in the subsequent movement.

Instead, the movement endpoint invariably fell between the baseline endpoint and the endpoint resulting from the execution of the baseline movement vector from the altered start location. However, these studies assumed that motor planning was based purely on movement vectors and explained their results entirely based on a visual-proprioceptive weighting rather than a MV-GL weighting. Correspondingly, they assumed that the motor system's estimate of the start location was the point from which the executed movement vector would have reached the movement goal. However, this need not be the case. Our paradigm alters the start location without creating a visual-proprioceptive mismatch, yet we find changes in endpoint similar to those previously observed. This demonstrates that the visual-proprioceptive weighting in estimating the start location is not entirely responsible for the intermediate endpoint locations observed with visual-proprioceptive mismatch, in line with the idea that motor planning is not purely MV-based. Instead, the results are due, at least in part, to the weighting of MV-based versus GL-based motor plans.

A number of recent studies have suggested that motor adaptation may differentially affect postural control and trajectory planning[32,41,75,76,103,110]. However, some studies have demonstrated the recalibration of movement control following postural adaptation[26,110] and several other studies have demonstrated the recalibration of postural control following movement adaptation[25,56,101,110], suggesting that postural control and trajectory planning are not entirely distinct. The current study provides a quantitative framework through which these results can be understood, since we show that trajectory control depends on both the weighting of and remapping of GL-based and MV-based motor planning. If this is the case, trajectory adaptation would partially affect location-based postural control and vice versa, in line with what has previously been observed experimentally[25,26,41,56,101,110]. Furthermore, the experiments designed

to quantitatively test our model employed some movement sequences that would be affected by trajectory remapping, some that would be affected by postural remapping, and some that would be affected by both. The ability of the CRF model to predict over 90% of the variance induced by motor adaptation across these different sequences indicates the capacity of our framework to quantitatively predict the effects of and interactions between trajectory control and postural control.

Chapter 4 – Conclusions and future work

4.1 – Variability and motor learning ability

In Chapter 2, we investigated how task-relevant variability affects the rate of adaptation of visually guided reaching movements. We demonstrated an interesting relationship between motor learning ability and the amount of task-relevant motor variability collected during a baseline period prior to learning. Confirming one of the central tenets of reinforcement learning theory, we show that higher levels of task-relevant variability produce faster learning rates for different individuals learning one task as well as for separate groups learning different tasks. First, we carefully studied the variability in movement paths during simple arm reaching movements. We then correlated the amount of variability related to a particular path with the rate at which subjects could modulate the magnitude of that path in their reaching movements, without an error signal to drive learning. Finding that subjects with greater amounts of task-relevant variability could adapt their reaching movements faster, we proceeded to examine this relationship in error-based force-field adaptation. Despite the error-based nature of this task, we found that differences in early learning rates were predicted in large part by task-relevant variability. However, these differences had disappeared by the tenth trial in the learning period. Our findings suggest that motor variability aids learning, such that motor tasks which are aligned with variability are learned faster. We find that this relationship is particularly strong when error signals are unavailable and during early learning when it is unclear how to reduce error. Moreover, in a separate experiment, we found evidence that variability is so integral to motor learning that the motor system can actively control and reshape the structure of motor output

variability, aligning it with a particular task to promote learning of that task. These results promote the view that motor variability is an essential feature of reinforcement learning[62,67,86,120,132] that is centrally-driven[19,20,86,117] and actively regulated[66-68,80] by the nervous system.

These findings not only enhance our basic understanding of the motor system, but also provide a potential avenue for the rational design of novel training procedures to improve motor learning and rehabilitation. For example, in stroke rehabilitation, clinical variables explain less than 50% of person-to-person differences in the rate and extent of recovery[94]. The existence of patient subpopulations with relatively rapid and complete recovery provides proof of principle that this type of recovery is possible. If we can understand why some patients with severe impairments can recover while others cannot, we might be able to enhance the recovery of those who show the least improvement. In our current results, the degree to which individual differences in variability explain individual differences in learning ability is striking. This suggests that training paradigms specifically designed to promote different types of variability or take advantage of the unique structure of each individual's variability could significantly improve the efficiency of motor learning.

4.2 – The planning of visually guided reaching movements

In Chapter 3, we investigated how motor adaptation affects the planning of visually guided reaching movements. We began by creating the Combined Remapped Feature (CRF) model through which we dissect the planning of visually guided reaching movements. The CRF

model allows the motor system to generate two feature-based motor plans in parallel, one based on the goal location of a movement, and the other based on an intended movement vector. Critically, each of these motor plans is affected by the remapping of the feature on which it is based, and these features can be simultaneously but differentially remapped by visuomotor adaptation. The CRF model proceeds to weight these two feature-based plans against each other to produce the final motor plan. Notably, in addition to generating motor plans based on a weighted average of movement-vector-based and goal-location-based planning, the CRF model can also account for pure movement vector planning or pure goal location planning by adjusting the weighting parameter between these two plans.

We performed a series of experiments to independently measure three key factors: the amount of movement vector remapping, the amount of goal location remapping, and the weighting of movement-vector-based plans versus goal-location-based plans. Remarkably, we found that this model accounted for over 90% of the adaptive changes in untrained movement sequences following adaptation to a visuomotor rotation. Our results demonstrate that multiple features contribute to the planning of both point-to-point and sequential reaching arm movements, and that a computational model which takes the remapping of both movement features into account accurately predicts how visuomotor adaptation affects the planning of movement sequences.

Interestingly, we find that movement vectors are remapped significantly more than goal locations, and are also weighted more heavily when determining the final motor plan. Preliminary analysis suggests that the relative variability in the initial movement direction of reaching movements is greater than the relative variability in movement endpoint, although the two are correlated. If initial movement direction is relevant to movement vector remapping and

endpoint position is relevant to goal location remapping, these findings may provide an explanation for why movement vectors display more remapping than goal locations and could provide a prediction for the individual differences in the levels of remapping of each feature. If a substantial amount of remapping occurs through reinforcement learning, subjects with more directional variability should display faster movement vector remapping, and subjects with more endpoint variability should display faster goal location remapping. However, the current experiments were not designed to investigate this hypothesis, and the current data is inconclusive. Moreover, since exposure to visuomotor rotations generates a clear error signal with a simple error gradient, the early-only differences in learning levels observed in Chapter 2 are likely to apply here as well. Hence, we would need to focus on remapping early in the training period, if feature remapping occurs primarily through error-based learning later on.

As a whole, dissecting motor adaptation in visually guided reaching movements provides insight into the mechanisms which underlie both motor adaptation and motor planning. Gaining additional understanding of these mechanisms will create opportunities for faster and more effective rehabilitation. Moreover, taken together, our results create a framework for the design of training paradigms to explicitly upregulate the variability associated with key features of complex tasks to improve the rate of learning for the task as a whole. It is my hope that future studies can leverage the groundwork which I have set forth here to create intelligently designed protocols which can enhance the rate and effectiveness of motor learning and motor rehabilitation.

Bibliography

1 Ackerman, P. L. Individual-Differences in Skill Learning - an Integration of Psychometric and Information-Processing Perspectives. *Psychol Bull* **102**, 3-27 (1987).

2 Ackerman, P. L. Determinants of Individual-Differences during Skill Acquisition - Cognitive-Abilities and Information-Processing. *J Exp Psychol Gen* **117**, 288-318 (1988).

3 Andalman, A. S. & Fee, M. S. A basal ganglia-forebrain circuit in the songbird biases motor output to avoid vocal errors. *P Natl Acad Sci USA* **106**, 12518-12523 (2009).

4 Andersen, R. A. & Buneo, C. A. Intentional maps in posterior parietal cortex. *Annu Rev Neurosci* **25**, 189-220 (2002).

5 Andersen, R. A. & Cui, H. Intention, Action Planning, and Decision Making in Parietal-Frontal Circuits. *Neuron* **63**, 568-583 (2009).

6 Andersen, R. A., Essick, G. K. & Siegel, R. M. Neurons of Area-7 Activated by Both Visual-Stimuli and Oculomotor Behavior. *Experimental Brain Research* **67**, 316-322 (1987).

7 Andersen, R. A., Snyder, L. H., Bradley, D. C. & Xing, J. Multimodal representation of space in the posterior parietal cortex and its use in planning movements. *Annu Rev Neurosci* **20**, 303-330 (1997).

8 Ashe, J. & Georgopoulos, A. P. Movement Parameters and Neural Activity in Motor Cortex and Area-5. *Cerebral Cortex* **4**, 590-600 (1994).

9 Avillac, M., Deneve, S., Olivier, E., Pouget, A. & Duhamel, J. R. Reference frames for representing visual and tactile locations in parietal cortex. *Nature neuroscience* **8**, 941-949 (2005).

10 Batista, A. P., Buneo, C. A., Snyder, L. H. & Andersen, R. A. Reach plans in eye-centered coordinates. *Science (New York, N.Y* **285**, 257-260 (1999).

11 Bays, P. M., Flanagan, J. R. & Wolpert, D. M. Interference between velocity-dependent and position-dependent force-fields indicates that tasks depending on different kinematic parameters compete for motor working memory. *Exp Brain Res* **163**, 400-405 (2005).

12 Berry, S. D. & Thompson, R. F. Prediction of learning rate from the hippocampal electroencephalogram. *Science* **200**, 1298-1300 (1978).

13 Beurze, S. M., de Lange, F. P., Toni, I. & Medendorp, W. P. Integration of target and effector information in the human brain during reach planning. *Journal of neurophysiology* **97**, 188-199 (2007).

14 Bottjer, S. W., Miesner, E. A. & Arnold, A. P. Forebrain lesions disrupt development but not maintenance of song in passerine birds. *Science* **224**, 901-903 (1984).

15 Buneo, C. A. & Andersen, R. A. The posterior parietal cortex: sensorimotor interface for the planning and online control of visually guided movements. *Neuropsychologia* **44**, 2594-2606 (2006).

16 Buneo, C. A., Jarvis, M. R., Batista, A. P. & Andersen, R. A. Direct visuomotor transformations for reaching. *Nature* **416**, 632-636 (2002).

17 Caminiti, R., Johnson, P. B., Galli, C., Ferraina, S. & Burnod, Y. Making Arm Movements within Different Parts of Space - the Premotor and Motor Cortical Representation of a Coordinate System for Reaching to Visual Targets. *Journal of Neuroscience* **11**, 1182-1197 (1991).

18 Carpenter, R. H. S. *Eye movements*. (CRC Press, 1991).

19 Chi, Z. Y. & Margoliash, D. Temporal precision and temporal drift in brain and behavior of zebra finch song. *Neuron* **32**, 899-910 (2001).

20 Churchland, M. M., Afshar, A. & Shenoy, K. V. A central source of movement variability. *Neuron* **52**, 1085-1096 (2006).

21 Clower, D. M. *et al.* Role of posterior parietal cortex in the recalibration of visually guided reaching. *Nature* **383**, 618-621 (1996).

22 Conditt, M. A., Gandolfo, F. & Mussa-Ivaldi, F. A. The motor system does not learn the dynamics of the arm by rote memorization of past experience. *Journal of Neurophysiology* **78**, 554-560 (1997).

23 Conditt, M. A. & Mussa-Ivaldi, F. A. Central representation of time during motor learning. *Proc Natl Acad Sci U S A* **96**, 11625-11630 (1999).

24 Connolly, J. D., Andersen, R. A. & Goodale, M. A. FMRI evidence for a 'parietal reach region' in the human brain. *Experimental Brain Research* **153**, 140-145 (2003).

25 Cressman, E. K. & Henriques, D. Y. Sensory recalibration of hand position following visuomotor adaptation. *Journal of neurophysiology* **102**, 3505-3518 (2009).

26 Cressman, E. K. & Henriques, D. Y. P. Reach Adaptation and Proprioceptive Recalibration Following Exposure to Misaligned Sensory Input. *Journal of neurophysiology* **103**, 1888-1895 (2010).

27 Della-Maggiore, V., Scholz, J., Johansen-Berg, H. & Paus, T. The rate of visuomotor adaptation correlates with cerebellar white-matter microstructure. *Hum Brain Mapp* **30**, 4048-4053 (2009).

28 Desmurget, M., Pelisson, D., Rossetti, Y. & Prablanc, C. From eye to hand: Planning goal-directed movements. *Neurosci Biobehav R* **22**, 761-788 (1998).

29 Deubel, H. Separate Adaptive-Mechanisms for the Control of Reactive and Volitional Saccadic Eye-Movements. *Vision Res* **35**, 3529-3540 (1995).

30 Deubel, H. Separate mechanisms for the adaptive control of reactive, volitional, and memory-guided saccadic eye movements. *Attention Perform* **17**, 697-721 (1999).

31 Diedrichsen, J., White, O., Newman, D. & Lally, N. Use-Dependent and Error-Based Learning of Motor Behaviors. *Journal of Neuroscience* **30**, 5159-5166 (2010).

32 Dizio, P. & Lackner, J. R. Motor Adaptation to Coriolis-Force Perturbations of Reaching Movements - End-Point but Not Trajectory Adaptation Transfers to the Nonexposed Arm. *Journal of neurophysiology* **74**, 1787-1792 (1995).

33 Duhamel, J. R., Bremmer, F., BenHamed, S. & Graf, W. Spatial invariance of visual receptive fields in parietal cortex neurons. *Nature* **389**, 845-848 (1997).

34 Edelman, J. A. & Goldberg, M. E. Dependence of saccade-related activity in the primate superior colliculus on visual target presence. *Journal of neurophysiology* **86**, 676-691 (2001).

35 Ferraina, S. & Bianchi, L. Posterior Parietal Cortex - Functional-Properties of Neurons in Area-5 during an Instructed-Delay Reaching Task within Different Parts of Space. *Exp Brain Res* **99**, 175-178 (1994).

36 Fox, S. I. & McGraw-Hill Companies. *Human physiology*. 12th edn, (McGraw-Hill, 2011).

37 Frank, M. J., Doll, B. B., Oas-Terpstra, J. & Moreno, F. Prefrontal and striatal dopaminergic genes predict individual differences in exploration and exploitation. *Nat Neurosci* **12**, 1062-1068 (2009).

38 Frens, M. A. & van Opstal, A. J. Transfer of Short-Term Adaptation in Human Saccadic Eye-Movements. *Experimental Brain Research* **100**, 293-306 (1994).

39 Gandolfo, F., Mussa-Ivaldi, F. A. & Bizzi, E. Motor learning by field approximation. *Proc Natl Acad Sci U S A* **93**, 3843-3846 (1996).

40 Georgopoulos, A. P., Schwartz, A. B. & Kettner, R. E. Neuronal Population Coding of Movement Direction. *Science (New York, N.Y* **233**, 1416-1419 (1986).

41 Ghez, C., Scheidt, R. & Heijink, H. Different learned coordinate frames for planning trajectories and final positions in reaching. *Journal of neurophysiology* **98**, 3614-3626 (2007).

42 Gonzalez-Castro, L. N., Hemphill, M. & Smith, M. A. in *Advances in Computational Motor Control.*

43 Gonzalez-Castro, L. N., Monsen, C. B. & Smith, M. A. The Binding of Learning to Action in Motor Adaptation. *Plos Comput Biol* **7** (2011).

44 Gordon, J., Ghilardi, M. F. & Ghez, C. Accuracy of Planar Reaching Movements .1. Independence of Direction and Extent Variability. *Experimental Brain Research* **99**, 97-111 (1994).

45 Graziano, M. S. A., Yap, G. S. & Gross, C. G. Coding of Visual Space by Premotor Neurons. *Science (New York, N.Y* **266**, 1054-1057 (1994).

46 Grefkes, C., Ritzl, A., Zilles, K. & Fink, G. R. Human medial intraparietal cortex subserves visuomotor coordinate transformation. *Neuroimage* **23**, 1494-1506 (2004).

47 Hall, J. E. & Guyton, A. C. *Guyton and Hall textbook of medical physiology*. 12th edn, (Saunders/Elsevier, 2011).

48 Halverson, H. M. *An experimental study of prehension in infants : by means of systematic cinema records*. (Clark university, 1931).

49 Hamilton, A. F., Jones, K. E. & Wolpert, D. M. The scaling of motor noise with muscle strength and motor unit number in humans. *Exp Brain Res* **157**, 417-430 (2004).

50 Harris, C. M. & Wolpert, D. M. Signal-dependent noise determines motor planning. *Nature* **394**, 780-784 (1998).

51 Hofsten, C. V. & Lindhagen, K. Observations on the Development of Reaching for Moving-Objects. *J Exp Child Psychol* **28**, 158-173 (1979).

52 Hopp, J. & Fuchs, A. E. The characteristics and neuronal substrate of saccadic eye movement plasticity. *Prog Neurobiol* **72**, 27-53 (2004).

53 Hopp, J. J. & Fuchs, A. F. Identifying sites of saccade amplitude plasticity in humans: transfer of adaptation between different types of saccade. *Experimental Brain Research* **202**, 129-145 (2010).

54 Howard, I. S., Franklin, D.W., Ingram, J.N., Wolpert, D. M. in *22nd Annual Meeting of the Society for the Neural Control of Movement.*

55 Huang, V. S., Haith, A., Mazzoni, P. & Krakauer, J. W. Rethinking Motor Learning and Savings in Adaptation Paradigms: Model-Free Memory for Successful Actions Combines with Internal Models. *Neuron* **70**, 787-801 (2011).

56 Izawa, J. & Shadmehr, R. Learning from Sensory and Reward Prediction Errors during Motor Adaptation. *Plos Comput Biol* **7** (2011).

57 Joiner, W. M., Ajayi, O., Sing, G. C. & Smith, M. A. Linear Hypergeneralization of Learned Dynamics Across Movement Speeds Reveals Anisotropic, Gain-Encoding Primitives for Motor Adaptation. *Journal of Neurophysiology* **105**, 45-59 (2011).

58 Joiner, W. M. & Smith, M. A. Long-Term Retention Explained by a Model of Short-Term Learning in the Adaptive Control of Reaching. *Journal of Neurophysiology* **100**, 2948-2955 (2008).

59 Jolliffe, I. T. *Principal component analysis*. 2nd edn, (Springer, 2002).

60 Jones, K. E., Hamilton, A. F. & Wolpert, D. M. Sources of signal-dependent noise during isometric force production. *J Neurophysiol* **88**, 1533-1544 (2002).

61 Jones, M. B. A 2-Process Theory of Individual Differences in Motor Learning. *Psychological Review* **77**, 353-& (1970).

62 Kaelbling, L. P., Littman, M. L. & Moore, A. W. Reinforcement learning: A survey. *J Artif Intell Res* **4**, 237-285 (1996).

63 Kagerer, F. A., ContrerasVidal, J. L. & Stelmach, G. E. Adaptation to gradual as compared with sudden visuo-motor distortions. *Exp Brain Res* **115**, 557-561 (1997).

64 Kalaska, J. F., Scott, S. H., Cisek, P. & Sergio, L. E. Cortical control of reaching movements. *Current Opinion in Neurobiology* **7**, 849-859 (1997).

65 Kandel, E. R., Schwartz, J. H. & Jessell, T. M. *Principles of neural science*. 4th edn, (McGraw-Hill, Health Professions Division, 2000).

66 Kao, M. H. & Brainard, M. S. Lesions of an avian basal ganglia circuit prevent context-dependent changes to song variability. *J Neurophysiol* **96**, 1441-1455 (2006).

67 Kao, M. H., Doupe, A. J. & Brainard, M. S. Contributions of an avian basal ganglia-forebrain circuit to real-time modulation of song. *Nature* **433**, 638-643 (2005).

68 Kao, M. H., Wright, B. D. & Doupe, A. J. Neurons in a Forebrain Nucleus Required for Vocal Plasticity Rapidly Switch between Precise Firing and Variable Bursting Depending on Social Context. *Journal of Neuroscience* **28**, 13232-13247 (2008).

69 Kawato, M. Internal models for motor control and trajectory planning. *Current Opinion in Neurobiology* **9**, 718-727 (1999).

70 Kertzman, C., Schwarz, U., Zeffiro, T. A. & Hallett, M. The role of posterior parietal cortex in visually guided reaching movements in humans. *Exp Brain Res* **114**, 170-183 (1997).

71 Kojima, S. & Doupe, A. J. Social performance reveals unexpected vocal competency in young songbirds. *Proc Natl Acad Sci U S A* **108**, 1687-1692 (2011).

72 Krakauer, J. W. Motor Learning and Consolidation: The Case of Visuomotor Rotation. *Adv Exp Med Biol* **629**, 405-421 (2009).

73 Krakauer, J. W., Ghilardi, M. F. & Ghez, C. Independent learning of internal models for kinematic and dynamic control of reaching. *Nature neuroscience* **2**, 1026-1031 (1999).

74 Krakauer, J. W., Pine, Z. M., Ghilardi, M. F. & Ghez, C. Learning of visuomotor transformations for vectorial planning of reaching trajectories. *J Neurosci* **20**, 8916-8924 (2000).

75 Kurtzer, I., Herter, T. M. & Scott, S. H. Random change in cortical load representation suggests distinct control of posture and movement. *Nature neuroscience* **8**, 498-504 (2005).

76 Lackner, J. R. & Dizio, P. Rapid Adaptation to Coriolis-Force Perturbations of Arm Trajectory. *Journal of neurophysiology* **72**, 299-313 (1994).

77 Lacquaniti, F., Guigon, E., Bianchi, L., Ferraina, S. & Caminiti, R. Representing spatial information for limb movement: role of area 5 in the monkey. *Cereb Cortex* **5**, 391-409 (1995).

78 Leigh, R. J. & Zee, D. S. *The neurology of eye movements*. 3rd edn, (Oxford University Press, 1999).

79 Malfait, N., Henriques, D. Y. & Gribble, P. L. Shape distortion produced by isolated mismatch between vision and proprioception. *Journal of neurophysiology* **99**, 231-243 (2008).

80 Mandelblat-Cerf, Y., Paz, R. & Vaadia, E. Trial-to-trial variability of single cells in motor cortices is dynamically modified during visuomotor adaptation. *J Neurosci* **29**, 15053-15062 (2009).

81 Mazzoni, P., Bracewell, R. M., Barash, S. & Andersen, R. A. Motor intention activity in the Macaque's lateral intraparietal area .1. Dissociation of motor plan from sensory memory. *Journal of neurophysiology* **76**, 1439-1456 (1996).

82 Mazzoni, P. & Krakauer, J. An Implicit Plan Overrides an Explicit Strategy during Visuomotor Adaptation. *The Journal of Neuroscience* **26**, 3642-3645 (2006).

83 Melendez-Calderon, A., Masia, L., Gassert, R., Sandini, G. & Burdet, E. Force Field Adaptation Can Be Learned Using Vision in the Absence of Proprioceptive Error. *Ieee T Neur Sys Reh* **19**, 298-306 (2011).

84 Mountcastle, V. B. Modality and Topographic Properties of Single Neurons of Cats Somatic Sensory Cortex. *Journal of neurophysiology* **20**, 408-434 (1957).

85 O'Sullivan, I., Burdet, E. & Diedrichsen, J. Dissociating Variability and Effort as Determinants of Coordination. *Plos Computational Biology* **5** (2009).

86 Olveczky, B. P., Andalman, A. S. & Fee, M. S. Vocal experimentation in the juvenile songbird requires a basal ganglia circuit. *PLoS Biol* **3**, e153 (2005).

87 Olveczky, B. P., Otchy, T. M., Goldberg, J. H., Aronov, D. & Fee, M. S. Changes in the neural control of a complex motor sequence during learning. *Journal of Neurophysiology* **106**, 386-397 (2011).

88 Paninski, L., Fellows, M. R., Hatsopoulos, N. G. & Donoghue, J. P. Spatiotemporal tuning of motor cortical neurons for hand position and velocity. *Journal of neurophysiology* **91**, 515-532 (2004).

89 Paz, R., Boraud, T., Natan, C., Bergman, H. & Vaadia, E. Preparatory activity in motor cortex reflects learning of local visuomotor skills. *Nature neuroscience* **6**, 882-890 (2003).

90 Paz, R., Boraud, T., Natan, C., Bergman, H. & Vaadia, E. Preparatory activity in motor cortex reflects learning of local visuomotor skills. *Nature neuroscience* **6**, 882-890 (2003).

91 Pelisson, D., Alahyane, N., Panouilleres, M. & Tilikete, C. Sensorimotor adaptation of saccadic eye movements. *Neurosci Biobehav R* **34**, 1103-1120 (2010).

92 Pesaran, B., Nelson, M. J. & Andersen, R. A. Dorsal premotor neurons encode the relative position of the hand, eye, and goal during reach planning. *Neuron* **51**, 125-134 (2006).

93 Polit, A. & Bizzi, E. Processes controlling arm movements in monkeys. *Science (New York, N.Y* **201**, 1235-1237 (1978).

94 Prabhakaran, S. *et al.* Inter-individual variability in the capacity for motor recovery after ischemic stroke. *Neurorehabil Neural Repair* **22**, 64-71 (2008).

95 Quaia, C., Joiner, W. M., FitzGibbon, E. J., Optican, L. M. & Smith, M. A. Eye movement sequence generation in humans: Motor or goal updating? *J Vision* **10** (2010).

96 Robinson, D. A. Mechanics of Human Saccadic Eye Movement. *J Physiol-London* **174**, 245-& (1964).

97 Robinson, D. L., Goldberg, M. E. & Stanton, G. B. Parietal Association Cortex in Primate - Sensory Mechanisms and Behavioral Modulations. *Journal of neurophysiology* **41**, 910-932 (1978).

98 Rosenbaum, D. A., Engelbrecht, S. E., Bushe, M. M. & Loukopoulos, L. D. A model for reaching control. *Acta psychologica* **82**, 237-250 (1993).

99 Rossetti, Y., Desmurget, M. & Prablanc, C. Vectorial coding of movement: vision, proprioception, or both? *Journal of neurophysiology* **74**, 457-463 (1995).

100 Rutishauser, U., Ross, I. B., Mamelak, A. N. & Schuman, E. M. Human memory strength is predicted by theta-frequency phase-locking of single neurons. *Nature* **464**, 903-907 (2010).

101 Salomonczyk, D., Cressman, E. K. & Henriques, D. Y. P. Proprioceptive recalibration following prolonged training and increasing distortions in visuomotor adaptation. *Neuropsychologia* **49**, 3053-3062 (2011).

102 Scheidt, R. A., Conditt, M. A., Secco, E. L. & Mussa-Ivaldi, F. A. Interaction of visual and proprioceptive feedback during adaptation of human reaching movements. *Journal of Neurophysiology* **93**, 3200-3213 (2005).

103 Scheidt, R. A. & Ghez, C. Separate adaptive mechanisms for controlling trajectory and final position in reaching. *Journal of neurophysiology* **98**, 3600-3613 (2007).

104 Scheidt, R. A., Reinkensmeyer, D. J., Conditt, M. A., Rymer, W. Z. & Mussa-Ivaldi, F. A. Persistence of motor adaptation during constrained, multi-joint, arm movements. *J Neurophysiol* **84**, 853-862 (2000).

105 Schmidt, R. A., Zelaznik, H., Hawkins, B., Frank, J. S. & Quinn, J. T., Jr. Motor-output variability: a theory for the accuracy of rapid motor acts. *Psychol Rev* **47**, 415-451 (1979).

106 Scholz, J. P. & Schoner, G. The uncontrolled manifold concept: identifying control variables for a functional task. *Experimental Brain Research* **126**, 289-306 (1999).

107 Scott, S. H., Sergio, L. E. & Kalaska, J. F. Reaching movements with similar hand paths but different arm orientations .2. Activity of individual cells in dorsal premotor cortex and parietal area 5. *Journal of neurophysiology* **78**, 2413-2426 (1997).

108 Shadmehr, R. & Mussa-Ivaldi, F. A. Adaptive representation of dynamics during learning of a motor task. *J Neurosci* **14**, 3208-3224 (1994).

109 Shadmehr, R. & Mussaivaldi, F. A. Adaptive Representation of Dynamics during Learning of a Motor Task. *Journal of Neuroscience* **14**, 3208-3224 (1994).

110 Simani, M. C., McGuire, L. M. & Sabes, P. N. Visual-shift adaptation is composed of separable sensory and task-dependent effects. *Journal of neurophysiology* **98**, 2827-2841 (2007).

111 Sing, G. C., Joiner, W. M., Nanayakkara, T., Brayanov, J. B. & Smith, M. A. Primitives for motor adaptation reflect correlated neural tuning to position and velocity. *Neuron* **64**, 575-589 (2009).

112 Sing, G. C. & Smith, M. A. Reduction in Learning Rates Associated with Anterograde Interference Results from Interactions between Different Timescales in Motor Adaptation. *Plos Comput Biol* **6** (2010).

113 Smith, M. A., Ghazizadeh, A. & Shadmehr, R. Interacting adaptive processes with different timescales underlie short-term motor learning. *PLoS Biol* **4**, e179 (2006).

114 Sober, S. J. & Brainard, M. S. Adult birdsong is actively maintained by error correction. *Nature Neuroscience* **12**, 927-U144 (2009).

115 Sober, S. J. & Sabes, P. N. Multisensory integration during motor planning. *J Neurosci* **23**, 6982-6992 (2003).

116 Sober, S. J. & Sabes, P. N. Flexible strategies for sensory integration during motor planning. *Nature neuroscience* **8**, 490-497 (2005).

117 Sober, S. J., Wohlgemuth, M. J. & Brainard, M. S. Central Contributions to Acoustic Variation in Birdsong. *Journal of Neuroscience* **28**, 10370-10379 (2008).

118 Sommer, M. A. & Wurtz, R. H. A pathway in primate brain for internal monitoring of movements. *Science (New York, N.Y* **296**, 1480-1482 (2002).

119 Stein, R. B., Gossen, E. R. & Jones, K. E. Neuronal variability: Noise or part of the signal? *Nat Rev Neurosci* **6**, 389-397 (2005).

120 Sutton, R. S. & Barto, A. G. *Reinforcement Learning: An Introduction*. (The MIT Press, 1998).

121 Takikawa, Y., Kawagoe, R., Itoh, H., Nakahara, H. & Hikosaka, O. Modulation of saccadic eye movements by predicted reward outcome. *Experimental Brain Research* **142**, 284-291 (2002).

122 Tamas Kincses, Z. *et al.* Model-free characterization of brain functional networks for motor sequence learning using fMRI. *Neuroimage* **39**, 1950-1958 (2008).

123 Tanaka, H., Sejnowski, T. J. & Krakauer, J. W. Adaptation to Visuomotor Rotation Through Interaction Between Posterior Parietal and Motor Cortical Areas. *Journal of neurophysiology* **102**, 2921-2932 (2009).

124 Tanaka, M. Contribution of signals downstream from adaptation to saccade programming. *Journal of neurophysiology* **90**, 2080-2086 (2003).

125 Thoroughman, K. A. & Shadmehr, R. Learning of action through adaptive combination of motor primitives. *Nature* **407**, 742-747 (2000).

126 Todorov, E. Cosine tuning minimizes motor errors. *Neural Comput* **14**, 1233-1260 (2002).

127 Todorov, E. Optimality principles in sensorimotor control. *Nat Neurosci* **7**, 907-915 (2004).

128 Todorov, E. & Jordan, M. I. Optimal feedback control as a theory of motor coordination. *Nat Neurosci* **5**, 1226-1235 (2002).

129 Tomassini, V. *et al.* Structural and functional bases for individual differences in motor learning. *Hum Brain Mapp* **32**, 494-508 (2011).

130 Tremblay, S., Shiller, D. M. & Ostry, D. J. Somatosensory basis of speech production. *Nature* **423**, 866-869 (2003).

131 Tseng, Y. W., Diedrichsen, J., Krakauer, J. W., Shadmehr, R. & Bastian, A. J. Sensory prediction errors drive cerebellum-dependent adaptation of reaching. *Journal of Neurophysiology* **98**, 54-62 (2007).

132 Tumer, E. C. & Brainard, M. S. Performance variability enables adaptive plasticity of 'crystallized' adult birdsong. *Nature* **450**, 1240-1244 (2007).

133 Unsworth, N. & Engle, R. W. Individual differences in working memory capacity and learning: evidence from the serial reaction time task. *Mem Cognit* **33**, 213-220 (2005).

134 van Beers, R. J., Baraduc, P. & Wolpert, D. M. Role of uncertainty in sensorimotor control. *Philos Trans R Soc Lond B Biol Sci* **357**, 1137-1145 (2002).

135 Wagner, M. J. & Smith, M. A. Shared Internal Models for Feedforward and Feedback Control. *Journal of Neuroscience* **28**, 10663-10673 (2008).

136 Wallman, J. & Fuchs, A. F. Saccadic gain modification: Visual error drives motor adaptation. *Journal of neurophysiology* **80**, 2405-2416 (1998).

137 Wang, J. & Sainburg, R. L. Adaptation to Visuomotor Rotations Remaps Movement Vectors, Not Final Positions. *The Journal of Neuroscience* **25**, 4024-4030 (2005).

138 Wang, W., Chan, S. S., Heldman, D. A. & Moran, D. W. Motor cortical representation of position and velocity during reaching. *Journal of neurophysiology* **97**, 4258-4270 (2007).

139 Warren, T. L., Tumer, E. C., Charlesworth, J. D. & Brainard, M. S. Mechanisms and time course of vocal learning and consolidation in the adult songbird. *Journal of Neurophysiology* **106**, 1806-1821 (2011).

140 White, B. L., Castle, P. & Held, R. Observations on the Development of Visually-Directed Reaching. *Child Dev* **35**, 349-364 (1964).

141 Wise, S. P., Moody, S. L., Blomstrom, K. J. & Mitz, A. R. Changes in motor cortical activity during visuomotor adaptation. *Exp Brain Res* **121**, 285-299 (1998).

142 Wolpert, D. M., Diedrichsen, J. & Flanagan, J. R. Principles of sensorimotor learning. *Nat Rev Neurosci* **12**, 739-751 (2011).

143 Wolpert, D. M., Miall, R. C. & Kawato, M. Internal models in the cerebellum. *Trends Cogn Sci* **2**, 338-347 (1998).

144 Woolley, S. C. & Doupe, A. J. Social context - induced song variation affects female behavior and gene expression. *Plos Biology* **6**, 525-537 (2008).

145 Wurtz, R. H. & Goldberg, M. E. *The Neurobiology of saccadic eye movements*. (Elsevier, 1989).

146 Zimmermann, E., Burr, D. & Morrone, M. C. Spatiotopic Visual Maps Revealed by Saccadic Adaptation in Humans. *Current Biology* **21**, 1380-1384 (2011).